2019

Cortical And Subcortical Mechanisms For Sound Processing

Jennifer Blackwell
University of Pennsylvania, blaje42@gmail.com

Cortical And Subcortical Mechanisms For Sound Processing

Abstract
The auditory cortex is essential for encoding complex and behaviorally relevant sounds. Many questions remain concerning whether and how distinct cortical neuronal subtypes shape and encode both simple and complex sound properties. In chapter 2, we tested how neurons in the auditory cortex encode water-like sounds perceived as natural by human listeners, but that we could precisely parametrize. The stimuli exhibit scale-invariant statistics, specifically temporal modulation within spectral bands scaled with the center frequency of the band. We used chronically implanted tetrodes to record neuronal spiking in rat primary auditory cortex during exposure to our custom stimuli at different rates and cycle-decay constants. We found that, although neurons exhibited selectivity for subsets of stimuli with specific statistics, over the population responses were stable. These results contribute to our understanding of how auditory cortex processes natural sound statistics. In chapter 3, we review studies examining the role of different cortical inhibitory interneurons in shaping sound responses in auditory cortex. We identify the findings that support each other and the mechanisms that remain unexplored. In chapter 4, we tested how direct feedback from auditory cortex to the inferior colliculus modulated sound responses in the inferior colliculus. We optogenetically activated or suppressed cortico-collicular feedback while recording neuronal spiking in the mouse inferior colliculus in response to pure tones and dynamic random chords. We found that feedback modulated sound responses by reducing sound selectivity by decreasing responsiveness to preferred frequencies and increasing responsiveness to less preferred frequencies. Furthermore, we tested the effects of perturbing intra-cortical inhibitory-excitatory networks on sound responses in the inferior colliculus. We optogenetically activated or suppressed parvalbumin-positive (PV) and somatostatin-positive (SOM) interneurons while recording neuronal spiking in mouse auditory cortex and inferior colliculus. We found that modulation of neither PV- nor SOM-interneurons affected sound-evoked responses in the inferior colliculus, despite significant modulation of cortical responses. Our findings imply that cortico-collicular feedback can modulate responses to simple and complex auditory stimuli independently of cortical inhibitory interneurons. These experiments elucidate the role of descending auditory feedback in shaping sound responses. Together these results implicate the importance of the auditory cortex in sound processing.

Degree Type
Dissertation

Degree Name
Doctor of Philosophy (PhD)

Graduate Group
Neuroscience

First Advisor
Maria N. Geffen

Second Advisor
Yale Cohen

CORTICAL AND SUBCORTICAL MECHANISMS FOR SOUND PROCESSING

Jennifer M. Blackwell

A DISSERTATION

in

Neuroscience

Presented to the Faculties of the University of Pennsylvania

in

Partial Fulfillment of the Requirements for the

Degree of Doctor of Philosophy

2019

Supervisor of Dissertation

_____

Maria N. Geffen, PhD
Associate Professor of Otorhinolaryngology

Graduate Group Chairperson

_____

Joshua I. Gold, PhD
Professor of Neuroscience

Dissertation Committee:
Yale Cohen, Professor of Otorhinolaryngology
Steven Eliades, Assistant Professor of Otorhinolaryngology
Christopher Fang-Yen, Associate Professor of Neuroscience
Daniel Polley, Associate Professor of Otolaryngology, Harvard Medical School

ACKNOWLEDGMENTS

There are so many people who have helped and supported me through my graduate school journey. First, I want to thank my advisor, Maria, for all the years of unwavering support. There were few ups and many downs during my time here and Maria was always able to stay positive and provide the space I needed to work through any difficulties I was facing. I also want to thank her for her support of my passion in teaching alongside my research. Even though the Geffen lab was always slightly too cold, the people have always been warm, supportive, and willing to help each other out in any way. I want to thank Laetitia Mwilambwe-Tshilobo, Drs. Mark Aizenberg, Ryan Natan, and Isaac Carruthers for their guidance when I first joined the lab. Our numbers have now expanded, but the lab environment continues to be friendly and collaborative. Thank you to Solymar Rolon-Martinez, Xiaomao Ding, Aaron Williams, Karmi Oxman, and Drs. Melanie Tobin and Linda Garami. I especially want to thank Chris Angeloni for always having the answers to all of my questions (Cy Twombly will always be the worst though) and Dr. Kath Wood for being, like me, willing to talk about literally anything (a kindred spirit). My fellow NGG students, Drs. Peter Dong, Preetika Gupta, Greg Artiushin, and CC Angelakos for the many years of friendship and laughter – I cannot imagine these years without you. For years of love and support, bringing me dinner when I was stuck in lab late at night, sending me terrible jokes from Reddit and many pictures of adorable animals just to brighten my day, I want to thank Dr. Andrew Moberly. Dad – thank you for being there while I was growing up and for introducing me to Terry Pratchett, who has gotten me through a lot of stressful times. Finally, I want to thank my mom, Dr. Kim Blackwell. I am lucky enough to know

that there is nothing in the world you would not do to help me achieve my dreams, including staying up to read my textbooks just to help me with my homework, or writing out math equations on our napkins at the dinner table. Thank you for always being there to talk about my achievements and my failures whenever I need, and also to bake some crazy things when I really just needed a break. You never pushed me into one career or another, yet somehow it turns out that I followed you right into Neuroscience.

ABSTRACT

CORTICAL AND SUBCORTICAL MECHANISMS FOR SOUND PROCESSING

Jennifer M. Blackwell

Maria N. Geffen

The auditory cortex is essential for encoding complex and behaviorally relevant sounds. Many questions remain concerning whether and how distinct cortical neuronal subtypes shape and encode both simple and complex sound properties. In chapter 2, we tested how neurons in the auditory cortex encode water-like sounds perceived as natural by human listeners, but that we could precisely parametrize. The stimuli exhibit scale-invariant statistics, specifically temporal modulation within spectral bands scaled with the center frequency of the band. We used chronically implanted tetrodes to record neuronal spiking in rat primary auditory cortex during exposure to our custom stimuli at different rates and cycle-decay constants. We found that, although neurons exhibited selectivity for subsets of stimuli with specific statistics, over the population responses were stable. These results contribute to our understanding of how auditory cortex processes natural sound statistics. In chapter 3, we review studies examining the role of different cortical inhibitory interneurons in shaping sound responses in auditory cortex. We identify the findings that support each other and the mechanisms that remain unexplored. In chapter 4, we tested how direct feedback from auditory cortex to the inferior colliculus modulated sound responses in the inferior colliculus. We optogenetically activated or suppressed cortico-collicular feedback while recording neuronal spiking in the mouse inferior colliculus in response to pure tones and dynamic random chords. We found that feedback modulated

sound responses by reducing sound selectivity by decreasing responsiveness to preferred frequencies and increasing responsiveness to less preferred frequencies. Furthermore, we tested the effects of perturbing intra-cortical inhibitory-excitatory networks on sound responses in the inferior colliculus. We optogenetically activated or suppressed parvalbumin-positive (PV) and somatostatin-positive (SOM) interneurons while recording neuronal spiking in mouse auditory cortex and inferior colliculus. We found that modulation of neither PV- nor SOM-interneurons affected sound-evoked responses in the inferior colliculus, despite significant modulation of cortical responses. Our findings imply that cortico-collicular feedback can modulate responses to simple and complex auditory stimuli independently of cortical inhibitory interneurons. These experiments elucidate the role of descending auditory feedback in shaping sound responses. Together these results implicate the importance of the auditory cortex in sound processing.

TABLE OF CONTENTS

CHAPTER 1: Introduction

Acoustic signals from the peripheral auditory system enter the cochlear nucleus in the brainstem via the auditory nerve. From the brainstem, information travels through the auditory midbrain, the inferior colliculus, to the auditory thalamus, the medial geniculate body, to the auditory cortex (AC). The auditory cortex is essential for encoding complex and behaviorally relevant sounds (Nelken, 2004; Aizenberg and Geffen, 2013; Carruthers et al., 2013, 2015; Mizrahi et al., 2014; Aizenberg et al., 2015). In this dissertation we address questions about processing of sounds important for everyday hearing in the auditory cortex.

The goal of our work is to elucidate whether and how distinct cortical neuronal subtypes and projections shape and encode both simple and complex sound properties. We address the following questions about auditory processing in the auditory cortex: (1) *How does the auditory cortex encode the statistics of a natural sound such as water?* Experimental auditory stimuli are typically designed to uniformly sample stimulus space. The particular spectro-temporal statistics of natural sounds are not captured by these stimuli. Testing how the auditory system processes these stimulus statistics is important for understanding how organisms interact with behaviorally relevant sounds. (2) *How do inhibitory-excitatory networks shape sound responses in the auditory cortex?* Extensive work has been done to characterize how different cortical neuronal subtypes interact functionally and anatomically. Here we examine this literature to identify cohesive themes

found and mechanisms that remain unclear. (3) *How does feedback from the auditory cortex to the inferior colliculus shape sound processing in the inferior colliculus?* Whereas information is typically thought of as integrated along the auditory system in a hierarchical fashion, there is extensive feedback within the auditory pathway, including from the auditory cortex, that can modulate auditory processing and auditory behaviors. However, the mechanisms by which information processing is shaped via the descending feedback pathway remain poorly characterized. Modulating direct feedback projections allows us to test the contributions of feedback in sound processing.

Understanding how different classes of neurons auditory cortex process simple and complex sounds provides insight into the role of auditory cortex in sound processing and, thus, auditory behaviors. To introduce these topics, we will describe scale-invariant properties of natural sounds and known functions of intracortical networks and feedback in shaping auditory processing.

SCALE-INVARIANT PROPERTIES OF NATURAL SOUNDS

In a rich and complex sensory world, an organism's sensory systems must extract and encode a plethora of behaviorally relevant signals from the environment. However, the computational capacity of neurons places physiological limits on the amount information we can process. The efficient coding hypothesis postulates that, to compensate for this, the brain evolved to efficiently process natural inputs by adapting to the statistics of natural scenes (Attneave, 1954; Barlow, 1961). Many natural signals, such as environmental

sounds, exhibit scale-invariant statistics. These statistical regularities can be used by the auditory system to recognize categories of sounds even with certain types of modulation, such as compression of an audio file. One characteristic of natural sounds, like music and speech, is that the power spectrum scales inversely with the frequency, following the 1/f statistics law (Voss and Clarke, 1975; Attias and Schreiner, 1997; Singh and Theunissen, 2003). The temporal modulation spectrum also obeys scale-invariant statistics within frequency bands (Voss and Clarke, 1975, 1978; Attias and Schreiner, 1997; Nelken et al., 1999; Singh and Theunissen, 2003; Garcia-Lazaro et al., 2006; Rodríguez et al., 2010; McDermott and Simoncelli, 2011).

Sounds with these statistical regularities in their structure are perceived as natural by human listeners and varying the correlation of spectro-temporal modulations affects the naturalness of this perception (Voss and Clarke, 1978; Geffen et al., 2011). There are also neural correlates demonstrating preference for these characteristics, in particular 1/f temporal modulation (Escabí and Read, 2005; Garcia-Lazaro et al., 2006; Rodríguez et al., 2010).

In chapter 2, we used an artificial stimulus perceived as natural water sounds, but that can be parametrized precisely (Geffen et al., 2011), to test how populations of neurons in auditory cortex encode different sets of parameters contributing to the ‘naturalness’ of water-like sounds.

THE ROLE OF INHIBITORY INTERNEURONS IN SHAPING ACTIVITY IN THE AUDITORY CORTEX

In AC, interactions between excitation and inhibition shape sound responses in excitatory cell populations. Cortical inhibitory interneurons are comprised of a vastly diverse population, with cells differing both morphologically and physiologically (**Figure 1.1**). Hundreds of inhibitory neuronal subtypes can be identified depending on the characteristics used for classification (Kawaguchi, 1997; DeFelipe et al., 2013; Kepecs and Fishell, 2014; Tremblay et al., 2016). The two most predominant classes in the sensory cortices, classified based on molecular markers, are: parvalbumin-positive (PV) and somatostatin-positive (SOM) interneurons (Rudy et al., 2011). PVs, the most common class in the sensory cortex, include the "basket cells", which target excitatory neuronal cell bodies (Wang et al., 2002). SOMs, the second most common class, contain a large population of Martinotti cells (Wang et al., 2004), which target the distal dendrites of excitatory neurons. These differences may have consequences in how PVs and SOMs shape sound tuning in auditory cortex. PVs are thought to provide global inhibition to excitatory neuronal populations (Packer and Yuste, 2011), while SOMs could exert a more specific effect of modulating excitatory neuronal responses to stimuli (Vu and Krasne, 1992; Urban-Ciecko and Barth, 2016). In the auditory cortex, activating PVs decreased frequency selectivity and increased tone-evoked responses of excitatory neurons (Hamilton et al., 2013; Aizenberg et al., 2015), producing a mixture of subtractive and divisive shifts in frequency tuning (Seybold et al., 2015). Suppression of PV interneurons had the opposite effect (Aizenberg et al., 2015), although a mixture of additive and multiplicative shifts in

tuning were still observed (Phillips and Hasenstaub, 2016). Activating or suppressing SOMs decreased or increased the activity of excitatory neurons respectively (Seybold et al., 2015; Phillips and Hasenstaub, 2016), but the effect was more often multiplicative when SOM activity was reduced as compared with PVs.

Activity in the auditory cortex change with stimulus temporal history, exhibiting stimulus-specific adaptation (SSA) by reducing response to repeated stimuli (Ulanovsky et al., 2003; Natan et al., 2015). Inhibitory-excitatory networks support this transformation, and PVs and SOMs were found to play a differential role in cortical adaptation. SSA is quantified as the change in response to a rare 'deviant' tone presented as part of a sequence with a common 'standard' tone. Suppressing either PVs or SOMs increased the response to repeated stimuli in excitatory neurons (Natan et al., 2015). However, suppression of SOMs increased excitatory responses to the standard, but not the deviant tones, whereas suppressing PVs led to a non-specific response increase (Natan et al., 2015). PVs and SOMs also differentially affected frequency tuning following adaptation. SOM suppression increased tone-evoked response to an adapted stimulus, but not upon initial presentation of the stimulus, specifically for preferred frequencies. In contrast, PV suppression increased tone-evoked responses to non-preferred frequencies consistently across stimulus repeats (Natan et al., 2017). These results suggest SOM inhibition increased with stimulus repetition, while PV inhibition remained stable.

A third class of cortical inhibitory interneuron, the vasoactive intestinal polypeptide-positive interneurons (VIPs) (Rudy et al., 2011; Tremblay et al., 2016), target both SOM (Lee et al., 2013; Pfeffer et al., 2013; Pi et al., 2013; Jiang et al., 2015; Walker et al., 2016) and PV interneurons (Pi et al., 2013), although they preferentially target

SOMs. Since SOM and PV interneurons target excitatory cells, VIP interneurons are ideally placed to modulate cortical activity through disinhibition of excitatory cells via inhibition of SOM interneurons (Pfeffer et al., 2013). In the auditory cortex, activation of VIPs caused an additive shift in frequency response curves, increasing in tone-evoked responses of putative excitatory cells across frequencies (Pi et al., 2013). Activating cholinergic inputs, which target VIPs, increased frequency selectivity of cortical excitatory cells by decreasing responses to preferred frequencies and increasing responses to less preferred frequencies (Nelson and Mooney, 2016). These findings are consistent with VIPs role in disinhibition of excitatory neurons.

In chapter 3, we discuss previous studies on the function of inhibitory neurons and microcircuits in audition and, in chapter 4, we test whether and how modulation of cortical inhibitory-excitatory microcircuits propagates to the inferior colliculus by optogenetically activating or suppressing cortical PV or SOM inhibitory interneurons and measuring the effect on spontaneous and sound-evoked activity in the inferior colliculus.

Figure 1.1

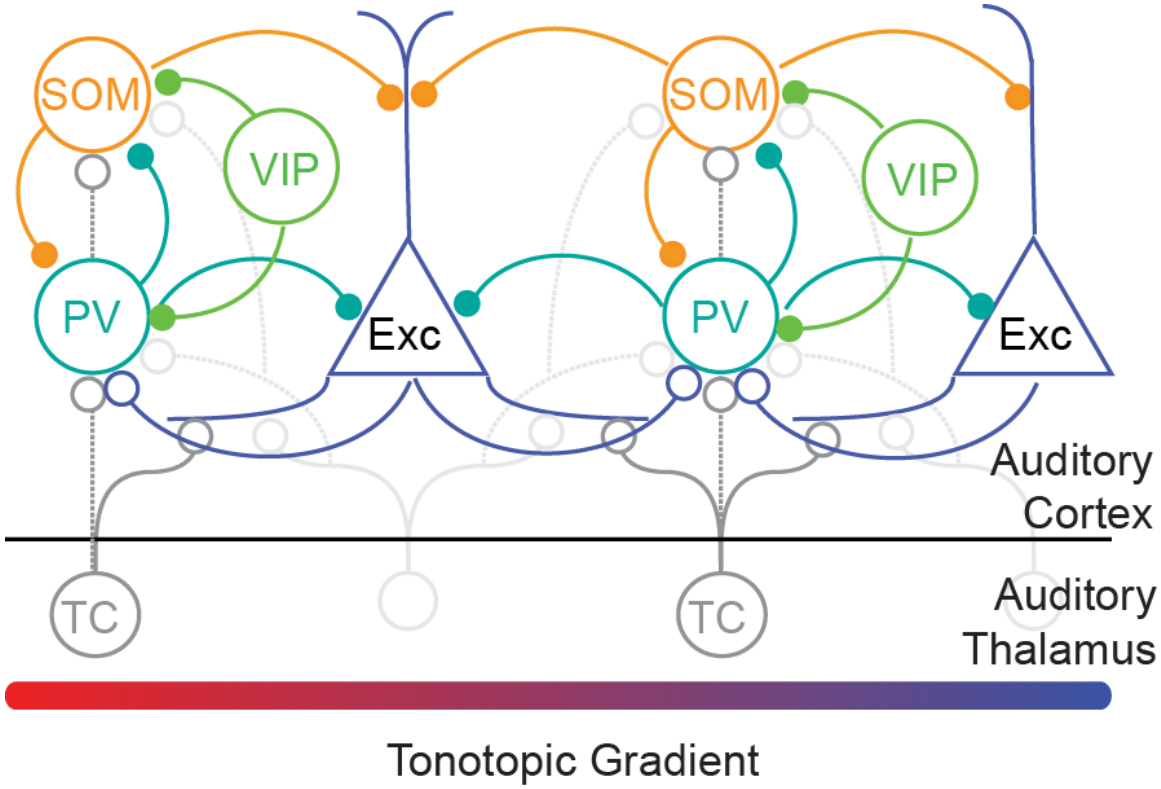
SOM
VIP
PV
Exc
SOM
VIP
PV
Exc
Auditory
Cortex
TC
TC
Auditory
Thalamus
Tonotopic Gradient

Figure 1.1 Schematic diagram of connectivity between select neurons in the auditory cortex (note that layer-specific information is omitted here): Exc: Excitatory neurons; PV: parvalbumin-positive interneurons; SOM: somatostatin-positive interneurons; VIP: vasopressin-positive interneurons; TC: Thalamo-cortical projection neurons. All neuron types receive additional inputs from other brain areas, which were omitted from the diagram for simplicity. Open circles: excitatory synapses; closed circles: inhibitory synapses. Solid lines indicate dominant projections; dashed lines indicate occasional connections

DESCENDING MODULATION FROM AUDITORY CORTEX

Descending feedback allows for modulation of inputs from nuclei earlier in the ascending pathway. There is extensive feedback within the auditory pathway, which drive changes in auditory processing and behaviors.

The auditory cortex sends descending projections to the auditory thalamus and auditory nuclei in the brainstem. Feedback to the medial geniculate body (MGB), the auditory thalamus, is one of the largest descending auditory pathways. Cortico-thalamic projections originate from AC layer 5 and 6 (Ojima, 1994; Bajo et al., 1995; Prieto and Winer, 1999; Williamson and Polley, 2019) and targets both principal neurons as well as thalamic inhibitory interneurons (Guo et al., 2017). Modulation of AC activity affected frequency tuning by shifting best frequency of thalamic neurons (Zhang et al., 1997), but inactivation by cooling had mixed effects on bandwidth, increasing or decreasing frequency tuning bandwidth in distinct thalamic subpopulations (Villa et al., 1991). Electrical stimulation of AC increased sound-evoked responses in MGB, although a small subpopulation of neurons was also suppressed (He et al., 2002). Consistent with this finding, activation of direct feedback also induced an increase in sound-evoked responses and similar patterns of change in frequency selectivity are seen in MGB and AC which depending on timing of activation (Guo et al., 2017). Selectively ablating cortico-thalamic feedback impaired detection of sound harmonicity (Homma et al., 2017) and activation modulated discrimination and detection of simple sounds depending on timing of activation (Guo et al., 2017). These mixed effects are not unexpected given that feedback targets both excitatory and inhibitory neurons.

Projections from auditory cortex terminate in the auditory brainstem, specifically in the lateral lemniscus (Beneyto et al., 1998; Budinger et al., 2000), superior olivary complex (Doucet et al., 2003; Coomes and Schofield, 2004), cochlear nucleus (Schofield and Coomes, 2005; Meltzer and Ryugo, 2006), and the pontine nuclei (Schofield and Coomes, 2005; Perales et al., 2006). Similar to the cortico-collicular projections, feedback to brainstem nuclei also originate exclusively in AC layer 5. There is evidence that modulation of auditory cortex indirectly affects activity of cochlear hair cells (Xiao and Suga, 2002; Perrot et al., 2006), but the role of cortical feedback in shaping upstream auditory processing in the brainstem is unclear.

The auditory cortex also sends extensive projections to the inferior colliculus (IC), the auditory midbrain nucleus, which have been observed in monkeys (Winer et al., 2002), cats (Winer and Prieto, 2001; Winer et al., 2002), ferrets (Bajo et al., 2007), guinea pigs (Coomes et al., 2005), gerbils (Bajo and Moore, 2005), and rats (Herbert et al., 1991; Saldaña et al., 1996; Doucet et al., 2003). This pathway originates predominantly from ipsilateral layer 5, but also includes projections from layer 6 (Saldaña et al., 1996; Winer et al., 1998; Doucet et al., 2003; Bajo and Moore, 2005; Coomes et al., 2005; Bajo et al., 2007; Schofield, 2009). There are also a small subset of projection neurons originating from the contralateral auditory cortex (Schofield, 2009; Bajo et al., 2010). Projections are not restricted to a specific region of auditory cortex, but rather from all regions of the auditory cortex (Winer et al., 1998), although the primary areas of cortex send the densest projections (Bajo et al., 2007). Cortico-collicular feedback is also tonotopically organized (Lim and Anderson, 2007; Markovitz et al., 2013; Barnstedt et al., 2015; Straka et al.,

2015), which provides a mechanism by which cortico-collicular feedback could modulate tuning properties of neurons in IC.

Previous studies demonstrated that neuronal responses to sounds in IC are altered by focal electrical stimulation and inactivation of AC. Cortical stimulation shifted tuning properties of IC neurons toward those of the stimulated neurons in frequency (Jen et al., 1998; Yan and Suga, 1998; Ma and Suga, 2001a; Jen and Zhou, 2003; Yan et al., 2005; Zhou and Jen, 2007), amplitude (Jen and Zhou, 2003; Yan et al., 2005; Zhou and Jen, 2007), azimuth (Zhou and Jen, 2005, 2007), and duration (Ma and Suga, 2001b). Stimulation of AC had mixed effects on sound-evoked responses in IC, increasing and decreasing responses in different subpopulations of neurons (Jen et al., 1998; Zhou and Jen, 2005). AC inactivation studies, on the other hand, found less consistent effects on IC responses. Cooling AC altered IC interaural level difference (ILD) sensitivity, causing shifts in preferred ILDs and increased selectivity bandwidth, although a subset of cells were unaffected (Nakamoto et al., 2008). It has been found that pharmacological inactivation of AC caused a shift in best frequency in IC neurons (Zhang et al., 1997). However, several studies show inactivation of AC had no effect on frequency selectivity in IC (Jen et al., 1998), but rather modulated sound-evoked and spontaneous activity (Gao and Suga, 1998; Popelář et al., 2003, 2016).

There is limited data exploring the role of direct cortico-collicular feedback in shaping sound responses in the inferior colliculus. Activation of cortico-collicular axon terminals in IC increased sound-evoked responses in IC, while suppression decreased sound-evoked responses (Xiong et al., 2015). Consistent with the findings that electrical stimulation of AC increased or decreased sound-evoked responses in distinct populations

of IC neurons, different patterns of direct cortico-collicular activation enhanced or suppressed white noise-induced responses in IC (Vila et al., 2019).

Cortico-collicular feedback is also critical for auditory learning. Pairing electrical leg stimulation with a tone induced a shift in best frequency of IC neurons, while presentation of a tone alone was insufficient to alter sound responses (Gao and Suga, 1998, 2000). Furthermore, cortico-collicular feedback is necessary for learning to adapt to a unilateral earplug during a sound localization task (Bajo et al., 2010). Furthermore, activation of cortico-collicular feedback can induce running in mice and feedback suppression attenuates running in response to a loud noise (Xiong et al., 2015), implicating the importance of this feedback pathway in an innate fear response to aversive sounds. Overall, these findings suggest that AC can modulate sound responses in IC and that the direct feedback pathway may play an important role in auditory learning.

In chapter 4, we test how direct feedback from the auditory cortex to the inferior colliculus shapes sound-evoked responses in the inferior colliculus by optogenetically activating or suppressing direct cortico-collicular projection neurons and measuring responses to pure tones and dynamic random chords in the inferior colliculus.

REFERENCES

Aizenberg M, Geffen MN (2013) Bidirectional effects of aversive learning on perceptual acuity are mediated by the sensory cortex. Nat Neurosci 16:994–996.

Aizenberg M, Mwilambwe-Tshilobo L, Briguglio JJ, Natan RG, Geffen MN (2015)

Bidirectional Regulation of Innate and Learned Behaviors That Rely on Frequency Discrimination by Cortical Inhibitory Neurons. PLoS Biol 13:1–32.

Attias H, Schreiner CE (1997) Temporal Low-Order Statistics of Natural Sounds. Adv Neural Inf Process Syst 9:27–33.

Attneave F (1954) Some informational aspects of visual perception.

Bajo VM, Moore DR (2005) Descending projections from the auditory cortex to the inferior colliculus in the gerbil, Meriones unguiculatus. J Comp Neurol 486:101–116.

Bajo VM, Nodal FR, Bizley JK, Moore DR, King a. J (2007) The Ferret Auditory Cortex: Descending Projections to the Inferior Colliculus. Cereb Cortex 17:475–491.

Bajo VM, Nodal FR, Moore DR, King AJ (2010) The descending corticocollicular pathway mediates learning-induced auditory plasticity. Nat Neurosci 13:253–260.

Bajo VM, Rouiller EM, Welker E, Clarke S, Villa AEP, Ribaupierre Y de, Ribaupierre F de (1995) Morphology and spatial distribution of corticothalamic terminals originating from the cat auditory cortex. Hear Res 83:161–174.

Barlow HB (1961) Possible Principles Underlying the Transformations of Sensory Messages. In: Sensory Communication (Rosenblith WA, ed), pp 217–234. MIT Press.

Barnstedt O, Keating P, Weissenberger Y, King AJ, Dahmen JC (2015) Functional

Microarchitecture of the Mouse Dorsal Inferior Colliculus Revealed through In Vivo Two-Photon Calcium Imaging. J Neurosci 35:10927–10939.

Beneyto M, Winer JA, Larue DT, Prieto JJ (1998) Auditory connections and neurochemistry of the sagulum. J Comp Neurol 401:329–351.

Budinger E, Heil P, Scheich H (2000) Functional organization of auditory cortex in the Mongolian gerbil (Meriones unguiculatus). IV. Connections with anatomically characterized subcortical structures. Eur J Neurosci 12:2452–2474.

Carruthers IM, Laplagne DA, Jaegle A, Briguglio JJ, Mwilambwe-Tshilobo L, Natan RG, Geffen MN (2015) Emergence of invariant representation of vocalizations in the auditory cortex. J Neurophysiol 114:2726–2740.

Carruthers IM, Natan RG, Geffen MN (2013) Encoding of ultrasonic vocalizations in the auditory cortex. J Neurophysiol 109:1912–1927.

Coomes DL, Schofield BR (2004) Projections from the auditory cortex to the superior olivary complex in guinea pigs. Eur J Neurosci 19:2188–2200.

Coomes DL, Schofield RM, Schofield BR (2005) Unilateral and bilateral projections from cortical cells to the inferior colliculus in guinea pigs. Brain Res 1042:62–72.

DeFelipe J et al. (2013) New insights into the classification and nomenclature of cortical GABAergic interneurons. Nat Rev Neurosci 14:202–216.

Doucet JR, Molavi DL, Ryugo DK (2003) The source of corticocollicular and corticobulbar projections in area Te1 of the rat. Exp Brain Res 153:461–466.

Escabí MA, Read HL (2005) Neural Mechanisms for Spectral Analysis in the Auditory Midbrain, Thalamus, and Cortex. Int Rev Neurobiol 70:207–252.

Gao E, Suga N (1998) Experience-dependent corticofugal adjustment of midbrain frequency map in bat auditory system. PNAS 95:12663–12670.

Gao E, Suga N (2000) Experience-dependent plasticity in the auditory cortex and the inferior colliculus of bats : Role of the corticofugal system. PNAS 97:8081–8086.

Garcia-Lazaro JA, Ahmed B, Schnupp JWH (2006) Tuning to Natural Stimulus Dynamics in Primary Auditory Cortex. Curr Biol 16:264–271.

Geffen MN, Gervain J, Werker JF, Magnasco MO (2011) Auditory Perception of Self-Similarity in Water Sounds. Front Integr Neurosci 5:15.

Guo W, Clause AR, Barth-Maron A, Polley DB (2017) A Corticothalamic Circuit for Dynamic Switching between Feature Detection and Discrimination. Neuron 95:180–194.e5.

Hamilton LS, Sohl-Dickstein J, Huth AG, Carels VM, Deisseroth K, Bao S (2013) Optogenetic activation of an inhibitory network enhances feedforward functional connectivity in auditory cortex. Neuron 80:1066–1076.

He J, Yu Y-Q, Xiong Y, Hashikawa T, Chan Y-S (2002) Modulatory Effect of Cortical Activation on the Lemniscal Auditory Thalamus of the Guinea Pig. J Neurophysiol 88:1040–1050.

Herbert H, Aschoff A, Ostwald J (1991) Topography of projections from the auditory

cortex to the inferior colliculus in the rat. J Comp Neurol 304:103–122.

Homma NY, Happel MFK, Nodal FR, Ohl FW, King AJ, Bajo VM (2017) A Role for Auditory Corticothalamic Feedback in the Perception of Complex Sounds. J Neurosci 37:6149–6161.

Jen PH-S, Chen QC, Sun XD (1998) Corticofugal regulation of auditory sensitivity in the bat inferior colliculus. J Comp Physiol A 183:683–697.

Jen PH-S, Zhou X (2003) Corticofugal modulation of amplitude domain processing in the midbrain of the big brown bat, Eptesicus fuscus. Hear Res 184:91–106.

Jiang X, Shen S, Cadwell CR, Berens P, Sinz F, Ecker AS, Patel S, Tolias AS (2015) Principles of connectivity among morphologically defined cell types in adult neocortex. Science (80-) 350:aac9462.

Kawaguchi Y (1997) Neostriatal cell subtypes and their functional roles. Neurosci Res 27:1–8 Available at: https://www.sciencedirect.com/science/article/pii/S0168010296011340?via%3Dihub [Accessed March 19, 2019].

Kepecs A, Fishell G (2014) Interneuron cell types are fit to function. Nature 505:318–326.

Lee S, Kruglikov I, Huang J, Fishell G, Rudy B (2013) A disinhibitory circuit mediates motor integration in the somatosensory cortex. Nat Neurosci 16:1662–1670.

Lim HH, Anderson DJ (2007) Antidromic Activation Reveals Tonotopically Organized

Projections From Primary Auditory Cortex to the Central Nucleus of the Inferior Colliculus in Guinea Pig. J Neurophysiol 97:1413–1427.

Ma X, Suga N (2001a) Plasticity of Bat's Central Auditory System Evoked by Focal Electric Stimulation of Auditory and/or Somatosensory Cortices. J Neurophysiol 85:1078–1087.

Ma X, Suga N (2001b) Corticofugal modulation of duration-tuned neurons in the midbrain auditory nucleus in bats. PNAS 98:14060–14065.

Markovitz CD, Tang TT, Lim HH (2013) Tonotopic and localized pathways from primary auditory cortex to the central nucleus of the inferior colliculus. Front Neural Circuits 7:1–11.

McDermott JH, Simoncelli EP (2011) Sound Texture Perception via Statistics of the Auditory Periphery: Evidence from Sound Synthesis. Neuron 71:926–940.

Meltzer NE, Ryugo DK (2006) Projections from auditory cortex to cochlear nucleus: A comparative analysis of rat and mouse. Anat Rec Part A Discov Mol Cell Evol Biol 288:397–408.

Mizrahi A, Shalev A, Nelken I (2014) Single neuron and population coding of natural sounds in auditory cortex. Curr Opin Neurobiol 24:103–110.

Nakamoto KT, Jones SJ, Palmer AR (2008) Descending projections from auditory cortex modulate sensitivity in the midbrain to cues for spatial position. J Neurophysiol 99:2347–2356.

Natan RG, Briguglio JJ, Mwilambwe-Tshilobo L, Jones SI, Aizenberg M, Goldberg EM, Geffen MN (2015) Complementary control of sensory adaptation by two types of cortical interneurons. Elife 4:1–27.

Natan RG, Rao W, Geffen Correspondence MN, Geffen MN (2017) Cortical Interneurons Differentially Shape Frequency Tuning following Adaptation. CellReports 21:878–890.

Nelken I (2004) Processing of complex stimuli and natural scenes in the auditory cortex. Curr Opin Neurobiol 14:474–480.

Nelken I, Rotman Y, Yosef OB (1999) Responses of auditory-cortex neurons to structural features of natural sounds. Nature 397:154–157.

Nelson A, Mooney R (2016) The Basal Forebrain and Motor Cortex Provide Convergent yet Distinct Movement-Related Inputs to the Auditory Cortex. Neuron 90:635–648.

Ojima H (1994) Terminal Morphology and Distribution of Corticothalamic Fibers Originating from Layers 5 and 6 of Cat Primary Auditory Cortex. Cereb Cortex 4:646–663.

Packer AM, Yuste R (2011) Dense, Unspecific Connectivity of Neocortical Parvalbumin-Positive Interneurons: A Canonical Microcircuit for Inhibition? J Neurosci 31:13260–13271.

Perales M, Winer JA, Prieto JJ (2006) Focal projections of cat auditory cortex to the pontine nuclei. J Comp Neurol 497:959–980.

Perrot X, Ryvlin P, Isnard J, Guénot M, Catenoix H, Fischer C, Mauguière F, Collet L (2006) Evidence for Corticofugal Modulation of Peripheral Auditory Activity in Humans. Cereb Cortex 16:941–948.

Pfeffer CK, Xue M, He M, Huang ZJ, Scanziani M (2013) Inhibition of inhibition in visual cortex : the logic of connections between molecularly distinct interneurons. Nat Publ Gr 16:1068–1076 Available at: http://dx.doi.org/10.1038/nn.3446.

Phillips EA, Hasenstaub AR (2016) Asymmetric effects of activating and inactivating cortical interneurons. Elife 5:1–22.

Pi H-J, Hangya B, Kvitsiani D, Sanders JI, Huang ZJ, Kepecs A (2013) Cortical interneurons that specialize in disinhibitory control. Nature 503:521–524.

Popelář J, Nwabueze-Ogbo FC, Syka J (2003) Changes in Neuronal Activity of the Inferior Colliculus in Rat after Temporal Inactivation of the Auditory Cortex. Physiol Res 52:615–628.

Popelář J, Šuta D, Lindovský J, Bureš Z, Pysanenko K, Chumak T, Syka J (2016) Cooling of the auditory cortex modifies neuronal activity in the inferior colliculus in rats. Hear Res 332:7–16.

Prieto JJ, Winer JA (1999) Layer VI in cat primary auditory cortex: Golgi study and sublaminar origins of projection neurons. J Comp Neurol 404:332–358.

Rodríguez FA, Chen C, Read HL, Escabí MA (2010) Neural modulation tuning characteristics scale to efficiently encode natural sound statistics. J Neurosci 30:15969–15980.

Rudy B, Fishell G, Lee S, Hjerling-Leffler J (2011) Three groups of interneurons account for nearly 100% of neocortical GABAergic neurons. Dev Neurobiol 71:45–61.

Saldaña E, Feliciano M, Mugnaini E (1996) Distribution of descending projections from primary auditory neocortex to inferior colliculus mimics the topography of intracollicular projections. J Comp Neurol 371:15–40.

Schofield BR (2009) Projections to the inferior colliculus from layer VI cells of auditory cortex. Neuroscience 159:246–258 Available at: http://linkinghub.elsevier.com/retrieve/pii/S0306452208016734 [Accessed October 2, 2015].

Schofield BR, Coomes DL (2005) Auditory cortical projections to the cochlear nucleus in guinea pigs. Hear Res 199:89–102.

Seybold BA, Elizabeth AK, Schreiner CE, Hasenstaub AR, Seybold BA, Phillips EAK, Schreiner CE, Hasenstaub AR (2015) Inhibitory Actions Unified by Network Integration Viewpoint Inhibitory Actions Unified by Network Integration. Neuron 87:1181–1192.

Singh NC, Theunissen FE (2003) Modulation spectra of natural sounds and ethological theories of auditory processing. J Acoust Soc Am 114:3394.

Straka MM, Hughes R, Lee P, Lim HH (2015) Descending and tonotopic projection patterns from the auditory cortex to the inferior colliculus. Neuroscience 300:325–337.

Tremblay R, Lee S, Rudy B (2016) GABAergic Interneurons in the Neocortex: From

Cellular Properties to Circuits. Neuron 91:260–292.

Ulanovsky N, Las L, Nelken I (2003) Processing of low-probability sounds by cortical neurons. Nat Neurosci 6:391–398.

Urban-Ciecko J, Barth AL (2016) Somatostatin-expressing neurons in cortical networks. Nat Rev Neurosci 17:401–409.

Vila C-H, Williamson RS, Hancock KE, Polley DB (2019) Optimizing optogenetic stimulation protocols in auditory corticofugal neurons based on closed-loop spike feedback. bioRxiv.

Villa AEP, Rouiller EM, Simm GM, Zurita P, De Ribaupierre Y, De Ribaupierre F (1991) Corticofugal modulation of the information processing in the auditory thalamus of the cat.

Voss RF, Clarke J (1975) "1/f noise" in music and speech. Wiley.

Voss RF, Clarke J (1978) "'1/f noise'" in music: Music from 1/f noise. Cit J Acoust Soc Am 63:258.

Vu ET, Krasne FB (1992) Evidence for a Computational Distinction Between Proximal and Distal Neuronal Inhibition. Science (80-) 255:1710–1712.

Walker F, Möck M, Feyerabend M, Guy J, Wagener RJ, Schubert D, Staiger JF, Witte M (2016) Parvalbumin- and vasoactive intestinal polypeptide-expressing neocortical interneurons impose differential inhibition on Martinotti cells. Nat Commun 7:13664.

Wang Y, Gupta A, Toledo-Rodriguez M, Wu CZ, Markram H (2002) Anatomical, Physiological, Molecular and Circuit Properties of Nest Basket Cells in the Developing Somatosensory Cortex. Cereb Cortex 12:395–410.

Wang Y, Toledo-Rodriguez M, Gupta A, Wu C, Silberberg G, Luo J, Markram H (2004) Anatomical, physiological and molecular properties of Martinotti cells in the somatosensory cortex of the juvenile rat. J Physiol 561:65–90.

Williamson RS, Polley DB (2019) Parallel systems for sound processing and functional connectivity among layer 5 and 6 auditory corticothalamic neurons. bioRxiv doi:10.1101/447276.

Winer JA, Chernock ML, Larue DT, Cheung SW (2002) Descending projections to the inferior colliculus from the posterior thalamus and the auditory cortex in rat, cat, and monkey. Hear Res 168:181–195.

Winer JA, Larue DT, Diehl JJ, Hefti BJ (1998) Auditory cortical projections to the cat inferior colliculus. J Comp Neurol 400:147–174.

Winer JA, Prieto JJ (2001) Layer V in cat primary auditory cortex (AI): Cellular architecture and identification of projection neurons. J Comp Neurol 434:379–412.

Xiao Z, Suga N (2002) Modulation of cochlear hair cells by the auditory cortex in the mustached bat. Nat Neurosci 5:57–63.

Xiong XR, Liang F, Zingg B, Ji X, Ibrahim LA, Tao HW, Zhang LI (2015) Auditory cortex controls sound-driven innate defense behaviour through corticofugal projections to inferior colliculus. Nat Commun 6:7224.

Yan J, Zhang Y, Ehret G, Yan J (2005) Corticofugal shaping of frequency tuning curves in the central nucleus of the inferior colliculus of mice. J Neurophysiol 93:71–83.

Yan W, Suga N (1998) Corticofugal modulation of the midbrain frequency map in the bat. Nat Neurosci 1:54–58.

Zhang Y, Suga N, Yan J (1997) Corticofugal modulation of frequency processing in bat auditory system. Nature 387:900–903.

Zhou X, Jen PH-S (2005) Corticofugal modulation of directional sensitivity in the midbrain of the big brown bat, Eptesicus fuscus. Hear Res 203:201–215.

Zhou X, Jen PH-S (2007) Corticofugal Modulation of Multi-Parametric Auditory Selectivity in the Midbrain of the Big Brown Bat. J Neurophysiol 98:2509–2516.

CHAPTER 2: STABLE ENCODING OF NATURAL SOUNDS IN THE AUDITORY CORTEX

Adapted from: Blackwell JM, Taillefumier TO, Natan RG, Carruthers IM, Magnasco MO, Geffen MN (2016) Stable encoding of sounds over a broad range of statistical parameters in the auditory cortex, *Eur. J. Neurosci*. 43:751-764

ABSTRACT

Natural auditory scenes possess highly structured statistical regularities, which are dictated by the physics of sound production in nature, such as scale-invariance. We recently identified that natural water sounds exhibit a particular type of scale invariance, in which the temporal modulation within spectral bands scales with the center frequency of the band. Here, we tested how neurons in the mammalian primary auditory cortex encode sounds that exhibit this property, but differ in their statistical parameters. The stimuli varied in spectro-temporal density and cyclo-temporal statistics over several orders of magnitude, corresponding to a range of water-like percepts, from pattering of rain to a slow stream. We recorded neuronal activity in the primary auditory cortex of awake rats presented with these stimuli. The responses of the majority of individual neurons were selective for a subset of stimuli with specific statistics. However, as a neuronal population, the responses were remarkably stable over large changes in stimulus statistics, exhibiting a similar range

in firing rate, response strength, variability and information rate, and only minor variation in receptive field parameters. This pattern of neuronal responses suggests a potentially general principle for cortical encoding of complex acoustic scenes: while individual cortical neurons exhibit selectivity for specific statistical features, a neuronal population preserves a constant response structure across a broad range of statistical parameters.

2.1 INTRODUCTION

Natural environmental sounds span a broad range of frequencies, and possess characteristic spectro-temporal statistical regularities in their structure (Voss and Clarke, 1975; Singh and Theunissen, 2003). Encoding information about these statistical regularities is an important processing step in the central auditory pathway, required for accurate analysis of an auditory scene (Chandrasekaran et al., 2009). Spectro-temporal statistical regularities in sounds can be used by the auditory system to recognize specific sounds and distinguish them from each other (Woolley et al., 2005; Geffen et al., 2011; McDermott and Simoncelli, 2011; McDermott et al., 2013; Gervain et al., 2014).

The power spectrum of natural sounds scales inversely with the frequency, following the $1/f$ statistics law (Voss and Clarke, 1975; Attias and Schreiner, 1997; Singh and Theunissen, 2003). Furthermore, the overall power spectrum and the temporal modulation spectrum also obey scale-invariant statistics. Neurons in the central auditory pathway encode small variations in spectro-temporally modulated stimuli (Elhilali et al., 2004) and respond preferentially to sounds exhibiting natural characteristics (Nelken et al.,

1999; Woolley et al., 2005), and 1/*f* frequency spectrum in particular (Escabí and Read, 2005; Garcia-Lazaro et al., 2006; Rodríguez et al., 2010). Changes in the statistical structure of stimuli, including the spectro-temporal density, or the spectro-temporal range, affect response properties of cortical neurons, leading to gain adaptation in their firing rate (Blake and Merzenich, 2002; Valentine and Eggermont, 2004; Asari and Zador, 2009; Pienkowski and Eggermont, 2009; Eggermont, 2011; Rabinowitz et al., 2011; Natan et al., 2015).

Recently, we identified an additional form of scale-invariance in environmental sounds (Geffen et al., 2011; Gervain et al., 2014). In sounds of running water, a subset of environmental sounds, the temporal modulation spectrum across spectral bands scales with the center frequency of the band (Geffen et al., 2011; Gervain et al., 2014). When the recording of running water was stretched or compressed temporally, it was still perceived as a natural, water-like sound (Geffen et al., 2011). Such a relationship corresponds to the optimal representation of a sound waveform under sparse coding assumptions (Lewicki, 2002; Garcia-Lazaro et al., 2006; Smith and Lewicki, 2006). Sounds that obeyed the invariant scaling relationship but which varied in cyclo-temporal coefficients and spectro-temporal sound density evoked different percepts, ranging from pattering of rain to sound of a waterfall to artificial ringing. In the present study, we adapted this set of stimuli to the hearing range of rats to examine how changing spectro-temporal statistical properties affect responses of neurons in the primary auditory cortex (A1), an essential area for encoding complex and behaviorally meaningful sounds (Nelken, 2004; Aizenberg and Geffen, 2013; Carruthers et al., 2013; Mizrahi et al., 2014; Aizenberg et al., 2015; Carruthers et al., 2015).

We recorded the responses of neurons in A1 of awake rats to naturalistic, scale-invariant sounds, designed to mimic the variety of natural water sounds, as their statistical structure was varied. We found that individual neurons exhibited tuning for a specific cyclo-temporal coefficient and spectro-temporal density of the stimulus, yet over the population of neurons, sounds with vastly different statistics evoked a similar range of response parameters.

2.2 RESULTS

We characterized the responses of neurons in the auditory cortex to acoustic stimuli designed to capture the statistical properties of natural water sounds. To construct these stimuli, we adapted the random droplet stimuli that were originally constructed to mimic the sound percept of water sounds (Geffen et al., 2011; Gervain et al., 2014), for presentation in the electrophysiological recordings to rats by expanding the frequency range and sample rate. The stimulus consisted of a superposition of gammatones, which can be thought of as individual droplet sounds, that are uniformly distributed in log-frequency space, and in time (**Figure 2.1A**). The amplitude of each droplet sound was drawn from a random probability distribution, as described in the Methods. The length of each droplet sound was scaled relative to its frequency, to mimic the statistical structure of environmental sounds (**Figure 2.1B**) (Geffen et al., 2011).

We varied two stimulus parameters: the cyclo-temporal coefficient, Q, and the droplet density, r (Geffen et al., 2011). Q denotes the ratio between the time constant of

decay for the individual droplets, and their center frequency. As such, it regulates how many cycles are contained within each droplet. Sounds with high Q have a sustained quality to them, sounding metallic. Sounds with Q = 2 sound natural, water-like. Sounds with low Q sound like pattering of rain. For very low Q, sounds are static-like, resembling fire crackling or similar fire-like sounds. r specifies how many droplets per second are combined to generate the stimulus. Sounds with r high and Q = 2 sound like a fast waterfall, and with r low and Q = 2 sound like dripping water (Geffen et al., 2011).

To cover the range of variability expected from natural sounds, we selected three values of Q and r to construct five random droplet stimuli (Geffen et al., 2011) (**Figure 2.1A**). The probability density of the stimulus gammatone transform exhibited a logarithmic relationship within distinct spectral bands. The density curves overlapped across a vast range of frequencies, demonstrating that the stimulus preserved the self-similar scaling structure, from 1 to 40 kHz (**Figure 2.1C**). Furthermore, these stimuli had a logarithmic power spectrum (**Figure 2.1D**). This indicates that these sounds possessed scale-invariance not just in the power spectrum, but also in temporal statistics across spectral channels. The random droplet stimulus allowed us to measure not only the response strength, but also the temporal and spectral time course of the dependency of the responses on the stimulus for the different statistical parameters.

Figure 2.1

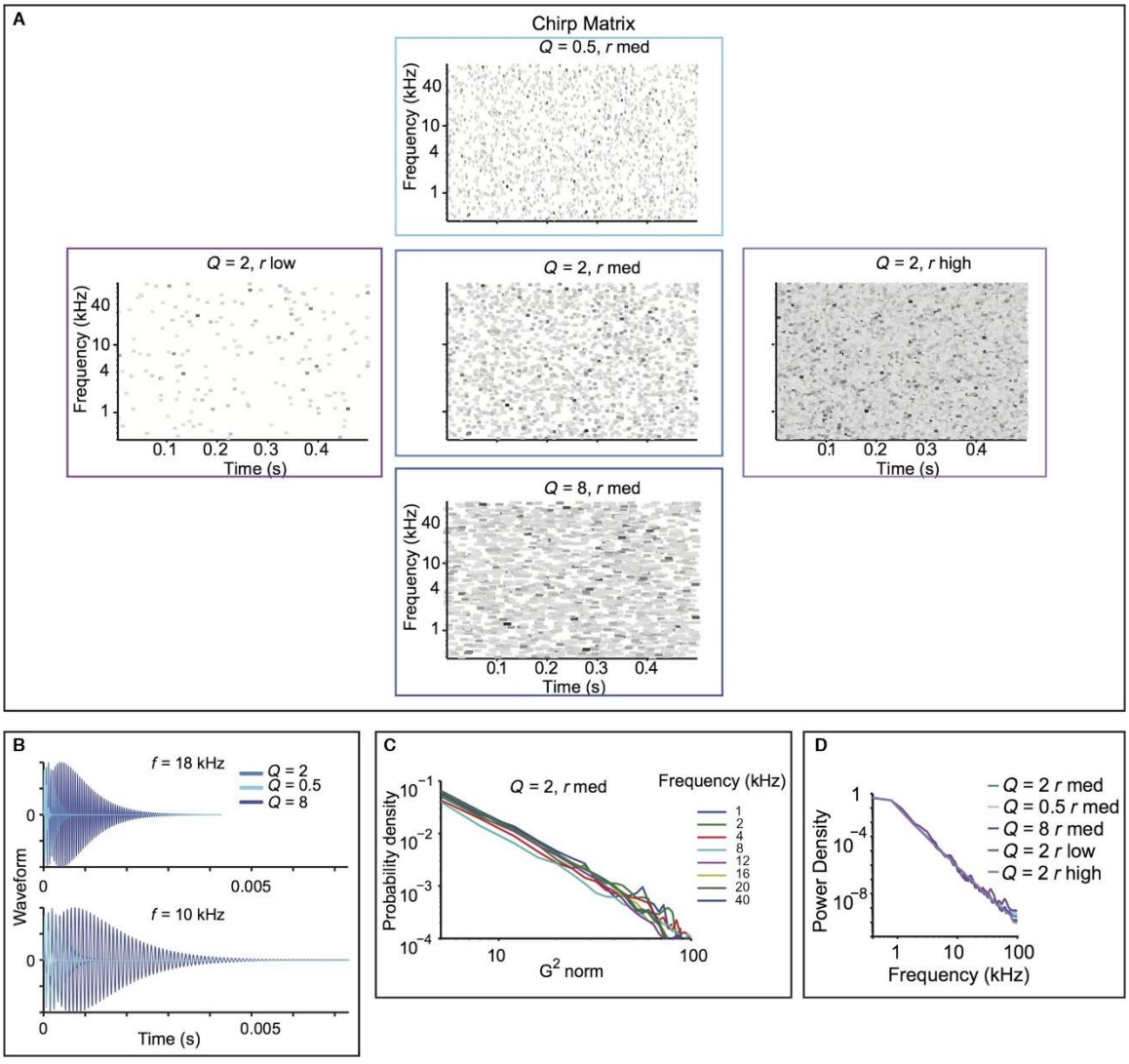
A
Chirp Matrix
Q = 0.5, r med
Q = 2, r low
Q = 2, r med
Q = 2, r high
Q = 8, r med
Frequency (kHz)
40
10
4
1
0.1
0.2
0.3
0.4
Time (s)
B
f = 18 kHz
Q = 2
Q = 0.5
Q = 8
f = 10 kHz
Waveform
0
0.005
Time (s)
C
Q = 2, r med
Frequency (kHz)
1
2
4
8
12
16
20
40
Probability density
G2 norm
D
Q = 2 r med
Q = 0.5 r med
Q = 8 r med
Q = 2 r low
Q = 2 r high
Power Density
Frequency (kHz)

Figure 2.1 The random droplet stimulus mimics scale-invariant structure of natural stimuli, while allowing spectro-temporal constant (Q) and density (rate) to vary. **A** Droplet onset matrix for the five stimuli used in the study. Each line depicts an individual droplet, plotted according to its center frequency and onset time. Color depicts relative maximum amplitude, darker colors corresponding to higher amplitudes. Width corresponds to Q. **B** Time course of the waveform for individual droplets. Top: center frequency of 18 kHz. Bottom: center frequency of 10 kHz. Droplets are depicted for $Q = 0.5$, 2 and 8. **C** Histogram of the gammatone transform of the $Q = 2$, r_{med} stimulus. **D** Power spectrum density for each of the five stimuli in eight frequency bands.

The stimulus reliably drives auditory-evoked responses in the primary auditory cortex

We recorded the activity of 654 units in the primary auditory cortex in awake rats, in response to the five variants of the random droplet stimulus. We used the stimulus with Q = 2, r_{med}, as the baseline stimulus, as this stimulus was perceived as most natural by human listeners (Geffen et al., 2011). Individual units reliably followed the stimulus, repeated 50 times, exhibiting a significantly modified level of activity during the stimulus presentation, as compared with baseline responses (n = 368 out of 654, response strength > 6, **Figure 2.2A–C**).

The types of responses ranged from sparse, time-locked responses to sustained responses (**Figure 2.2B, C**). Two representative neuronal responses are depicted in Figure 2.2B and C. Neuron 1 exhibited elevated responses throughout the stimulus presentation (**Figure 2.2B**), whereas neuron 2 exhibited sparse responses (**Figure 2.2C**).

The recorded units spanned a broad range of best frequencies, corresponding to the hearing range of rats. Neurons across the full range of best frequencies exhibited significant responses to the stimulus (**Figure 2.2D**, n = 368), as expected for a broadband stimulus.

Figure 2.2

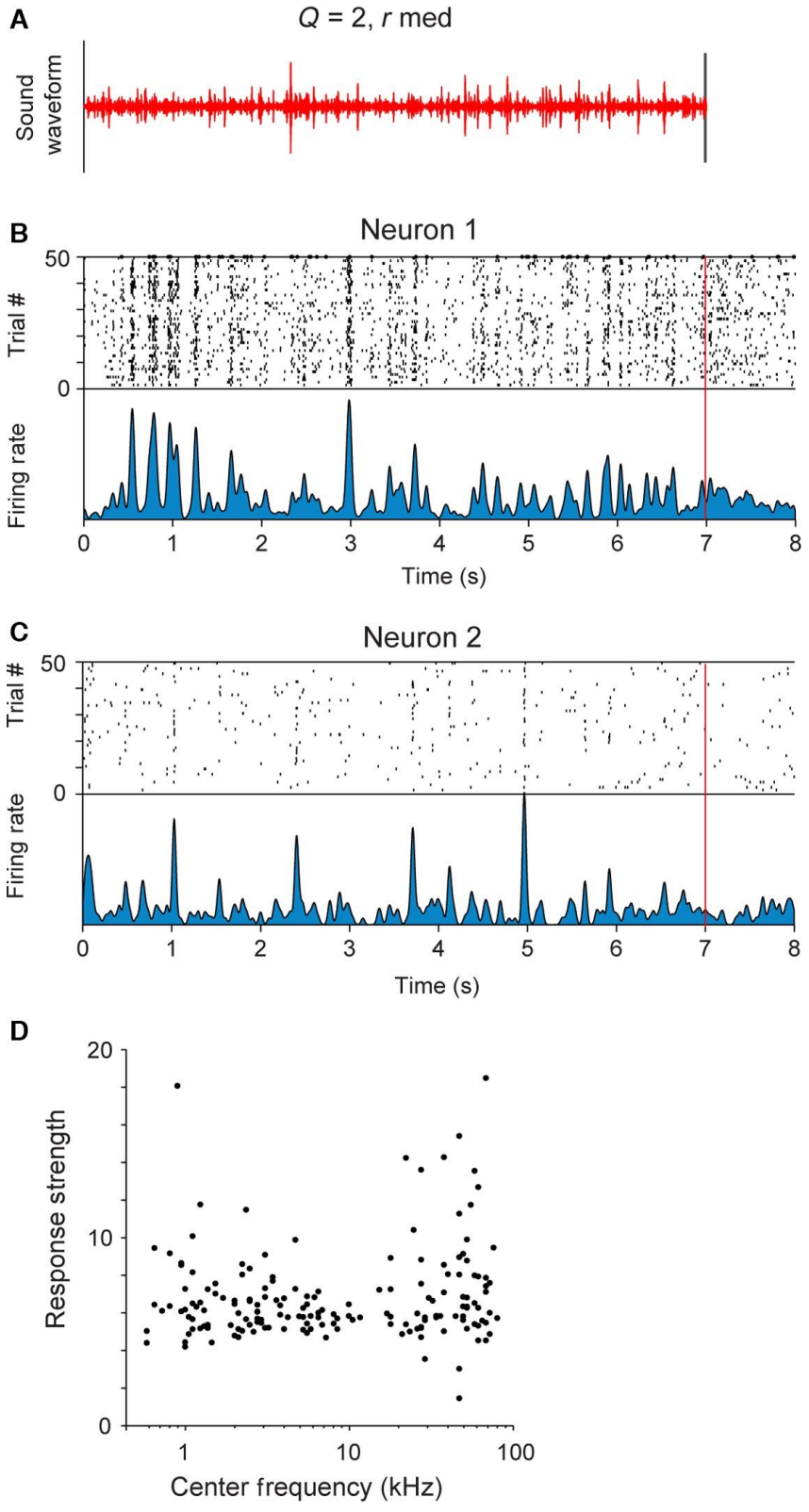
A
Q = 2, r med
Sound waveform
B
Neuron 1
50
Trial #
0
Firing rate
0 1 2 3 4 5 6 7 8
Time (s)
C
Neuron 2
50
Trial #
0
Firing rate
0 1 2 3 4 5 6 7 8
Time (s)
D
20
10
0
Response strength
1
10
100
Center frequency (kHz)

Figure 2.2 Neurons in primary auditory cortex exhibit reliable responses to the stimulus. **A** Stimulus waveform for the baseline stimulus ($Q = 2$, r_{med}). **B, C** Raster plot and firing rate of responses of a representative unit showing time-locking responses to the stimulus. Top panel: raster plot – each black line denotes an action potential produced by the neuron at a particular delay from stimulus onset (*x*-axis) in a particular trial (*y*-axis). Bottom panel: mean firing rate of the neuron. **D** Mean response strength of recorded units to the stimulus vs. their center frequency ($n = 368$).

Selectivity of neuronal responses for specific stimulus statistics

We next tested whether and how changing the spectro-temporal statistical structure of the stimulus affected neuronal response patterns. The responses of the same neuron to variants of the stimuli included time-locked excitatory responses, elevated sustained responses or suppressed responses (**Figure 2.3**).

The majority of recorded units exhibited selectivity for a subset of the stimuli. Time-locked responses to a subset of stimuli were more common (**Figure 2.3A**). Figure 2.3A depicts a neuron that exhibited time-locked, sparse responses to stimuli of Q = 2, r_{low} or r_{med}, and Q = 8, rate r_{high}. The faster fluctuating (Q = 0.5) or more dense (r_{high}) stimuli were less efficient in driving this neuron. Some neurons exhibited sustained responses (**Figure 2.3B**). The neuron whose response is depicted in Figure 2.3B exhibited an elevated firing rate, but not precise time locking to the stimulus. It was most responsive for the stimulus with Q = 0.5, r_{med}. Some neurons responded significantly to all five stimuli (**Figure 2.3C, D**). While elevated responses (**Figure 2.3C**) were more common, some suppressed responses were also observed (**Figure 2.3D**).

Figure 2.3

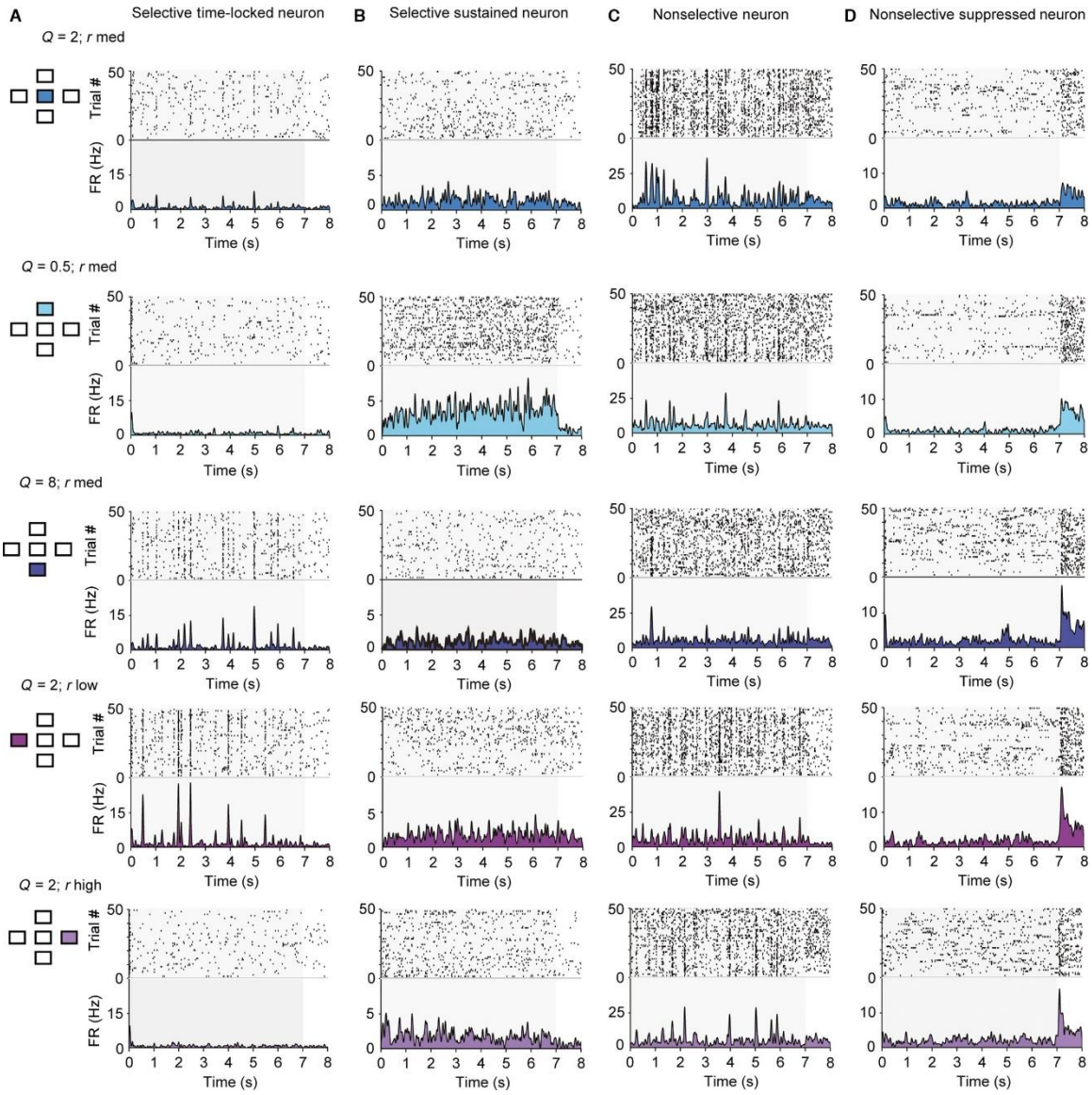
A
Selective time-locked neuron
B
Selective sustained neuron
C
Nonselective neuron
D
Nonselective suppressed neuron
Q = 2; r med
Q = 0.5; r med
Q = 8; r med
Q = 2; r low
Q = 2; r high
Trial #
FR (Hz)
Time (s)

Figure 2.3 Neurons in primary auditory cortex exhibit diverse responses to the five stimuli used in the study. Responses of four sample units to the five stimuli used in the study. Each row depicts raster plot and firing rate of responses to one of the five stimuli. Left inset: diagram depicting which stimulus was used (compare with **Figure 2.1A**). **A** Responses of a selective time-locked neuron. **B** Responses of a selective sustained neuron. **C** Responses of a non-selective neuron. **D** Responses of a non-selective suppressed neuron.

To assay selectivity in neuronal responses to different stimuli, we computed the selectivity index and the sparseness index. The selectivity index was measured as the difference between the strongest and the mean response strength to the five stimuli for each unit, normalized by the strongest response (**Figure 2.4A**). This measure is 1 if the neuron responds to only one stimulus and 0 if it responds to all stimuli with equal strength. The sparseness index quantified how specific the neuronal responses were to a particular stimulus (**Figure 2.4B**). We found that, typically, neurons were responsive to more than a single stimulus. Still, most neurons exhibited a non-zero selectivity ratio (mean selectivity index = 0.24) and sparseness index (mean sparseness index = 0.069). These values were higher than when responses were randomly shuffled across stimuli (**Figure 2.4**, selectivity: P = 1.9e-9; sparseness, P = 4.1e-57, Wilcoxon sign rank test), such that ~50% of neurons were above the 5% significance threshold for the shuffled data. These results indicate that most neurons exhibited higher selectivity for a subset of stimuli than would be expected by chance.

Did selectivity for a specific stimulus imply that a neuron encoded more information about its structure? We estimated the information conveyed about the stimulus by neuronal responses across different stimulus conditions. We applied an information-theoretic calculation following a previously developed procedure (Magri et al., 2009; Kayser et al., 2010) by estimating the information (in bits) in six successive 2-ms bins between the neuronal responses and the stimulus over seven 1-s stimulus 'chunks'. Neurons exhibited significantly higher mutual information for stimuli to which they

responded most strongly as compared with those that they responded to least strongly (**Figure 2.4C**, n = 304, P = 0.009).

Mutual information may be increased due to an increase in reliability of neuronal responses (Kayser et al., 2010). Consistently, we found a positive correlation between mutual information and the inverse of the Fano factor for responses of neurons to both most and least preferred stimuli (most preferred: correlation coefficient = 0.12, P = 0.04; least preferred: correlation coefficient = 0.31, P = 2.1e-8). However, there was no difference in the Fano factor between responses to the most preferred and the least preferred stimulus (sign rank test, P > 0.05). Therefore, the increase in mutual information may be attributed to increased responses of individual neurons to the preferred stimuli.

Figure 2.4

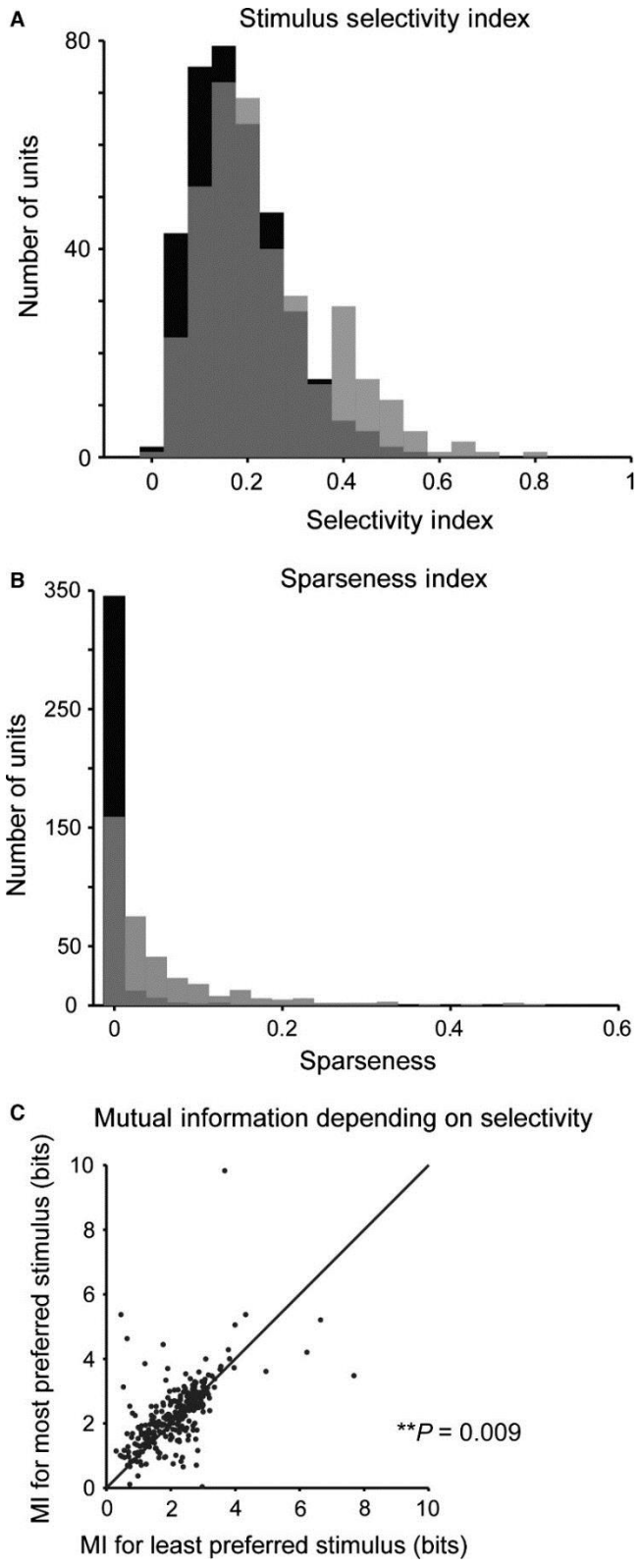
A
Stimulus selectivity index
Number of units
80
40
0
0
0.2
0.4
0.6
0.8
1
Selectivity index
B
Sparseness index
Number of units
350
250
150
50
0
0
0.2
0.4
0.6
Sparseness
C
Mutual information depending on selectivity
MI for most preferred stimulus (bits)
10
8
6
4
2
0
0
2
4
6
8
10
MI for least preferred stimulus (bits)
**P = 0.009

Figure 2.4 Neurons in primary auditory cortex exhibit selectivity for specific spectro-temporal statistics. **A** Histogram of stimulus selectivity index across the recorded neuronal population (grey) and for randomly shuffled responses (black). Many units exhibit selective responses to a subset of stimuli. The selectivity index is higher for recorded than for shuffled responses. **B** Histogram of the sparseness of responses across the recorded neuronal population (grey) and for randomly shuffled responses (black). Sparseness is higher for the recorded population than for shuffled responses. **C** Mutual information between the responses and the stimulus is higher for the stimulus, for which the neuron exhibits high selectivity. $P = 0.009$, paired *t*-test.

Droplet onset and spectrogram fits of the linear/non-linear model to neuronal responses

We next sought to characterize which parameters of neuronal responses change with the spectro-temporal statistics of the stimuli. Responses of neurons in the auditory cortex to an acoustic stimulus have previously been successfully modelled through a linear/non-linear (LN) model (Eggermont et al., 1983b; deCharms et al., 1998; Depireux et al., 2001; Escabí and Read, 2003; Linden et al., 2003; Gourévitch and Eggermont, 2008). This model is used to predict the firing rate of a neuron in response to a new stimulus by first convolving the stimulus with a linear filter, and then passing the linear prediction through an instantaneous non-linearity (Geffen et al., 2007, 2009). The linear filter can be thought of as the receptive field of the neuron, and the instantaneous non-linearity to represent the transformation from inputs that change membrane voltage to neuronal spiking.

We fitted the parameters of the linear and non-linear components of the responses of each neuron to the stimulus. There was, however, an important problem in comparing these parameters. Typically, the receptive field of the neuron is computed as the reverse correlation of the firing rate of the neuron to the spectrogram of the stimulus. In the case of a white noise stimulus, this operation is equivalent to a spike-triggered average of the stimulus. The changing cyclo-temporal coefficient of the stimulus introduces dependencies across time within spectro-temporal channels, resulting in temporal correlations. These correlations are further exaggerated in the spectrogram-based representation of the stimulus due to binned sampling. To overcome this uneven sampling of the stimulus space,

a standard approach is to use decorrelation, in which the linear prediction from the spike-triggered average is divided by the auto-correlation of the stimulus (Theunissen et al., 2001; Baccus and Meister, 2002). We applied this approach to the spectrogram-based representation of the stimulus. However, the time scale of correlations would typically dominate over the time course of neuronal responses, effectively smoothing them and therefore precluding the analysis of the receptive field changes across different statistics of the stimulus.

The construction of the droplet-based stimulus allowed us to innovatively extend an existing approach to estimate the linear filter (deCharms et al., 1998). Instead of the spectrogram-based representation, the stimulus was represented by the droplet-onset matrix. This matrix, by construction, does not contain any correlations, and therefore the optimal filter can be computed as the spike-triggered average of the droplet-onset matrix, normalized by mean amplitude of each spectral channel. The droplet-onset matrix does not contain information about Q, so the matrix is the same for all stimuli at the same rate. Using this matrix as the stimulus representation allowed us to test the hypothesis that the neurons respond predominantly to the onsets of the droplets in the stimulus, rather than their sustained structure. In other words, the information about the sustained 'ringing' of droplets may prove less important to the majority of neurons than the timing of the droplet onsets. Such a response pattern would allow the neurons to create a sparse representation of the stimulus, and would be consistent with previous hypotheses on sparse representation of natural acoustic stimuli in the auditory cortex (Smith and Lewicki, 2006; Hromádka et al., 2008). An analogous representation is provided by the cochleagram, a standard method

for representing acoustic stimuli (Lyon, 1982; Meddis et al., 1990). In a cochleagram, the acoustic waveform is transformed across spectro-temporally delimited channels using kernels that scale the bandwidth relative to the center frequency (Smith and Lewicki, 2006; McDermott et al., 2013).

Therefore, we fitted the LN model to the responses of each neuron under three different representations of the stimulus. The stimulus was represented as either a spectrogram or a cochleagram, and the filter was computed as the spectro-temporal receptive field; or in the droplet onset representation, in which only the information about the droplet onset time, amplitude and frequency was contained –DTRF (**Figure 2.5A–C**).

We analyzed the performance of the model by fitting it based on responses on a random subset of 50% of trials, and computing the correlation coefficient between the prediction for the firing rate and the measured firing rate for the remaining 50% of the trials (Carruthers et al., 2013; Ahn et al., 2014). We found that the droplet-based and cochleagram-based representation provided more accurate predictions of the neuronal responses than the spectrogram-based model (**Figure 2.5D–F**, n = 232). This relationship held when computed over all stimuli [Droplet: 45%, P (all stimuli) = 2.2e-15, Cochleagram: 60%, P (all stimuli) = 5.8e-43], but also for most individual stimuli [Droplet: P ($Q = 2, r_{med}$) = 2.7e-6; P ($Q = 0.5, r_{med}$) = 0.0031; P ($Q = 8, r_{med}$) = 0.0026; P ($Q = 2, r_{low}$) = 2.8e-8; P ($Q = 2, r_{high}$) > 0.05 - not significant, Cochleagram: P ($Q = 2, r_{med}$) = 7.5e-13; P ($Q = 0.5, r_{med}$) = 1.1e-6; P ($Q = 8, r_{med}$) = 7.6e-10; P ($Q = 2, r_{low}$) = 1.3e-8; P ($Q = 2, r_{high}$) = 2.8e-10], except $Q = 2, r_{high}$. Because this stimulus $Q = 2, r_{low}$ corresponds to the highest r value (densest dynamics), the result is probably due to the spectrogram approximation

being more similar to the droplet matrix under the fastest stimulus dynamics as compared to the other stimuli. The predictions based on the cochleagram-based representations were more accurate than the droplet-based representations over all stimuli, but the improvement was not as great as for droplet-based prediction over the spectrogram-based prediction [35%, P (all stimuli) = 7.7e-12] and for stimuli 1, 3 and 5 [P (Q = 2, r_{med}) = 2.9e-4; P (Q = 0.5, r_{med}) > 0.05, not significant; P (Q = 8, r_{med}) = 9.3e-6; P (Q = 2, r_{low}) > 0.05, not significant; P (Q = 2, r_{high}) = 1.7e-8]. In some studies, neurons in the auditory cortex have been shown to be more sensitive to stimulus onsets, rather than the prolonged 'ringing' of distinct spectral components. This observation may provide an explanation for the improved performance of the LN model when using droplet-based representation of the stimulus, as this model is more sensitive to the stimulus onsets by design.

Figure 2.5

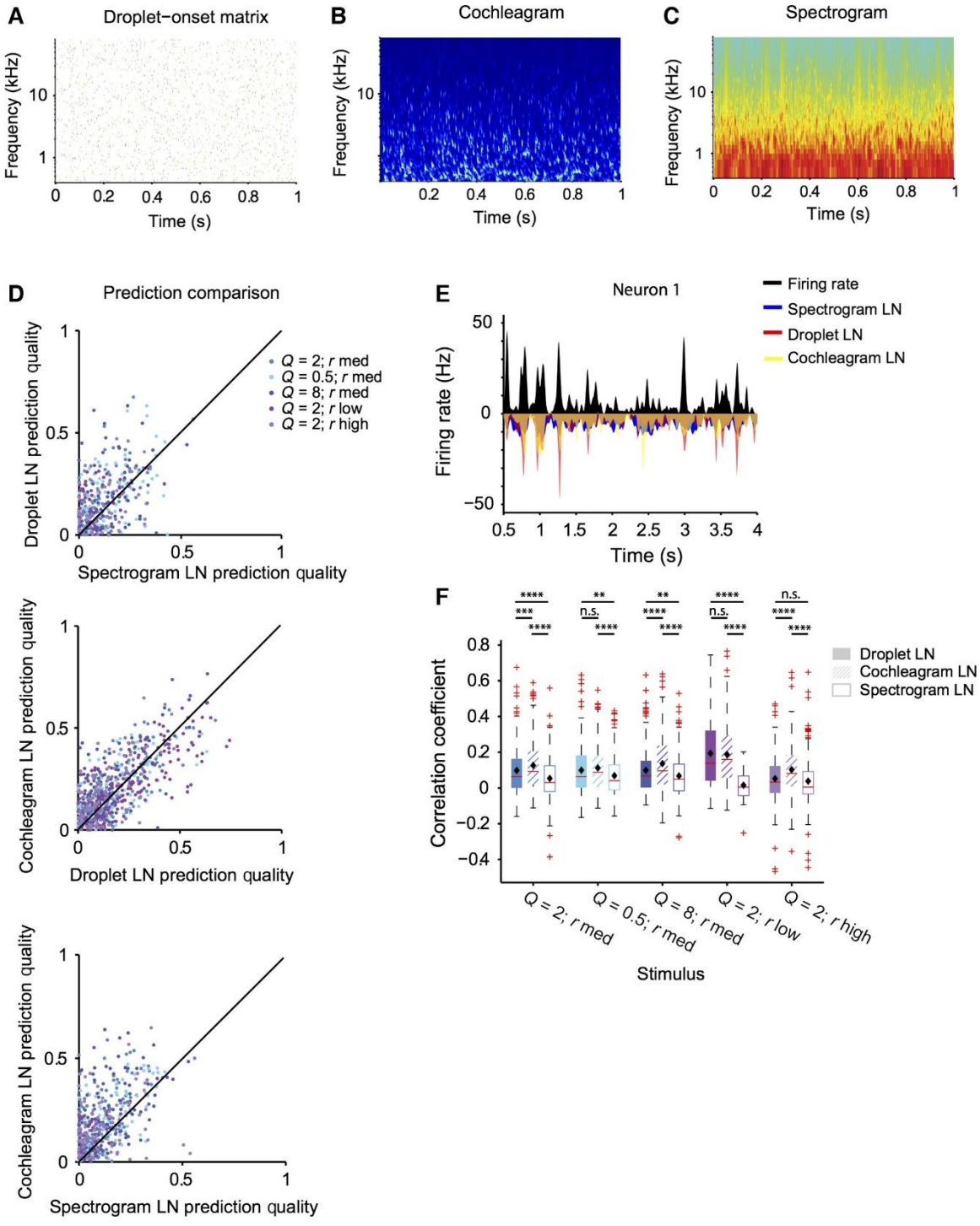
A
Droplet−onset matrix
Frequency (kHz)
10
1
0 0.2 0.4 0.6 0.8 1
Time (s)
B
Cochleagram
Frequency (kHz)
10
0.2 0.4 0.6 0.8 1
Time (s)
C
Spectrogram
Frequency (kHz)
10
1
0 0.2 0.4 0.6 0.8 1
Time (s)
D
Prediction comparison
Droplet LN prediction quality
Spectrogram LN prediction quality
Q = 2; r med
Q = 0.5; r med
Q = 8; r med
Q = 2; r low
Q = 2; r high
Cochleagram LN prediction quality
Droplet LN prediction quality
Cochleagram LN prediction quality
Spectrogram LN prediction quality
E
Neuron 1
Firing rate
Spectrogram LN
Droplet LN
Cochleagram LN
Firing rate (Hz)
50
0
−50
0.5 1 1.5 2 2.5 3 3.5 4
Time (s)
F
Correlation coefficient
0.8
0.6
0.4
0.2
0
−0.2
−04
Droplet LN
Cochleagram LN
Spectrogram LN
Q = 2; r med
Q = 0.5; r med
Q = 8; r med
Q = 2; r low
Q = 2; r high
Stimulus

Figure 2.5 LN model based on droplet-onset matrix predicts responses to the stimulus better than spectrogram-based LN model. **A** Representation of the acoustic waveform of the droplet stimulus as a droplet-onset matrix. **B** Representation of the acoustic waveform of the droplet stimulus as a spectrogram. **C** Representation of the acoustic waveform of the droplet stimulus as a cochleagram. **D** Prediction quality based on the droplet, spectrogram, or cochleagram-based prediction. Prediction quality is significantly higher for droplet and cochleagram-based prediction than spectrogram (for droplet: P (all stimuli) = 2.2e-15; for cochleagram: P (all stimuli) = 5.8e-43]. **E** LN prediction and recorded firing rate (black) for the spectrogram-based (blue), droplet-based (red) and cochleagram-based (yellow) model for a representative neuron. **F** Quartile plot for the prediction quality for the droplet, spectrogram and cochleagram based prediction (filled bars: droplet-temporal receptive field-based prediction, open bars: spectro-temporal receptive field-based prediction, cross-hatched bars: cochleagram-based prediction). $^{**}P < 0.01$, $^{***}P < 0.001$, $^{****}P < 0.0001$, Wilcoxon sign rank test, corrected for multiple comparisons.

Response parameters of the receptive field of A1 neurons do not exhibit systematic change with changing cyclo-temporal constant

We next examined whether there were any systematic changes in the time course and the spectral structure of the receptive field depending on the stimulus (**Figure 2.6**). We measured the spectral width, temporal delay and temporal length of the positive lobes of the cyclo-temporal receptive fields (the linear component of the model computed using the droplet-onset matrix as the stimulus) of the recorded units (Woolley et al., 2006; Shechter and Depireux, 2007; Schneider and Woolley, 2010). Across the neuronal population, there were only modest changes in a small subset of DTRF parameters (**Figure 2.6C**): for Q = 0.5, r med stimulus, the peak frequency was slightly reduced (P = 0.008); for Q = 2, r low stimulus, temporal width of DTRF increased (P = 0.004) whereas spectral width decreased (P = 0.011) as compared with the baseline Q = 2, r_{med} stimulus. This difference is attributed to the temporal delay between droplet onsets in the low-droplet-rate stimulus, which allows for more sustained neuronal responses. This suggests that rather than scaling the receptive field's temporal response with changing Q and droplet rate, over the population of neurons, the receptive fields cover the same range of parameters despite the change in the statistical structure of the stimulus.

We also tested whether over repeated presentations of the same stimulus there was adaptation in the receptive field parameters over time. We computed DRTFs separately for both the first and the last 20 trials and the first and last five trials of each stimulus repeat. We found no significant differences for any parameters for any stimulus over the first and last halves of stimulus blocks ($P > 0.06$ for all comparisons). These results demonstrate

that there is no adaptation to stimulus repeats over time within presentation of the same stimulus.

Nonetheless, we found that the prediction accuracy for each neuron's response was significantly higher using the LN parameters from the corresponding stimulus (same condition) than from the baseline condition (cross-prediction) (**Figure 2.7**, n = 165, P = 4e-12 over all five stimuli, $P < 0.05$ for stimuli 2 and 4). This analysis demonstrates that while there are no systematic changes over the neuronal population, at the level of individual units, the LN parameters differ between the stimuli.

Figure 2.6

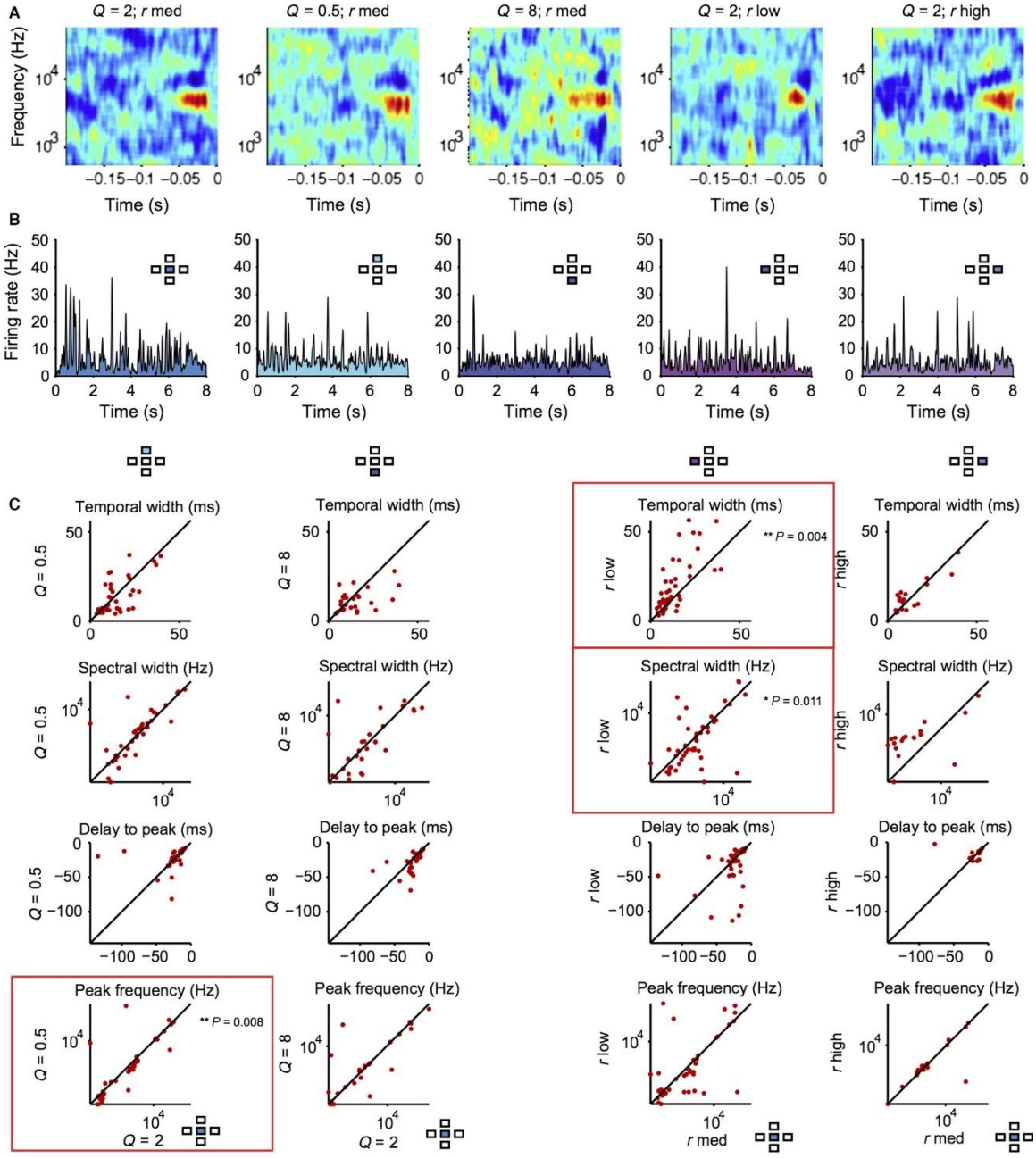
A
Q = 2; r med
Q = 0.5; r med
Q = 8; r med
Q = 2; r low
Q = 2; r high
Frequency (Hz)
Time (s)
B
Firing rate (Hz)
Time (s)
C
Temporal width (ms)
Spectral width (Hz)
Delay to peak (ms)
Peak frequency (Hz)
Q = 0.5
Q = 8
r low
r high
** P = 0.004
* P = 0.011
** P = 0.008
Q = 2
r med

Figure 2.6 Spectro-temporal receptive fields of neurons do not exhibit consistent changes with the stimulus statistics. **A** Droplet-temporal receptive field of a representative neuron for the five stimuli. **B** Firing rate of the neuron to five stimuli. **C** Parameters of droplet-temporal receptive field for each measured neuron for stimuli with different statistics vs. baseline ($Q = 2$, r_{med}) stimulus: temporal width, spectral width, delay to peak and peak frequency of the DTRF. *$P < 0.05$, **$P < 0.01$, Wilcoxon signed-rank test.

Figure 2.7

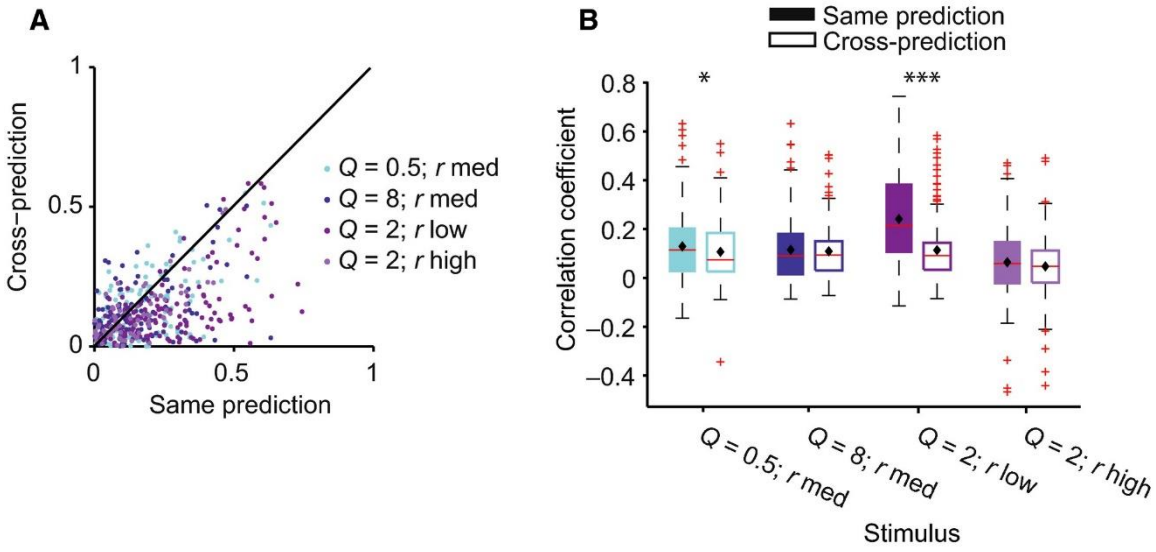
A
Cross−prediction
Same prediction
0
0.5
1
Q = 0.5; r med
Q = 8; r med
Q = 2; r low
Q = 2; r high
B
Same prediction
Cross-prediction
Correlation coefficient
0.8
0.6
0.4
0.2
0
−0.2
−0.4
*
***
Q = 0.5; r med
Q = 8; r med
Q = 2; r low
Q = 2; r high
Stimulus

Figure 2.7 LN model fails in predicting the responses of neurons to stimulus with different statistical parameters. **A** Prediction quality of the LN model, for neuronal responses to four stimuli based on a model that was fitted based on the responses to 'cross-condition' (baseline, $Q = 2$, r_{med}) vs. to the 'same-condition'. Prediction quality is significantly higher for responses to 'same' vs. 'cross' stimulus (P = 3.9e-32 across all stimuli). **B** Quartile plot for the prediction quality of the model fitted to the 'same' (filled bars) vs. 'baseline' (open bars) stimulus. ***$P < 0.001$; *$P < 0.05$: paired t-test.

Neuronal population maintains stable mean response profiles across varying stimulus statistics

Whereas for individual neurons there were large differences in response strength for different stimuli, across the population there were no significant differences in the response strength or mean firing rate between stimuli. Over the population of neurons, the mean response strength (**Figure 2.8A**) did not change significantly with Q or rate as compared with the baseline stimulus (n = 368, $P > 0.05$ for each comparison, Stimulus 1: Q = 2, r_{med}; Stimulus 2: Q = 0.5, r_{med}; Stimulus 3: Q = 8, r_{med}; Stimulus 4: Q = 2, r_{low}; Stimulus 5: Q = 2, r_{high}). The mean firing rate was also remarkably stable: it did not differ from baseline for stimuli 2, 3 and 4 (**Figure 2.8B**, n = 368), and was only marginally smaller for stimulus 5 (Q = 2, r_{high}: difference 8.8%, P = 0.0068).

We next assayed the variability of the firing rate of neuronal responses. We calculated the Fano factor, which indicates how variable the discharge count is over trials relative to the mean firing rate. For a Poisson neuron, the standard deviation of the response is equal to the mean, and Fano factor is 1. Typical Fano factors for neurons recorded in the awake mammalian cortex exceed 1. Indeed, our calculations of the Fano factor demonstrate that it exceeded 1 on average for all stimuli. The mean Fano factor did not differ from the baseline for stimuli 2, 3 and 4 (**Figure 2.8C**, n = 368, $P > 0.05$), and was only marginally increased for stimulus 5 (Q = 2, r_{high}: difference 7.5%, P = 0.026). Importantly, the mutual information was not significantly different in a population pairwise comparison across all neurons tested (**Figure 2.8D**, n = 304, $P > 0.05$) between the stimuli, further underlining the stability of the distribution of neuronal response parameters across different stimulus statistics.

Overall, our data demonstrate that stimuli with different cyclo-temporal statistics or density are stable in their representation over the neuronal population.

Figure 2.8

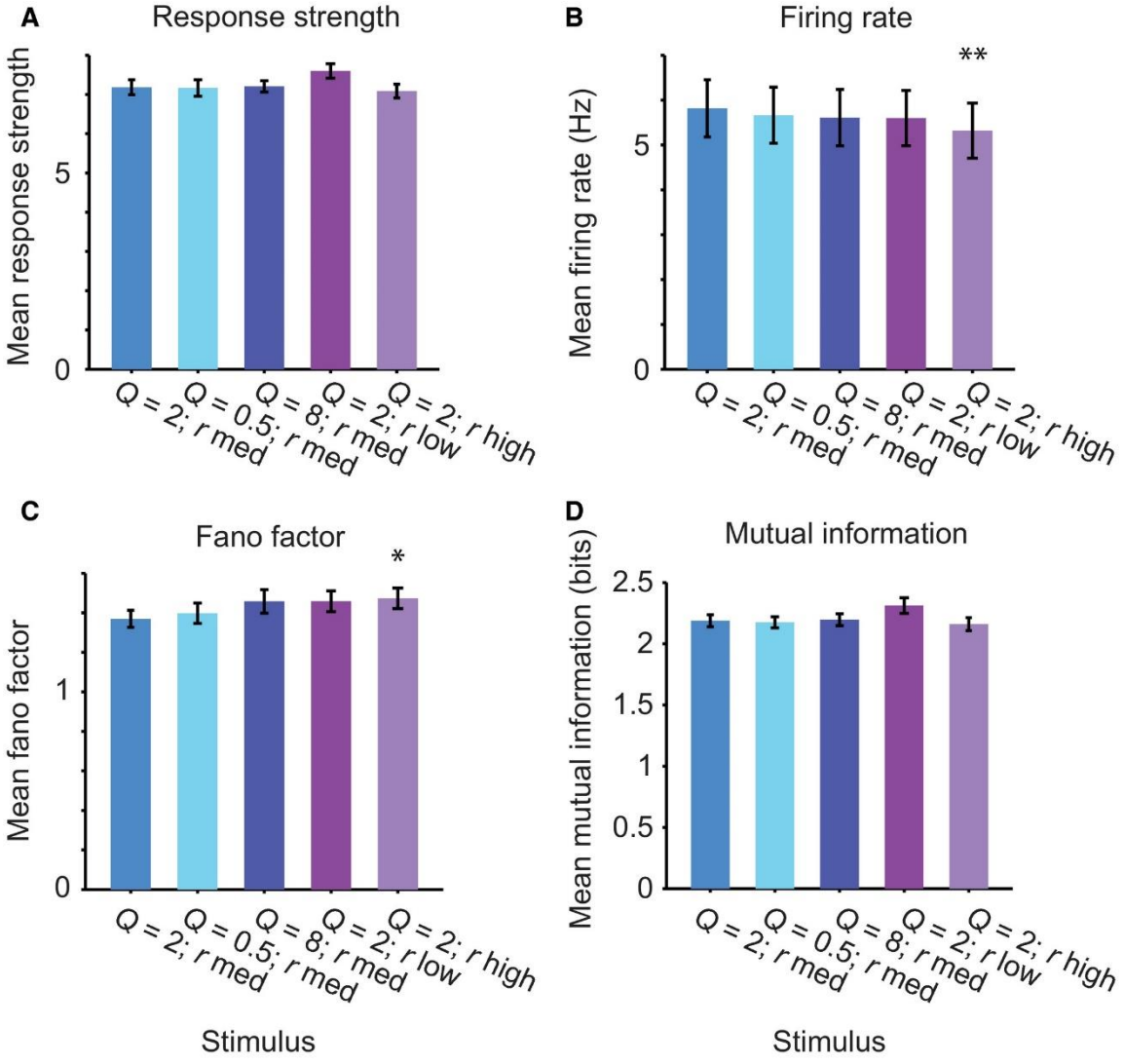
A
Response strength
Mean response strength
5
0
Q = 2; r med
Q = 0.5; r med
Q = 8; r med
Q = 2; r low
Q = 2; r high
B
Firing rate
**
Mean firing rate (Hz)
5
0
Q = 2; r med
Q = 0.5; r med
Q = 8; r med
Q = 2; r low
Q = 2; r high
C
Fano factor
*
Mean fano factor
1
0
Q = 2; r med
Q = 0.5; r med
Q = 8; r med
Q = 2; r low
Q = 2; r high
Stimulus
D
Mutual information
Mean mutual information (bits)
2.5
2
1.5
1
0.5
0
Q = 2; r med
Q = 0.5; r med
Q = 8; r med
Q = 2; r low
Q = 2; r high
Stimulus

Figure 2.8 Neuronal population exhibits even responses to stimuli with different stimulus statistics. **A** Mean response strength over the population of neurons to the five stimuli. **B** Mean firing rate over the population of neurons to the five stimuli. **C** Mean Fano factor over the population of neurons to the five stimuli. **D** Mean mutual information between the response and the stimulus for the five stimuli. $^{**}P < 0.01$; $^{*}P < 0.05$: paired *t*-test to responses to baseline stimulus.

2.3 DISCUSSION

Natural water sounds exhibit spectro-temporal regularities in their structure, which are characterized by scale-invariant statistics. The goal of this study was to establish how populations of neurons in the auditory cortex respond to sounds across a wide range of spectro-temporal parameters that correspond to a range of acoustic percepts (Geffen et al., 2011). We focused on two statistical quantities, which we had previously identified as perceptually relevant for distinguishing water-like sounds. Cyclo-temporal coefficient, *Q*, refers to the ratio of temporal change within a particular frequency band to its centre frequency. Droplet rate corresponds to the spectro-temporal density of sounds. We found that most units recorded in A1 exhibited tuning for specific combinations of *Q* and droplet rate. However, over the neuronal population, the responses and response parameters were stable across the broad range of the spectro-temporal statistics of the stimulus. These results suggest that tuning to spectro-temporal statistics in neurons may be distributed in such a way as to preserve the mean responses over the population, rather than individual neurons.

Even population responses across changed stimulus statistics

Spectro-temporal statistics vary greatly between different acoustic environments. Within different water sounds, the statistics can differ over several orders of magnitude, from a loud gurgling brook to rain pattering on the roof to droplets falling from a slowly melting icicle. Yet our auditory system needs to be able to represent the multitude of sounds with a limited set of resources. This limited set of resources is generally constrained by the range of the firing rate of neurons, as well as their noise level. Our results demonstrate that, for

the group of water-like sounds, the response properties are matched over the neuronal population across a large range of stimulus statistics. Conservation of the mean firing rate and other response characteristics of neurons is considered an important organizational principle for sensory systems. Neuronal selectivity can be thus thought of as a process that enables neurons to preserve mean response parameters in the context of stimuli with vastly different statistical structure. The specialization of response properties of individual neurons to specific subsets of spectro-temporal stimulus statistics may arise from a combination of inputs tuned to relatively simple statistics of the stimulus (McDermott and Simoncelli, 2011), and facilitate perceptual discrimination of acoustic environmental sounds (McDermott et al., 2013).

Naturalistic stimulus to probe spectro-temporal receptive field properties of auditory neurons under naturalistic conditions

Typically, responses of neurons in the auditory cortex to sounds are characterized by identifying their spectro-temporal receptive fields (Depireux et al., 2001; Escabí and Schreiner, 2002; Theunissen et al., 2004). The stimuli that are used to map the spectro-temporal receptive field include random pip and random chord sequences (Eggermont et al., 1983b; deCharms et al., 1998; Blake and Merzenich, 2002; Escabí and Read, 2003; Linden et al., 2003; Gourévitch and Eggermont, 2008). These stimuli differ from the scale-invariant stimulus set because the temporal dynamics are at the same timescale within each spectral band. Similarly, white noise (Eggermont et al., 1983a) or dynamic ripple stimuli (Klein et al., 2000; Depireux et al., 2001; Elhilali et al., 2004), designed to measure the

responses of neurons for sound with continuously changing temporal modulations, apply temporal modulations uniformly across all spectral channels. By contrast, the random droplet stimuli probe the auditory system within the statistical regime characteristic of water-like sounds, in which the temporal modulation of the structure of sounds scales with the centre frequency of the droplet (Geffen et al., 2011; Gervain et al., 2014).

Numerous studies have shown that the response properties of neurons depend on the statistical make-up of the stimuli with which they are probed. A receptive field measured with a white-noise stimulus can differ from that measured with a stimulus with scale-invariant statistics (Sharpee et al., 2004). Therefore, the use of the droplet stimulus is advantageous in measuring the receptive fields of neurons in that it reflects an important property of natural sounds. In estimating the linear receptive field of neurons, using a stimulus that follows a random distribution of parameters is furthermore of an advantage for practical reasons: as the stimulus space is sampled uniformly, the optimal filter can be constructed without a correction for stimulus auto-correlation. The present stimulus provides such a representation in the droplet-based matrix because the timing of the droplets as well as their amplitude are picked from a random distribution that does not have correlations in either time or frequency.

Changing *Q* modulates both the rise/fall time of the amplitude of each droplet as well as the bandwidth, and therefore can affect auditory responses through several mechanisms at different stages of auditory processing. Temporal envelope and modulation frequency are important parameters that have previously been shown to be important for psychoacoustic (Irino and Patterson, 1996) and physiological responses to sounds (Heil et

al., 1992; Heil, 1997; Lu et al., 2001; Krebs et al., 2008; Lesica and Grothe, 2008; Zheng and Escabi, 2008; Lin and Liu, 2010). Therefore, the selective responses for different *Q*–*r* combinations may be a result of integration of changes in the auditory periphery (Lu et al., 2001; Lin and Liu, 2010; Heil and Peterson, 2015) as well as central processing (Blake and Merzenich, 2002; Valentine and Eggermont, 2004).

Variability of neuronal responses and time course of spectro-temporal receptive fields

The temporal width of the receptive fields that we identified in the study is very tight – some of the receptive fields contained a positive lobe with a width of <10 ms (**Figure 2.6C**). This is consistent with several previous studies that have demonstrated that neuronal responses in A1 provide important information about the stimulus at the time scale of 1–3 ms (Yang et al., 2008; Kayser et al., 2010). Remarkably, our analysis revealed that as the droplet presentation rate slowed, the temporal integration window of the receptive field became longer. This suggests that under the regime of slower modulations, the droplet onsets trigger more sustained responses than under the regime with fast scale of modulations. It is plausible that higher-order statistics, which differ between stimuli with short and long *Q* parameters, may account for this change.

Non-linear transformation of the stimulus

The droplet-based LN model belongs to a greater family of non-linear linear – non-linear models as the droplet-onset matrix can be thought of as a non-linear transformation of the stimulus (Marmarelis and Marmarelis, 1978; Butts et al., 2011; McFarland et al.,

2013). We note that this stimulus representation differs from the commonly used cochlear gammatone-like filter bank, constructing a cochleagram (Klein et al., 2000; Elhilali et al., 2004) in that the gammatone onsets are specified during stimulus construction, and rather than being used as filters, are components of the stimulus. In a recent study, we found that for A1 responses to another class of stimuli, rat ultrasonic vocalizations, a non-linear transformation of the stimulus into a dominant amplitude- and frequency-modulated parametrized tone led to a more accurate prediction of the LN model (Carruthers et al., 2013). Similarly, in the present study, the representation of the stimulus as a droplet-based matrix provides a more accurate prediction than a spectrogram-based representation for all but the most sluggish stimulus. A similar stimulus was used to model the receptive fields of neurons in response to sounds with constant temporal statistics across different frequency bands (deCharms et al., 1998), but that approach did not extend to scale-invariant sounds, in which the spectro-temporal coefficient Q is presented across frequency bands. While our representation probably oversimplifies the operations that are performed within the auditory periphery, it is consistent with previous predictions and experimental observations for processing of acoustic stimuli by the cochlea and the auditory nerve (Robles and Ruggero, 2001).

Although LN models have been successfully used to study the linear components and receptive fields of neurons throughout the auditory pathway, these models carry significant limitations, which pose constraints on the interpretation of our results. In using a single-stage model, it is difficult to pinpoint at which stage of the pathway the transformation takes place. On the other hand, more complex models that include several

linear and non-linear terms may preclude a summary of the effect of statistics of the stimulus on a subset of response parameters (Ahrens et al., 2008; Christianson et al., 2008). Adding the pre-processing step for representing the stimulus as an ensemble of gammatones expands the ability of the LN model to predict the stimulus responses, while simplifying the representation of the stimulus.

Generalization of the random droplet stimulus to probe speech and other communication signals

An additional advantage of this stimulus is that the droplet-like representation can be used to construct a representation of an arbitrary complex sound, and that such a representation is optimal for sparsely firing neurons (Smith and Lewicki, 2006; Carlson et al., 2012). It has been previously demonstrated that the optimal sparse code for representing natural sounds consists of unitary scale-invariant impulses that correspond to the auditory revcorr filters (Smith and Lewicki, 2006). The random droplet stimulus can be modified to probe specificity of neuronal responses to speech and communication signals. To represent a speech signal, the acoustic waveform could be projected on the impulse functions, used as band-passed filters, and represented as 'spikes'. The droplets used in the present stimulus can be viewed as a simplified, generalizable version of such impulses, and would produce a similar representation of different environmental sounds, beyond the range of measured water sounds. Decomposing a speech acoustic waveform on spectro-temporal channels will then allow us to compute the cross-correlation functions across those channels. A

random droplet signal can be constructed to match the cross-correlation functions, and the responses across different statistical dependencies can be compared.

Speech contains important information at different time scales, which is relevant for different aspects of speech comprehension (Rosen, 1992; Poeppel, 2003). Introducing the dependencies at varying time scales into the random droplet stimulus would allow us to test neuronal responses to different aspects of speech and vocalization processing.

2.4 METHODS

This study was performed in strict accordance with the recommendations in the Guide for the Care and Use of Laboratory Animals of the National Institutes of Health. The protocol was approved by the Institutional Animal Care and Use Committee of the University of Pennsylvania.

Animals

Subjects in all experiments were adult male rats. Rats were housed in a temperature- and humidity-controlled vivarium on a reversed 24- light–dark cycle with food and water provided *ad libiditum*.

Surgery

Sprague Dawley or Long Evans adult male rats ($n = 5$) were anaesthetized with an intraperitoneal injection of a mixture of ketamine (60 mg per kg body weight) and

dexmedetomidine (0.25 mg/kg). Buprenorphine (0.1 mg/kg) was administered as an operative analgesic with ketoprofen (5 mg/kg) as post-operative analgesic. Rats were implanted with chronic custom-built multi-tetrode microdrives as previously described (Otazu et al., 2009). The animal's head was secured in a stereotactic frame (David Kopf Instruments, Tujunga, CA, USA). Following the recession of the temporal muscle, a craniotomy and durotomy were performed over the location of the primary auditory cortex. A microdrive housed eight tetrodes, of which two were used for reference and six for signal channels. Each tetrode consisted of four polyimide-coated Nichrome wires (Kenthal-PalmCoast, FL, USA; wire diameter of 12 μm) twisted together and was controlled independently with a turn of a screw. Two screws (one reference and one ground) were inserted in the skull at locations distal from A1. The tetrodes were implanted 4.5–6.5 mm posterior to bregma and 6.0 mm left of the midline, covered with agar solution (3.5%) and secured to the skull with dental acrylic (Metabond) and dental cement. The location of the electrodes was verified based on the stereotaxic coordinates, the electrode position in relation to brain surface blood vessels, and through histological reconstruction of the electrode tracks post-mortem. The electrodes were gradually advanced below the brain surface in daily increments of 40–50 μm. The location was also confirmed by identifying the frequency tuning curve of the recorded units. The recorded units' best frequency, which elicited the highest firing rate, spanned the range of rat hearing and was consistent with previous studies (Sally and Kelly, 1988).

Stimulus construction

To generate scale-invariant sounds, the sound waveform, $y(t)$, was modelled as a sum of droplets, where each droplet, $x_i(a_i, f_i, Q, \tau_i; t)$ was modelled as a gammatone function (Geffen et al., 2011):

$$y(t) = \sum_i x_i(a_i, f_i, Q, \tau_i; t) = \sum_i a_i \frac{f_i}{Q}(t - \tau_i)e^{-f(t-\tau_i)/Q_i} \sin(2\pi f_i(t - \tau_i))$$

with parameters amplitude, a_i, frequency, f_i, onset time, τ_i, and cycle constant of decay, Q, drawn at random from distinct probability distributions. f_i was uniform random in log-frequency space, between 400 and 80000 Hz; onset time was uniform random with mean rate r. Five distinct 7-s stimuli were generated, each comprising a different set of values of Q and r (in units of droplets/octave/s), chosen from: Stimulus 1: $Q = 2$, $r_{med} = 530$; Stimulus 2: $Q = 0.5$, $r_{med} = 530$; Stimulus 3: $Q = 8$, $r_{med} = 530$; Stimulus 4: $Q = 2$, $r_{low} = 53$; Stimulus 5: $Q = 2$, $r_{high} = 5300$. The resulting waveforms were normalized for equal root-mean-square sound pressure level. Further, to make the signal punctate within each spectral band, the amplitude distribution of the droplets was drawn from an inverse square distribution, $p(z) \sim \frac{1}{z^2}$ (Geffen et al., 2011). The distributions of droplet amplitude and frequencies were exactly matched between the stimuli – all sounds generated at the same rate were produced with the same random seed. Each stimulus was 7 s long, and repeated at least 40 times with an inter-stimulus interval of 1 s.

Neural recordings

Neural signals were analysed as previously described (Carruthers et al., 2013, 2015; Aizenberg et al., 2015; Natan et al., 2015). Neuronal signals were acquired daily from 24 chronically implanted electrodes in awake, freely moving rats using a Neuralynx Cheetah system. The neuronal signal was filtered between 0.6 and 6.0 kHz, digitized and recorded at 32 kHz. Discharge waveforms were clustered into single-unit and multi-unit clusters using either Neuralynx Spike Sort 3D or Plexon Off-line Spike Sorter software (Carruthers et al., 2013). Discharge waveforms had to form a visually identifiable distinct cluster in a projection onto a three-dimensional subspace (Otazu et al., 2009; Bizley et al., 2010; Brasselet et al., 2012).

The acoustical stimulus was delivered via a magnetic speaker (MF-1, Tucker-Davis Technologies, Alachua, FL, USA) positioned above the recording chamber. The speaker output was calibrated using Bruel and Kjaer 1/4-inch free-field microphone type 4939, which was placed at the location that would normally be occupied by the animal's ear, by presenting a recording of repeated white noise bursts and tone pips between 400 and 80 000 Hz. From these measurements, the speaker transfer function and its inverse were computed. The input to the microphone was adjusted using the inverse of the transfer function such that the speaker output was 70 dB (sound pressure level relative to 20 μP, SPL) tones, within 3 dB, between 400 and 80 000 Hz. Spectral and temporal distortion products were measured in response to tone pips between 1 and 80 kHz, and were found to be >50 dB below the SPL of the fundamental (Carruthers et al., 2013). All stimuli were presented at 400 kHz sampling rate, using custom-built software based on a commercially

available data acquisition toolbox (Mathworks, Inc., Natick, MA, USA), and a high-speed data acquisition card (National Instruments, Inc., Austin, TX, USA).

Frequency response analysis

We first presented a stimulus designed to map the frequency response function of the recorded units: consisting of 50 tones, each 50 ms long, between 400 and 80 000 Hz, logarithmically spaced, at 70 dB SPL, repeated five times. The response strength, which combined onset and offset responses, was computed as the mean firing rate of neurons during 0–80 ms after tone onset. The best frequency was computed as the frequency of the tone that evoked the maximum response strength (Brown and Harrison, 2009; Carruthers et al., 2013).

Droplet stimulus representation

The stimulus, $s(f, t)$, was represented either as the spectrogram of the sound waveform (2048-point spectrogram computed in Matlab) or as a matrix of droplet onset time/magnitude. The droplet onset matrix was computed from the stimulus design matrix, by binning the droplet onset time into 5-ms bins, and droplet center frequency into 0.0772-octave windows. The value of each point of the matrix was the sum of magnitudes of all droplets originating in that bin.

Firing rate and response strength

The discharge times in each trial were histogrammed in 1-ms bins after stimulus onset (0–8 s), averaged across trials, and smoothed with a Gaussian filter with 3-ms standard deviation. Mean firing rate was computed as the response averaged across the first 7 s of stimulus presentation. The response strength was computed as the difference between the firing rate during the stimulus and that during the baseline, divided by the standard error of the mean of the firing rate at the baseline over trials. The response was considered significant if the response strength exceeded 6.

Selectivity index and sparseness

For each neuron, the selectivity index was computed as the difference between the strongest and the mean response strength to the five stimuli for each unit, normalized by the strongest response.

For each neuron, sparseness, *S*, was computed using the following formula (Weliky et al., 2003):

$$S = 1 - \frac{\left(\sum_i \frac{v_i}{N}\right)^2}{\sum_i \frac{v_i^2}{N}}$$

where v_i is the firing rate (spikes/s) of a single neuron to the *i*th stimulus, and *n* is the total number of stimuli ($n = 5$). *S* takes a value between 0 and 1, where a higher value indicates that the neuron responds to a narrow range of stimuli and a lower value indicates that the neuron responds to a broad range of stimuli.

Linear-Non-Linear model fit

The response of each unit, $r(t)$, was computed as the probability of emitting a discharge within a 5-ms temporal bin relative to the onset of the stimulus. We fitted a linear – non-linear model (LN model) computed using a standard reverse correlation technique (Theunissen et al., 2001; Baccus and Meister, 2002; Escabí and Read, 2003; Geffen et al., 2007), using a spectrogram or the droplet-based representation as an input.

To determine the droplet-temporal receptive field (DTRF), the stimulus was represented in terms of the onset time and maximum amplitude of each droplet within its frequency band. One hundred uniformly, logarithmically distributed frequency bands were used (range: 0.4–80 kHz). DTRF was computed as the normalized average of the stimulus preceding each discharge.

To determine the spectrogram-based spectro-temporal receptive field (STRF), the stimulus was represented as a spectrogram of the waveform. We used the Auditory Toolbox to compute a cochleagram-based representation of the stimulus (Lyon, 1982; Meddis et al., 1990) with sampling rate of 400 kHz and decimation factor 100. STRF and cochleagram-based receptive fields were computed as reverse-correlation between discharge times and the spectrogram or cochleagram of the stimulus, using ridge regression (Theunissen et al., 2001).

The linear prediction of the firing rate was computed as the convolution of the stimulus with DTRF, cochleagram-based receptive field or STRF. The instantaneous non-linearity was computed directly from firing rate vs. linear prediction plot (Baccus and Meister, 2002; Geffen et al., 2007).

The model parameters were fitted to the data over randomly selected 50% of trials. The remaining 50% of trials were used to test the prediction accuracy of the model (Ahn et al., 2014). The prediction accuracy of the LN model was assessed by computing the coefficient of correlation between the predicted and recorded firing rate. Only neurons with correlation coefficient above 0.13 for either droplet-based or spectrogram-based prediction for at least one stimulus were included in the comparisons for model prediction quality over different variants of the model (**Figures 2.5, 2.7**). This value was chosen as the elbow in the histogram of model prediction correlation coefficients, followed by visual inspection of the predicted and actual firing rates for the cases close to the chosen threshold.

Receptive field measurement

The spectral width, temporal width, time to peak and peak frequency of the positive lobe of the DTRF were computed using standard methods (Woolley et al., 2006; Shechter and Depireux, 2007; Schneider and Woolley, 2010). DTRF was denoised by setting all values outside of a significant positive cluster of pixels to 0. To determine the significance of the cluster, the *z*-score of pixels was computed relative to the baseline values from a DTRF generated with scrambled spike trains, using the Stat4ci toolbox (Chauvin et al., 2005). To measure temporal parameters of the receptive field, the positive portion of the cluster-corrected DTRF was averaged across frequencies and fitted with a one-dimensional gaussian filter. Delay to peak was defined as the center of the gaussian fit. Temporal width was defined as twice the standard deviation of the gaussian fit. Likewise, to measure spectral parameters of the DTRF, the DTRF was averaged across time, and fitted with a

one-dimensional gaussian. Peak frequency and spectral width were defined as the center and 2 × standard deviation of the gaussian fit, respectively. Only DTRFs that produced prediction accuracy of 0.13 or higher over the full set of trials for at least one of the stimuli were included in the analysis.

Fano factor

A Fano factor was computed as the mean of the variance of the firing rate over individual trials (in 50-ms bins), divided by the mean firing rate in each bin. Because of the sparseness of responses, only ten bins with the highest firing rates were used for each neuron.

Information measured

Mutual information was computed between the response and the stimulus as previously described (Magri et al., 2009; Kayser et al., 2010). The mutual information between stimuli *S* and neural responses *V* is defined as:

$$I(S;V) = \sum_{v,s} P(s)P(v|s)log_2 \frac{P(v|s)}{P(v)}$$

where $P(s)$ is the probability of presenting stimulus s, $P(v|s)$ is the probability of observing response v when stimulus s is presented, and $P(v)$ is the probability of observing response v across all trials to any stimulus. A value of zero would indicate that there is no relationship between the stimulus and the response.

The 7-s stimulus was separated into seven 'chunks', each 1 s long. Mutual information was computed for 50 randomly selected responses to each of the stimulus 'chunks', and averaged. Each instance of the response was a randomly selected spike count

in six consecutive 2-ms bins to a stimulus chunk (Kayser et al., 2010). These parameters were selected following a pilot calculation of mutual information on a subset of data with variable timing and number of bins.

Statistical comparisons

Samples with $n < 50$ that did not pass the Shapiro–Wilk test for normality were compared using a Wilcoxon signed rank test. Measurements across different stimulus conditions with $n > 50$ were compared via paired Student's *t*-test, with a post-hoc Bonferroni multiple-comparison correction when appropriate unless otherwise noted. $P < 0.05$ was considered significant, unless otherwise noted.

2.4 REFERENCES

Ahn J, Kreeger LJ, Lubejko ST, Butts DA, MacLeod KM (2014) Heterogeneity of intrinsic biophysical properties among cochlear nucleus neurons improves the population coding of temporal information. J Neurophysiol 111:2320–2331.

Ahrens MB, Linden JF, Sahani M (2008) Nonlinearities and Contextual Influences in Auditory Cortical Responses Modeled with Multilinear Spectrotemporal Methods. J Neurosci 28:1929–1942.

Aizenberg M, Geffen MN (2013) Bidirectional effects of aversive learning on perceptual acuity are mediated by the sensory cortex. Nat Neurosci 16:994–996.

Aizenberg M, Mwilambwe-Tshilobo L, Briguglio JJ, Natan RG, Geffen MN (2015) Bidirectional Regulation of Innate and Learned Behaviors That Rely on Frequency

Discrimination by Cortical Inhibitory Neurons. PLoS Biol 13:1–32.

Asari H, Zador AM (2009) Long-Lasting Context Dependence Constrains Neural Encoding Models in Rodent Auditory Cortex. J Neurophysiol 102:2638–2656.

Attias H, Schreiner CE (1997) Temporal Low-Order Statistics of Natural Sounds. Adv Neural Inf Process Syst 9:27–33.

Baccus SA, Meister M (2002) Fast and Slow Contrast Adaptation in Retinal Circuitry. Neuron 36:909–919.

Bizley JK, Walker KMM, King AJ, Schnupp JWH (2010) Neural ensemble codes for stimulus periodicity in auditory cortex. J Neurosci 30:5078–5091.

Blake DT, Merzenich MM (2002) Changes of AI Receptive Fields With Sound Density. J Neurophysiol 88:3409–3420.

Brasselet R, Panzeri S, Logothetis NK, Kayser C (2012) Neurons with Stereotyped and Rapid Responses Provide a Reference Frame for Relative Temporal Coding in Primate Auditory Cortex. J Neurosci 32:2998–3008.

Brown TA, Harrison R V. (2009) Responses of Neurons in Chinchilla Auditory Cortex to Frequency-Modulated Tones. J Neurophysiol 101:2017–2029.

Butts DA, Weng C, Jin J, Alonso J-M, Paninski L (2011) Temporal Precision in the Visual Pathway through the Interplay of Excitation and Stimulus-Driven Suppression. J Neurosci 31:11313–11327.

Carlson NL, Ming VL, DeWeese MR (2012) Sparse Codes for Speech Predict Spectrotemporal Receptive Fields in the Inferior Colliculus Behrens T, ed. PLoS Comput Biol 8:1–15.

Carruthers IM, Laplagne DA, Jaegle A, Briguglio JJ, Mwilambwe-Tshilobo L, Natan

RG, Geffen MN (2015) Emergence of invariant representation of vocalizations in the auditory cortex. J Neurophysiol 114:2726–2740.

Carruthers IM, Natan RG, Geffen MN (2013) Encoding of ultrasonic vocalizations in the auditory cortex. J Neurophysiol 109:1912–1927.

Chandrasekaran C, Trubanova A, Stillittano S, Caplier A, Ghazanfar AA (2009) The Natural Statistics of Audiovisual Speech Friston KJ, ed. PLoS Comput Biol 5:1–18.

Chauvin A, Worsley KJ, Schyns PG, Arguin M, Gosselin F (2005) Accurate statistical tests for smooth classification images. J Vis 5:659–667.

Christianson GB, Sahani M, Linden JF (2008) The consequences of response nonlinearities for interpretation of spetrotemporal receptive fields. J Neurosci 28:446–455.

deCharms RC, Blake DT, Merzenich MM (1998) Optimizing sound features for cortical neurons. Science 280:1439–1443.

Depireux DA, Simon JZ, Klein DJ, Shamma SA (2001) Spectro-Temporal Response Field Characterization With Dynamic Ripples in Ferret Primary Auditory Cortex. J Neurophysiol 85:1220–1234.

Eggermont JJ (2011) Context dependence of spectro-temporal receptive fields with implications for neural coding. Hear Res 271:123–132.

Eggermont JJ, Aertsen AMHJ, Johannesma PIM (1983a) Quantitative characterisation procedure for auditory neurons based on the spectro-temporal receptive field. Hear Res 10:167–190.

Eggermont JJ, Johannesma PM, Aertsen AM (1983b) Reverse-correlation methods in auditory research. Q Rev Biophys 16:341–414.

Elhilali M, Fritz JB, Klein DJ, Simon JZ, Shamma SA (2004) Dynamics of Precise Spike Timing in Primary Auditory Cortex. 24:1159–1172.

Escabí MA, Read HL (2003) Representation of spectrotemporal sound information in the ascending auditory pathway. Biol Cybern 89:350–362.

Escabí MA, Read HL (2005) Neural Mechanisms for Spectral Analysis in the Auditory Midbrain, Thalamus, and Cortex. Int Rev Neurobiol 70:207–252.

Escabí MA, Schreiner CE (2002) Nonlinear spectrotemporal sound analysis by neurons in the auditory midbrain. J Neurosci 22:4114–4131.

Garcia-Lazaro JA, Ahmed B, Schnupp JWH (2006) Tuning to Natural Stimulus Dynamics in Primary Auditory Cortex. Curr Biol 16:264–271.

Geffen MN, Broome BM, Laurent G, Meister M (2009) Neural Encoding of Rapidly Fluctuating Odors. Neuron 61:570–586.

Geffen MN, de Vries SEJ, Meister M (2007) Retinal Ganglion Cells Can Rapidly Change Polarity from Off to On Sterling P, ed. PLoS Biol 5:640–650.

Geffen MN, Gervain J, Werker JF, Magnasco MO (2011) Auditory Perception of Self-Similarity in Water Sounds. Front Integr Neurosci 5:15.

Gervain J, Werker JF, Geffen MN (2014) Category-Specific Processing of Scale-Invariant Sounds in Infancy Malmierca MS, ed. PLoS One 9:e96278.

Gourévitch B, Eggermont JJ (2008) Spectro-temporal sound density-dependent long-term adaptation in cat primary auditory cortex. Eur J Neurosci 27:3310–3321.

Heil P (1997) Auditory Cortical Onset Responses Revisited. II. Response Strength. J Neurophysiol 77:2642–2660.

Heil P, Peterson AJ (2015) Basic response properties of auditory nerve fibers: a review.

Cell Tissue Res 361:129–158.

Heil P, Rajan R, Irvine DRF (1992) Sensitivity of neurons in cat primary auditory cortex to tones and frequency-modulated stimuli. I: Effects of variation of stimulus parameters. Hear Res 63:108–134.

Hromádka T, DeWeese MR, Zador AM (2008) Sparse Representation of Sounds in the Unanesthetized Auditory Cortex Plenz D, ed. PLoS Biol 6:124–137.

Irino T, Patterson RD (1996) Temporal asymmetry in the auditory system. Cit J Acoust Soc Am 99:2316.

Kayser C, Logothetis NK, Panzeri S (2010) Millisecond encoding precision of auditory cortex neurons. Proc Natl Acad Sci U S A 107:16976–16981.

Klein DJ, Depireux DA, Simon JZ, Shamma SA (2000) Robust Spectrotemporal Reverse Correlation for the Auditory System: Optimizing Stimulus Design.

Krebs B, Lesica NA, Grothe B (2008) The Representation of Amplitude Modulations in the Mammalian Auditory Midbrain. J Neurophysiol 100:1602–1609.

Lesica NA, Grothe B (2008) Dynamic spectrotemporal feature selectivity in the auditory midbrain. J Neurosci 28:5412–5421.

Lewicki MS (2002) Efficient coding of natural sounds. Nat Neurosci 5:356–363.

Lin FG, Liu RC (2010) Subset of Thin Spike Cortical Neurons Preserve the Peripheral Encoding of Stimulus Onsets. J Neurophysiol 104:3588–3599.

Linden JF, Liu RC, Sahani M, Schreiner CE, Merzenich MM (2003) Spectrotemporal Structure of Receptive Fields in Areas AI and AAF of Mouse Auditory Cortex. J Neurophysiol 90:2660–2675.

Lu T, Liang L, Wang X (2001) Neural Representations of Temporally Asymmetric

Stimuli in the Auditory Cortex of Awake Primates. J Neurophysiol 85:2364–2380.

Lyon RF (1982) A computational model of filtering, detection, and compression in the cochlea. Acoust Speech, Signal Process IEEE Int Conf ICASSP 7:1282–1285.

Magri C, Whittingstall K, Singh V, Logothetis NK, Panzeri S (2009) A toolbox for the fast information analysis of multiple-site LFP, EEG and spike train recordings. BMC Neurosci 10:81.

Marmarelis PZ, Marmarelis VZ (1978) Analysis of physiological systems: the white noise approach. New York, NY: Plenum Press.

McDermott JH, Schemitsch M, Simoncelli EP (2013) Summary statistics in auditory perception. Nat Neurosci 16:493–498.

McDermott JH, Simoncelli EP (2011) Sound Texture Perception via Statistics of the Auditory Periphery: Evidence from Sound Synthesis. Neuron 71:926–940.

McFarland JM, Cui Y, Butts DA (2013) Inferring Nonlinear Neuronal Computation Based on Physiologically Plausible Inputs Bethge M, ed. PLoS Comput Biol 9:1–18.

Meddis R, Hewitt MJ, Shackleton TM (1990) Implementation details of a computation model of the inner hair-cell auditory-nerve synapse. J Acoust Soc Am 87:1813.

Mizrahi A, Shalev A, Nelken I (2014) Single neuron and population coding of natural sounds in auditory cortex. Curr Opin Neurobiol 24:103–110.

Natan RG, Briguglio JJ, Mwilambwe-Tshilobo L, Jones SI, Aizenberg M, Goldberg EM, Geffen MN (2015) Complementary control of sensory adaptation by two types of cortical interneurons. Elife 4:1–27.

Nelken I (2004) Processing of complex stimuli and natural scenes in the auditory cortex. Curr Opin Neurobiol 14:474–480.

Nelken I, Rotman Y, Yosef OB (1999) Responses of auditory-cortex neurons to structural features of natural sounds. Nature 397:154–157.

Otazu GH, Tai L-H, Yang Y, Zador AM (2009) Engaging in an auditory task suppresses responses in auditory cortex. Nat Neurosci 12:646–654.

Pienkowski M, Eggermont JJ (2009) Effects of adaptation on spectrotemporal receptive fields in primary auditory cortex. Neuroreport 20:1198–1203.

Poeppel D (2003) The analysis of speech in different temporal integration windows: cerebral lateralization as 'asymmetric sampling in time.' Speech Commun 41:245–255.

Rabinowitz NC, Willmore BDB, Schnupp JWH, King AJ (2011) Contrast Gain Control in Auditory Cortex. Neuron 70:1178–1191.

Robles L, Ruggero MA (2001) Mechanics of the Mammalian Cochlea. Physiol Rev 81:1305–1352.

Rodríguez FA, Chen C, Read HL, Escabí MA (2010) Neural modulation tuning characteristics scale to efficiently encode natural sound statistics. J Neurosci 30:15969–15980.

Rosen S (1992) Temporal information in speech: acoustic, auditory and linguistic aspects. Philos Trans R Soc Lond B Biol Sci 336:367–373.

Sally SL, Kelly JB (1988) Organization of auditory cortex in the albino rat: sound frequency. J Neurophysiol 59:1627–1638.

Schneider DM, Woolley SMN (2010) Discrimination of Communication Vocalizations by Single Neurons and Groups of Neurons in the Auditory Midbrain. J Neurophysiol 103:3248–3265.

Sharpee T, Rust NC, Bialek W (2004) Communicated by Pamela Reinagel Analyzing Neural Responses to Natural Signals: Maximally Informative Dimensions. Neural Comput 16:223–250.

Shechter B, Depireux DA (2007) Stability of spectro-temporal tuning over several seconds in primary auditory cortex of the awake ferret. Neuroscience 148:806–814.

Singh NC, Theunissen FE (2003) Modulation spectra of natural sounds and ethological theories of auditory processing. J Acoust Soc Am 114:3394.

Smith EC, Lewicki MS (2006) Efficient auditory coding. Nature 439:978–982.

Theunissen FE, David SV, Singh NC, Hsu A, Vinje WE, Gallant JL (2001) Estimating spatio-temporal receptive fields of auditory and visual neurons from their responses to natural stimuli. Network 12:289–316.

Theunissen FE, Woolley SMN, Hsu A, Fremouw TE (2004) Methods for the Analysis of Auditory Processing in the Brain. Ann N Y Acad Sci 1016:187–207.

Valentine PA, Eggermont JJ (2004) Stimulus dependence of spectro-temporal receptive fields in cat primary auditory cortex. Hear Res 196:119–133.

Voss RF, Clarke J (1975) "1/f noise" in music and speech. Wiley.

Weliky M, Fiser J, Hunt RH, Wagner DN (2003) Coding of Natural Scenes in Primary Visual Cortex. Neuron 37:703–718.

Woolley SMN, Fremouw TE, Hsu A, Theunissen FE (2005) Tuning for spectro-temporal modulations as a mechanism for auditory discrimination of natural sounds. Nat Neurosci 8:1371–1379.

Woolley SMN, Gill PR, Theunissen FE (2006) Stimulus-Dependent Auditory Tuning Results in Synchronous Population Coding of Vocalizations in the Songbird

Midbrain. J Neurosci 26:2499–2512.

Yang Y, DeWeese MR, Otazu GH, Zador AM (2008) Millisecond-scale differences in neural activity in auditory cortex can drive decisions. Nat Neurosci 11:1262–1263.

Zheng Y, Escabi MA (2008) Distinct Roles for Onset and Sustained Activity in the Neuronal Code for Temporal Periodicity and Acoustic Envelope Shape. J Neurosci 28:14230–14244.

CHAPTER 3: THE FUNCTION OF CORTICAL MICROCIRCUITS IN AUDITORY PROCESSING

Adapted from: Blackwell JM, Geffen MN (2017) Progress and challenges for understanding the function of cortical microcircuits in auditory processing. *Nature communications* 8:2165

In auditory processing, a long-standing question has been the function of cortical architecture in specific sensory functions. Auditory cortex (AC) is comprised of neurons of many different types, providing the ability to perform an astonishing number of computations. Even the most basic distinction between neurons into excitatory and inhibitory units dramatically expand the computational capacity of a network, and a quest in auditory neuroscience has been to unravel the function of specific micro-circuits in sound encoding and plasticity. A particularly interesting aspect of cortical connectivity is the diversity of inhibitory neurons in their morphology and synaptic properties (Kepecs and Fishell, 2014) (**Figure 3.1A**). Interneurons form reciprocal connections not only with the excitatory neurons, but also with each other (**Figure 3.1B**). Furthermore, the diversity of connections between different types of inhibitory interneurons can affect how information is processed in the network (**Figure 3.1C**).

Recent advances in optogenetics and imaging (Roux et al., 2014) facilitate the exploration of the role of cortical circuits comprised of distinct inhibitory neurons in basic auditory functions, such as frequency discrimination and adaptation to temporal stimulus statistics. In combination with computational techniques for inhibitory-excitatory network analysis, these experimental approaches offer promise for unraveling the microcircuits within auditory cortex for representing sounds. Here, we discuss progress and limitations in our understanding that emerges from recent investigations of the function of cortical micro-circuits in audition.

Role of inhibition in auditory frequency discrimination.

Spectral differences between sounds are fundamental cues for identifying a dangerous sound, be it the sound of an approaching predator or screeching brakes; recognizing a familiar speaker; or distinguishing different animal vocalizations (Bregman, 1990; Feng and Ratnam, 2000; Aizenberg and Geffen, 2013). Frequency selectivity, originating with spectral decomposition of the acoustic signal by the cochlea, is a strong organizing feature of neuronal responses in the auditory pathway. Neurons in the auditory cortex exhibit frequency selectivity (Abeles and Goldstein, 1970; Shamma et al., 1993; Wehr and Zador, 2003), responding to a subset of frequencies more strongly than others. This selectivity is thought to support perceptual frequency discrimination acuity (Talwar and Gerstein, 2001; Tramo et al., 2002; Dykstra et al., 2012) (but see (Ohl et al., 1999; Gimenez et al., 2015)): the greater the difference either in individual or population neuronal responses for tones of neighboring frequencies, the higher frequency discrimination acuity.

Either more narrowly tuned neurons, or neurons with higher signal-to-noise ratio in tone-evoked responses would support higher frequency discrimination acuity, as the difference in responses to neighboring tones will be higher in these neurons than in broadly tuned/low signal-to-noise neurons. One of the most extensively tested roles of cortical inhibition in auditory processing has been in shaping frequency selectivity of excitatory neurons. Inhibition may sharpen frequency tuning and increase the signal-to-noise ratio in excitatory tone-evoked responses by suppressing spontaneous excitatory activity; alternatively, either broad or co-tuned inhibitory inputs may sharpen frequency selectivity due to the rectifying non-linear integration (such as the spiking non-linearity) (Liu et al., 2007; Wu et al., 2008; Schinkel-Bielefeld et al., 2012). Differential timing of excitatory and inhibitory co-tuned inputs can further refine frequency tuning of excitatory neurons (Oswald et al., 2006). Experimental evidence from pharmacological experiments and intra-cellular recordings has supported either effect (Chen and Jen, 2000; Wang et al., 2000; Wehr and Zador, 2003; Oswald et al., 2006; Wu et al., 2008; Tan and Wehr, 2009). An interesting possibility is that distinct inhibitory neuronal cell types may contribute differentially to shaping frequency selectivity. The development of optogenetic manipulations has promised to disambiguate the effects of different specific neuronal cell types (Lee et al., 2012).

Figure 3.1

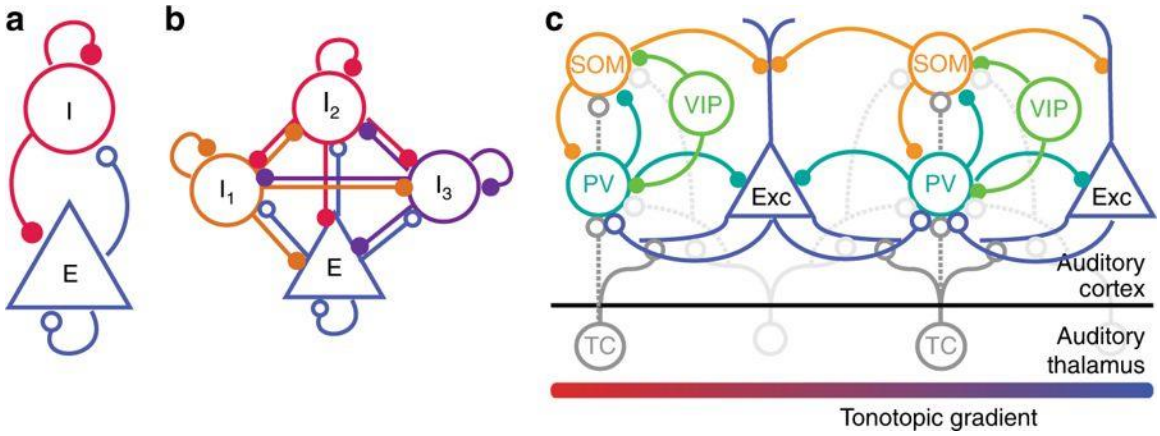
a
I
E
b
I2
I1
I3
E
c
SOM
VIP
PV
Exc
SOM
VIP
PV
Exc
Auditory cortex
TC
TC
Auditory thalamus
Tonotopic gradient

Figure 3.1 Simplified views of cortical circuits. **A**. Diagram of excitatory-inhibitory circuit with recurrent connections. Theoretical and experimental studies demonstrate that inhibition stabilizes between excitatory and inhibitory neurons in the auditory cortex. **B**. Inhibitory-excitatory network can be extended to include several interneuron subtypes. **C**. Schematic diagram of connectivity between select neurons in the auditory cortex (note that layer-specific information is omitted here): Exc: Excitatory neurons; PV: parvalbumin-positive interneurons; SOM: somatostatin-positive interneurons; VIP: vasopressin-positive interneurons; TC: Thalamo-cortical projection neurons. All neuron types receive additional inputs from other brain areas, which were omitted from the diagram for simplicity. Open circles: excitatory synapses; closed circles: inhibitory synapses. Solid lines indicate dominant projections; dashed lines indicate occasional connections.

A series of studies that optogenetically manipulated the most common interneuron type, parvalbumin-positive interneurons (PVs) confirmed that inhibitory neurons modulate frequency tuning in AC: Activating PVs enhanced feedforward connectivity between excitatory units. The spontaneous activity of excitatory neurons was decreased, and the frequency tuning width was narrower, increasing frequency selectivity (Hamilton et al., 2013). Consistently, PV activation also increased the strength of tone-evoked responses and improved behavioral frequency discrimination acuity, while suppression decreased the strength and tuning width of the tone-evoked responses in putative excitatory neurons, and drove an impairment in behavioral frequency discrimination acuity (**Figure 3.2A-C**) (Aizenberg et al., 2015).

But are the effects different between distinct interneuron types? There is a range of interneuron classifications available, with at least two major groups of neurons emerging besides PVs, somatostatin (SOMs), and serotonin receptor 5HT3aR, of which a major group are also positive for vassopressin (VIPs) (Markram et al., 2004; Rudy et al., 2011; Kepecs and Fishell, 2014). Although each interneuron class includes a number of different cell types and may change with development and experience (Spitzer, 2017), these classes of neurons have received prominent attention, as they approximate a canonical cortical circuit (**Figure 3.1**), and due to availability of transgenic mouse lines. Optogenetic activation of either PVs or SOMs exerted a similar mix of effects on tone-evoked activity in excitatory cells, with activation providing either multiplicative scaling, as would be expected from co-tuned inhibition, or linear amplification, as would be expected from broad inhibitory inputs (Seybold et al., 2015). This variability in combination with spiking threshold non-linearity and strength of suppression across different neurons can both

amplify and sharpen tuning properties of excitatory neurons (Seybold et al., 2015). On average, suppressing interneurons had differential effects: suppressing SOMs increased the gain of excitatory neurons, whereas suppressing PVs weakened frequency tuning (Phillips and Hasenstaub, 2016). Nonetheless, as with activation, in individual neurons inactivation of either type of interneuron showed a range of effects, thus supporting a number of models for interactions between PVs, SOMs and excitatory neurons. Measuring the tuning widths of individual PVs, excitatory neurons and SOMs neurons furthermore did not yield clear distinctions (Moore and Wehr, 2013; Li et al., 2015), potentially because these classes of neurons are themselves comprised of multiple cell types. These differences may be exacerbated across studies by the various biases toward specific subclasses by different recording techniques. Indeed, a recent review of SOMs estimated over 100 subtypes of SOM neurons (Yavorska and Wehr, 2016). Thus, whereas the optogenetic perturbations of PVs and SOMs confirmed their role in shaping frequency tuning in the auditory cortex, the results were consistent with the range of results in the pharmacological literature, and a clear distinction between the function of the two interneuron subtypes in frequency tuning has not emerged.

By targeting the electrophysiological recordings to specific cell types, it has begun possible to assess the diversity of neuronal responses in both stimulus selectivity and timecourse. Interestingly, in the temporal domain, responses of PVs had faster onsets on average than excitatory neurons, while SOM neurons exhibited slower response onsets than excitatory neurons (Moore and Wehr, 2013; Li et al., 2015). Such differential activation timing may provide an additional mechanism for sharpening of tone-evoked responses in AC (Denève and Machens, 2016): the differences between inhibitory and excitatory

response onsets would drive more precise response onsets over the excitatory population. The timing differences in suppression between PVs and SOMs could support a number of other functional effects, for example when applied to suppression of responses due to the stimulus history. These observations, facilitated by targeted recordings, provide information about specific neuronal synaptic parameters that should inform the design of computational models. Future studies are required for understanding whether the timing differences in tone-evoked responses of PVs and SOMs results in distinct function of these neurons in frequency discrimination.

Figure 3.2

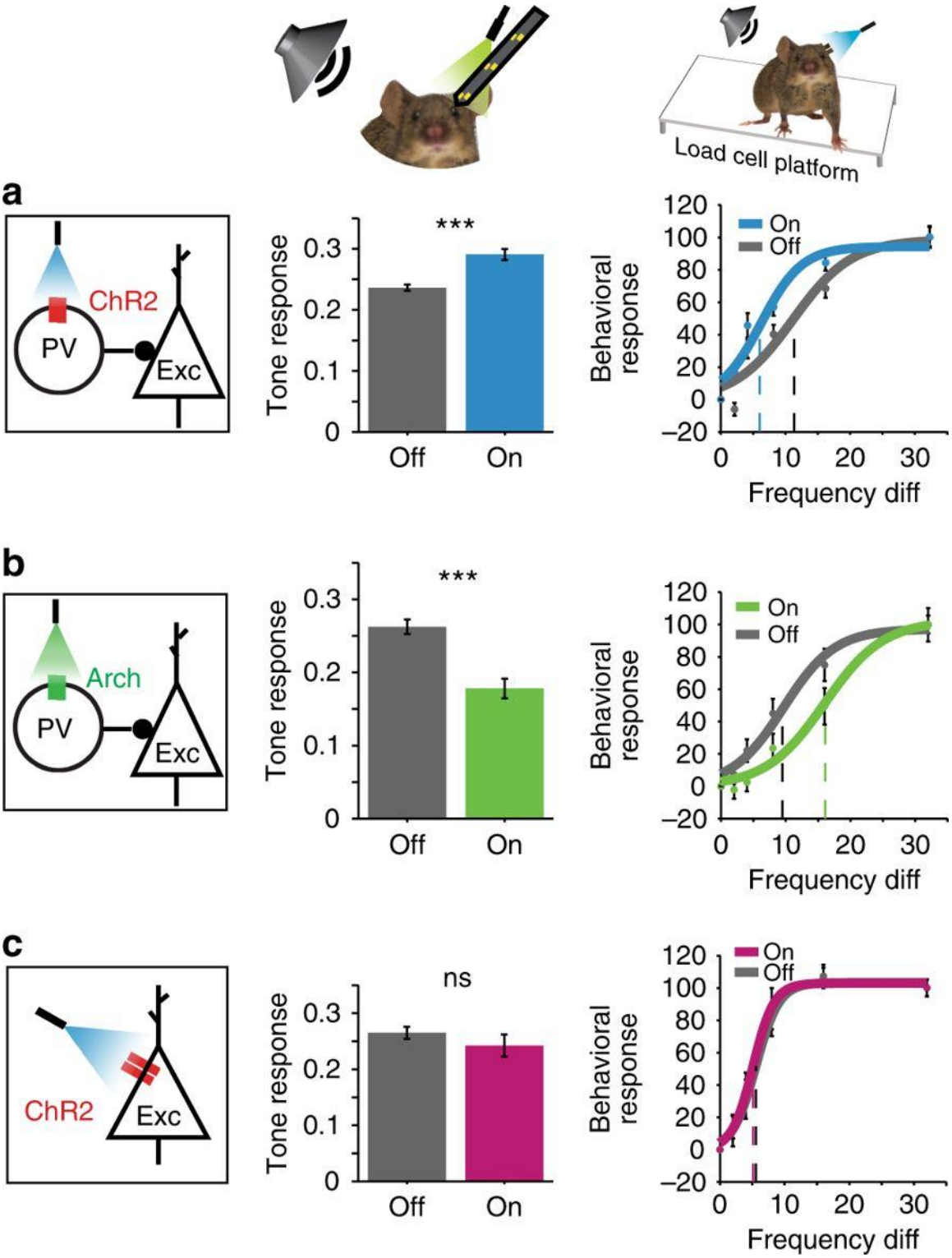
Load cell platform
a
ChR2
PV
Exc
Tone response
***
Off
On
Behavioral response
On
Off
Frequency diff
b
Arch
PV
Exc
Tone response
***
Off
On
Behavioral response
On
Off
Frequency diff
c
ChR2
Exc
Tone response
ns
Off
On
Behavioral response
On
Off
Frequency diff

Figure 3.2 Inhibitory interneurons affect auditory cortical responses and behavior. Activating PVs with ChR2 **A** increases tone-evoked responses and improves behavioral frequency discrimination acuity, whereas suppressing PVs using Arch has the opposite effect **B**. **C** Direct activation of excitatory neurons with ChR2 does not change tone-evoked responses or behavioral frequency discrimination acuity on average. **A-C**. Left: diagram of optogenetic manipulation. Center: Mean tone-evoked response magnitude under light-off and light-on conditions based on neuronal recordings. Right: Behavioral response to a shift in frequency under light-off and light-on conditions. Adapted from (Aizenberg et al., 2015).

Role of inhibition in adaptation to stimulus statistics

Time processing is particularly important for auditory perception. Perception is formed as much by the present stimulus as by the history of preceding stimuli; it is an interaction between the representation of new events and memory of past events. Sensory cortex constantly reshapes responses to present stimuli dependent on the context. Responses of nearly all neurons in the auditory cortex (95%) change with stimulus temporal history, exhibiting stimulus-specific adaptation (SSA) (Ulanovsky et al., 2003; Natan et al., 2015). Typically, the firing rate is reduced in response to repeated stimuli through a process that involves integration of stimulus statistics over time (Ulanovsky et al., 2003; Natan et al., 2015). Inhibitory-excitatory networks support this transformation, and PVs and SOMs were found to play a differential role in cortical adaptation. SSA is quantified as the index of change in the firing rate in response to a rare 'deviant' tone presented as part of a sequence with another common 'standard' tone, at varying presentation probabilities (for example, 10%, deviant versus 90% standard). SSA is thought to be supported by a combination of thalamo-cortical depression and intra-cortical inhibitory-excitatory circuit effects (Nelken, 2014). Indeed, suppressing either PVs or SOMs optogenetically increased the strength of adaptation in excitatory neurons (Natan et al., 2015) (**Figure 3.3A, B**). However, PVs and SOMs differed in their contribution to adaptation: suppression of SOMs evoked a stimulus-selective increase in excitatory responses to the standard, but not the deviant tones, whereas suppressing PVs led to a non-specific response increase. When examining the effect of SOM suppression on excitatory responses to repeated presentations of the standard tones following a deviant tone, disinhibition of the excitatory response increased with repeated presentations (**Figure**

3.2A-C), further confirming that SOMs provided a selective inhibitory contribution to stimulus-specific adaptation. PV and SOM interneurons themselves both exhibit SSA (Chen et al., 2015; Natan et al., 2015), so that the unique contribution of SOMs in stimulus-specific inhibition of excitatory responses was possible through selective suppression of this cell type.

Further work revealed that stimulus specific inhibition mediated by SOMs persisted over a longer time scale, in habituation following passive exposure to sounds over several days (Kato et al., 2015) (**Figure 3.3C, D**). Whereas the excitatory and PV neuronal responses to habituated sounds were reduced over several weeks of exposure, SOM responses increased, as did inhibition from SOMs. Thus, in temporal domain, the function of SOMs is consistent with regulation of the gain of cortical responses to sounds based on their behavioral prominence or relevance. SOMs thus contribute to adaptation and habituation, acting on several time scales to control the gain in response to commonly presented acoustic stimuli, exerting a more specific modulation than PVs. Such modulation of excitatory activity may contribute to the more general context-specific gain modulation and adaptation observed within AC (Williamson et al., 2016). As discussed earlier, the temporal history of the stimulus accounts for the differential function of interneuron modulation. This functional dissociation likely underlies other temporally differentiated functions, such as integration of stimulus sequences, or more general computation of spectro-temporal statistical regularities in sound sequences. A promising direction for future studies would be to continue the exploration of the function not just over the instantaneous responses to tones, but in understanding how, over a range of time scales, inhibition may modulate dynamic changes in sound response properties.

Inhibitory cascades within the auditory cortex

While the above studies mainly considered the effects of PVs and SOMs on excitatory neurons, understanding how PVs and SOMs act within a cortical microcircuit is of particular importance given the modulatory roles these interneurons play when targeted by feedback from other brain regions and different neuromodulatory projections. In a circuit that supports reduction of auditory responses during locomotion, a subset of secondary motor cortex neurons, which are active during movement, suppresses excitatory tone-evoked responses in AC by activating PVs, which in turn suppress excitatory neurons (Nelson et al., 2013; Schneider et al., 2014). Additionally, PVs are involved in inter-hemispheric information integration, as callossal projections terminate on PVs, which suppress cortico-cortical excitatory neurons (Rock and Apicella, 2015). PVs and SOMs can be activated by oxytocin, which likely supports the sharpening of responses to pup calls observed in mothers (Marlin et al., 2015). PVs also shape cortical responses to tones coupled with aversive stimuli (Letzkus et al., 2011), as part of circuit, which includes projections from the amygdala to layer 1 neurons in AC. Thus, projections from cognitive and emotional brain centers likely preferentially target inhibitory interneurons and may affect behavioral and emotional processing.

Other inhibitory neuronal subtypes further contribute to inhibitory cascades in the cortex. For example, there is extensive evidence that PVs and SOMs are regulated by VIPs. Cortical VIP interneurons are recruited by projections from other brain regions (Lee et al., 2013; Zhang et al., 2014) and can be modulated by cholinergic projections (Fu et al., 2014;

Poorthuis et al., 2014; Koukouli et al., 2016; Kuchibhotla et al., 2017) allowing for external control of these local microcircuits. In the auditory cortex, engagement in an auditory task enhanced the activity of PVs, SOMs, and VIPs, attributed to cholinergic modulation (Kuchibhotla et al., 2017). Activation of VIP interneurons disinhibited excitatory responses (Pi et al., 2013), consistent with an additional inhibitory synapse between VIPs, another inhibitory neuron and excitatory neuron. Indeed, *in vitro* activation of VIPs suppresses PV and SOM activity, thereby providing a mechanism for delayed activation of excitatory tone-evoked responses. Interestingly, VIP neurons were driven by sounds at much lower intensities than either PV or SOM neurons (Mesik et al., 2015). The increased excitatory neuronal activity due to VIP activation may contribute to increased gain of sensory inputs, although it remains to be determined whether the relative timing of disinhibition may provide an increase in gain, rather than nonspecific elevation in cortical activity. VIP neurons have also been implicated in integration of cross-modal activity, as responses of VIPs in the visual cortex are suppressed by sound (Ibrahim et al., 2016). This wide range of effects of VIP activation suggests that the connections between VIPs and inhibitory and excitatory neurons are likely modulated in a task- and modality- specific fashion, and therefore the interpretation of their function should inherently be studied in a specific statistical and behavioral context. To understand whether and how these circuits integrate with each other and what biophysical constraints are required for their function, the results of these studies need to be incorporated in a circuit-level model that includes interactions between the different circuits.

Caveats in optogenetic result interpretation

In interpreting these rich and varied experimental results, it is important to account for limitations and potentially confounding factors: An important caveat to grouping the interneurons into classes based on molecular markers is that each of these classes are comprised of multiple interneuron subtypes, and those subtypes are distributed differentially across the different cortical laminae. For instance, PV interneurons are comprised of not only two already diverse large groups of neurons, basket and chandelier cells, but also of a number of other neurons (Kepecs and Fishell, 2014). SOM interneurons include Martinotti cells, whose axons target the distal dendrites of pyramidal neurons, as well as at least two other classes of layer 2/3 targeting neurons (McGarry et al., 2010). A recent review estimated between 4 and 100 subtypes of SOMs depending on classification method, such as differential labeling and projection patterns (Yavorska and Wehr, 2016). Incorporating some specific aspects of neuronal morphology, such as by building multi-compartment neuronal models and accounting for expression of different molecules involved in neuronal communication, may prove essential for differentiating between the effects of dendrite-targeting SOMs and cell-body targeting interneurons. Indeed, the excitatory-inhibitory circuit composition likely differs between cortical layers with some neuronal types being overrepresented and targeting different parts of the excitatory cell body, leading to differences in integration and non-linearity (DeFelipe et al., 2013; Fino et al., 2013; Naka and Adesnik, 2016). Different recording techniques, such as extracellular recordings of activity of optically tagged neurons versus two-photon guided patch-clamp recordings might be biased toward different subclasses within the optogenetically identified groups and different cortical sublayers, potentially reporting conflicting results on the response properties of different cell types (Moore and Wehr, 2013; Li et al., 2015).

By measuring a number of essential connectivity parameters, the strength and time constant of synapses between different neuronal types within different layers, it should be possible to further develop models to extrapolate the results across different cortical connectivity patterns. In turn, electrophysiological experiments, including multiple-neuron intracellular recordings, could be used to establish the specific parameters for connectivity between different neuronal cell types (Song et al., 2005). The computational approaches to implement such detailed biophysical models have been developed, and, as detailed in the next section, a small number of studies started using these computational frameworks to build models incorporating multiple neuronal subtypes in a variety of circuit motifs.

Figure 3.3

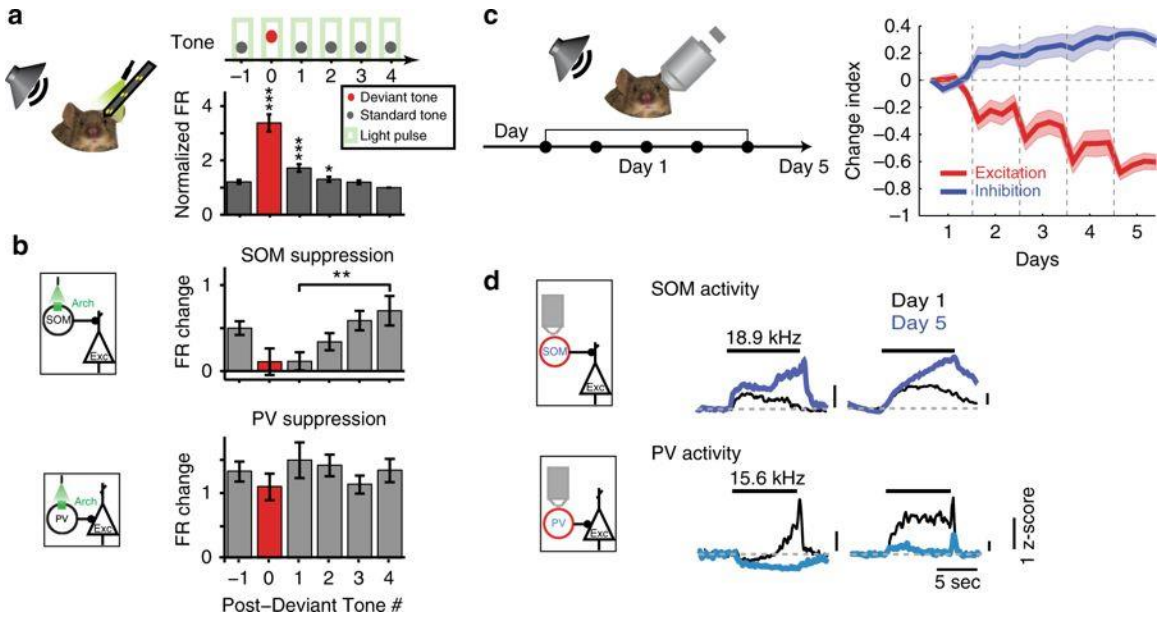
a
Tone
−1 0 1 2 3 4
Deviant tone
Standard tone
Light pulse
Normalized FR
b
SOM suppression
FR change
PV suppression
Post−Deviant Tone #
c
Day
Day 1
Day 5
Change index
Excitation
Inhibition
Days
d
SOM activity
18.9 kHz
Day 1
Day 5
PV activity
15.6 kHz
1 z-score
5 sec

Figure 3.3 Specific inhibitory neuron type mediates auditory adaptation. **A**. Top: The effect of SOM and PV inactivation on stimulus-specific adaptation to frequent tones was tested using an oddball stimulus, with two tones at 10-90 ratio, light every 5th tone. Bottom: The mean firing rate (FR) during repeated tones adapted with successive presentations of the standard tone. **B**. SOMs provide stimulus-specific inhibition, as the effect of SOM suppression increased with repeated standard tones. PVs provided constant inhibition regardless of adaptation. **A, B** adapted from (Natan et al., 2015). **C**. Passive exposure to a tone stimulus lead to a decrease in excitatory and an increase in inhibitory activity over 5 days. Left: Calcium activity was imaged using two-photon microscopy in populations of identified inhibitory and excitatory neurons before and after subjecting the mouse to prolonged exposure to tones. Neuronal activity was measured as spike counts inferred from the imaged fluorescence signal. Right: Change index of the mean activity in response to the tone to which the mouse was exposed, averaged over populations of excitatory (red) or inhibitory (blue) neurons, over days since prolonged tone exposure onset. Mean excitatory activity decreased with exposure, whereas mean inhibitory activity increased. **D**. Among the inhibitory neurons, the activity of SOMs increased following passive tone exposure, whereas the activity of PVs decreased. Mean z-scored time course of Calcium activity of SOMs or PVs in response to a tone at day 1 (black traces) and day 5 (blue traces). **C, D** adapted from (Kato et al., 2015).

Computational models for excitatory-inhibitory interactions.

The approaches for incorporating inhibition into modeling sensory cortical function have ranged from implementing massive inhibition, forming inhibition-stabilized networks (Tsodyks et al., 1997; Latham and Nirenberg, 2004; Ozeki et al., 2009) to fine-tuning parameters of individual neuronal feedback circuits (Sussillo, 2014). Indeed, the large range of response profiles to activation of interneurons in inter-connected networks was extensively studied in the context of inhibition-stabilized networks that interpret the function of inhibition as supporting "stability" in neuronal pattern discharges across neuronal population activity (Aizenberg et al., 2015; Seybold et al., 2015). Stabilization of excitatory neuron activity by recurrent inhibition can be explained by analyzing the dynamics of firing rates of excitatory and inhibitory populations over time, including feedback propagation of activity **(Figure 3.4A**). This relatively simple model also explained heterogeneous findings from experiments testing the effect of increasing inhibition on network activity (Aizenberg et al., 2015; Seybold et al., 2015; Phillips and Hasenstaub, 2016) as providing input to inhibitory neurons resulting in increased activity of excitatory neurons in a model of an excitatory-inhibitory network (Tsodyks et al., 1997). Additional studies of inhibition-stabilized circuits focused on the role of inhibition in improving tuning of neurons for specific sensory features, such as orientation selectivity in the visual cortex using more abstract supra-linear networks with feedback inhibition (Rubin et al., 2015), and the ability to tightly track the stimulus fluctuations in a balanced excitatory-inhibitory regime (Denève and Machens, 2016). Extending the inhibitory-excitatory network model to incorporate the connectivity patterns between different types

of interneurons, including PVs, SOMs and VIPs, required a different set of constraints for explaining cortical tuning properties than when only one inhibitory subtype was used (Litwin-Kumar et al., 2016) (**Figure 3.1B**). Moreover, the resulting network did not require the massive inhibitory feedback consistent with inhibition-stabilized networks to model the observed effects for tuning properties. This was particularly important for understanding the tuning properties of neurons in layers 2/3 of the visual cortex, where only weak inhibition was identified experimentally.

In the auditory cortex, simpler models have already proved useful for understanding the heterogeneity of the effects of optogenetic manipulations. A static model illustrated the origin of the heterogeneous effects of optogenetic perturbations of PVs and SOMs on excitatory neuronal activity by shifting the threshold as well as the strength of inhibitory-excitatory conductances (Seybold et al., 2015). This model demonstrated plausibility that linear scaling and additive effects are produced by the same underlying mechanism – addition followed by rectification. A mutually coupled excitatory-inhibitory firing rate model reproduced the differential effects of manipulating PVs and excitatory neurons on the baseline and tone-evoked responses by adjusting the non-linearity at the inhibitory-excitatory synapse (Aizenberg et al., 2015). Differential synaptic strength of connections between the excitatory and inhibitory neurons could account for the differences between SOM and PV effects on adaptation in excitatory neurons, including flat and saturating non-linearities for synapses between PVs or SOMs and excitatory neurons, respectively (**Figure 3.4B**). The principles outlined by the simplified models illustrate that by manipulating a specific aspect of input integration, the same wiring pattern can produce the heterogeneous results observed experimentally.

Several additional studies have used similar approaches to explore the role of distinct interneurons in cortical processing across sensory modalities. Using a combination of anatomical and optogenetic data in the somatosensory cortex (Avermann et al., 2012), a model could identify correlations in connection strengths between different neuronal subtypes (Tomm et al., 2014). Furthermore, a model of mutually coupled, fast-spiking and non-fast-spiking interneurons, revealed the limitations in the role of fast-spiking neurons in cortical oscillations (Vierling-Claassen et al., 2010). Beyond the sensory cortex, model circuits incorporating several inhibitory interneuron subtypes exhibited recurrent memory across a number of biophysically plausible configurations (Merolla et al., 2014; Markram et al., 2015). Indeed, recurrence in neuronal circuits increased the network's capacity to efficiently store and recall memories (Wang et al., 2004), as originally proposed (Hopfield, 1982). Measuring whether and how inhibitory neuronal populations control and contribute to recurrent activity using recently developed methods for efficient model training (Sussillo, 2014) should prove a fruitful way forward for understanding not only the key cell types that are affected by optogenetic perturbations, but also the time scales of their modulatory effects.

The temporal impact of optogenetic manipulations on auditory activity might differ between opsins, and thus have variable behavioral effects (Guo et al., 2015). Expanding current models to account for the effects of inhibition at a circuit level will clarify how inhibition shapes trajectories of neuronal population dynamics (Loewenstein et al., 2015). In a complex network, where stimulus-evoked activity and neuronal connectivity patterns are highly heterogeneous (Bandyopadhyay et al., 2010; Rothschild et al., 2010; Aizenberg et al., 2015), computational models incorporating mutually coupled excitatory-inhibitory

cells can reveal network features that may otherwise be obscured by results of electrophysiological and imaging experiments, which are biased toward stronger connections (Chambers and MacLean, 2015). Recurrent circuit dynamics may be the dominating feature of cortical circuits, and the interpretation of results based on optogenetic perturbations need to incorporate feedback dynamics in their design (Aljadeff et al., 2015; Landau et al., 2016; Rajan et al., 2016).

As the number of simultaneously observed neurons has increased with recent advances in functional imaging and dense electrophysiological recording techniques, there is a growing need to efficiently represent how units in a large population relate to one another and how these relations change over time (Yatsenko et al., 2015). To meet these demands, current computational approaches address the dynamics of neuronal populations that exhibit non-random dynamics and form higher-degree connectivity (Song et al., 2005; Ko et al., 2013; Timme et al., 2016). The study of the structure of excitatory-inhibitory connectivity can be combined with synaptic organizational principles to understand the basis for cortical dynamics (Ocker et al., 2015; Landau et al., 2016).

One such approach is to apply principles from network science to tracking the dynamics of neuronal cortical populations (**Figure 3.4C**). Network science has been extensively used to characterize large-scale brain networks, revealing modular, hierarchical or random organization (Bassett et al., 2008, 2011). There is extensive evidence that neuronal populations exhibit stereotyped, temporally precise tone-activated patterns of activity in AC (Harris et al., 2011), which are repeated during spontaneous firing, reflecting stereotypical population activity organization (Luczak et al., 2009). Such population activity patterns may differ between the synchronized and the desynchronized

state of the cortical network (Pachitariu et al., 2015), and identifying interconnected modules using network science methods can reveal whether and how the modules are transformed between the different brain states. Shared variability in neuronal populations can potentially be explained by distinct patterns of connections between neurons (Lin et al., 2015), whereas diverse response patterns may correspond to different coupling patterns between single neurons and neuronal populations (Okun et al., 2015) – network analysis of activity in cortical slices already identifies functional modules, that exhibit similar organization across sensory cortex (Sadovsky and MacLean, 2013; Gururangan et al., 2014) (**Figure 3.4C**). Two-photon imaging of calcium activity in large networks of neurons identified similar population activity modes in the auditory cortex (Deneux et al., 2016). Such modes correlated with behavioral responses (Bathellier et al., 2012). Analyzing neuronal activity in terms of population firing rate or activity variability discounts the complex temporal structure of these cellular networks, and thus might underestimate the information contained in neuronal responses (Pachitariu et al., 2015; Kuczala and Sharpee, 2016). Network analysis can furthermore reveal whether and how the neurons within functional modules reorganize with adaptation and learning, and whether specific inhibitory neurons assume specialized roles within networks.

Outlook/future directions.

The diversity of these computational approaches for modeling the function of excitatory – inhibitory circuits and population neuronal activity in cortical sensory processing provides for the basic framework for moving forward in identifying the cortical

circuits involved in auditory scene analysis. The complex effects of network interactions can only partially be understood in the context of natural audition when tested with a limited set of isolated stimuli. To the extent that we can view audition through the lens of temporal processing, recurrent inhibitory-excitatory networks can yield unique capabilities for storing and recalling complex temporal sequences, detecting unexpected events, and recognizing patterns of activation characteristic of more complex stimuli (Aljadeff et al., 2015; Landau et al., 2016; Rajan et al., 2016), such as speech/vocalizations/music. The models should be fitted on data from experiments that would incorporate progressively complex acoustic stimuli; constructed either by varying spectro-temporal complexity, based on the scale-invariant statistical structure of environmental sounds (Geffen et al., 2011; Gervain et al., 2014), or using statistical methods for shaping random signals to match different sound textures (McDermott and Simoncelli, 2011). Taking advantage of the full computational toolset provided by inhibitory-excitatory network modeling, recurrent network dynamics and network science will allow us to tackle the complex richness of cortical circuits and generalize results across sensory modalities and behavioral paradigms.

The use of dynamic analysis tools to explore sets of possible neuronal activity regimes makes inhibitory-excitatory networks a powerful framework for testing hypotheses on population responses in the cortex. The expansion of these models to include different cell types and wiring schemes in combination with analysis of the network structure dynamics is required for understanding the functions and sources of variability within specific neuronal populations. In order to fully understand cortical network function,

our computational models must take into account the field's wealth of data concerning neuronal subtypes, how they are connected locally and to other areas, how they respond to stimuli, and how optogenetic manipulation perturbs them in order to make testable predictions about how these networks behave. Thus, modeling studies need to be combined with a range of experimental techniques that would allow measurement of the strength of synaptic connections between neurons within specific layers and more precisely defined cellular classes.

Figure 3.4

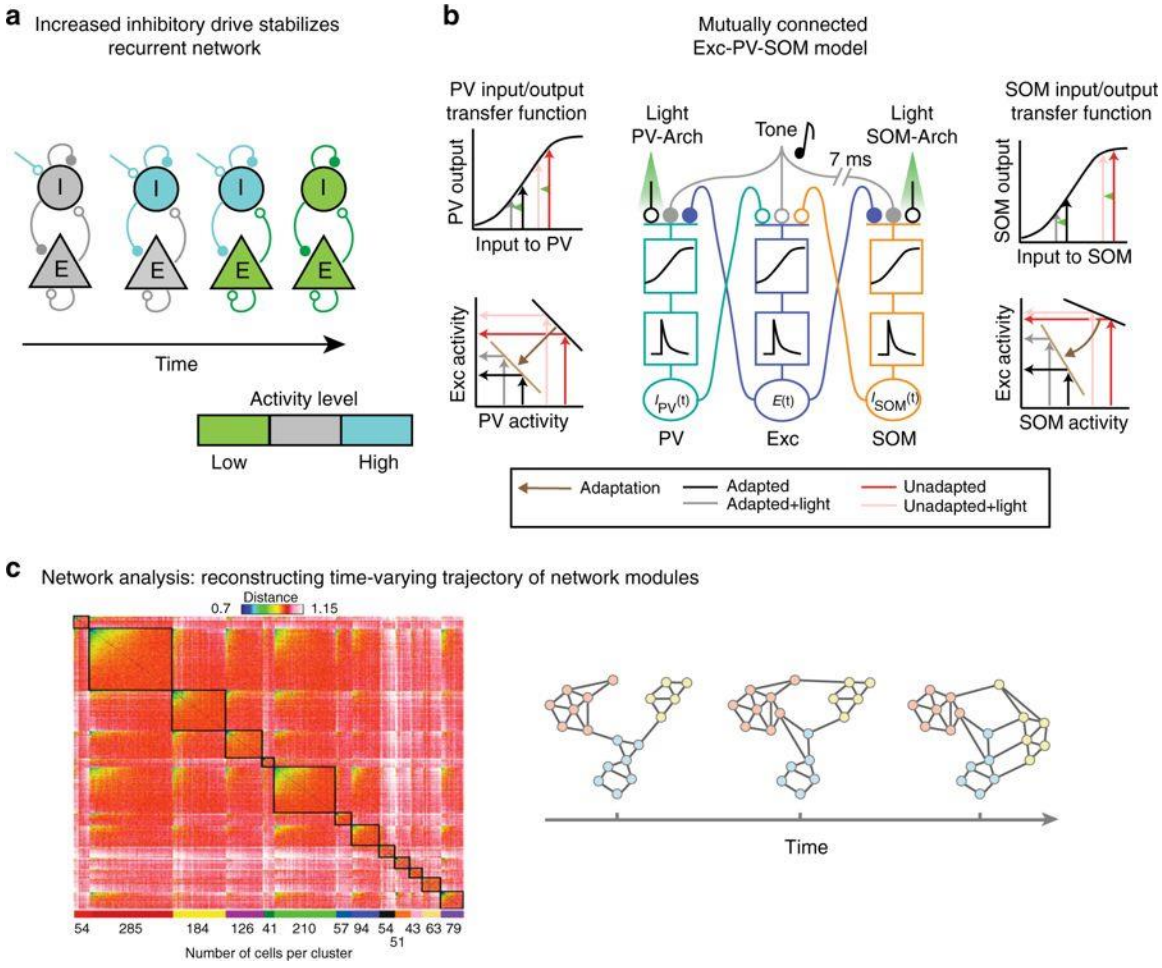
a
Increased inhibitory drive stabilizes recurrent network
I
E
Time
Activity level
Low
High
b
Mutually connected Exc-PV-SOM model
PV input/output transfer function
PV output
Input to PV
Exc activity
PV activity
Light PV-Arch
Tone
7 ms
Light SOM-Arch
SOM input/output transfer function
SOM output
Input to SOM
Exc activity
SOM activity
PV
Exc
SOM
Adaptation
Adapted
Adapted+light
Unadapted
Unadapted+light
c
Network analysis: reconstructing time-varying trajectory of network modules
Distance
0.7
1.15
54
285
184
126
41
210
57
94
54
51
43
63
79
Number of cells per cluster
Time

Figure 3.4 Progressively complex view of cortical dynamics. **A**. Diagram of the time course of inhibition-stabilized recurrent dynamics. Adapted from (Ozeki et al., 2009). **B**. Reduced model of mutually coupled Excitatory (Exc) – PV – SOM network. Exc rate is a non-linear – linear function of excitatory synaptic inputs (filled circles) evoked by the tone, as well as inhibitory inputs (open circles) from PVs and SOMs. PV and SOM firing rate is a non-linear – linear function of excitatory synaptic inputs from excitatory cells and tone-evoked excitatory inputs. Optogenetic manipulation by Arch is modeled as an inhibitory synaptic input. Adapted from (Natan et al., 2015). **C**. Left: network modules identified based on the correlation network structure. Adapted from (Deneux et al., 2016). Right: Diagram of the time course of transformation in brain network structure with learning: Nodes belonging to the same module are colored in the same color. Black lines refer to the edges of the network. Note that with learning, the connectivity within and between modules is transformed. Adapted from (Bassett and Sporns, 2017).

3.1 REFERENCES

Abeles M, Goldstein MH (1970) Functional architecture in cat primary auditory cortex: columnar organization and organization according to depth. J Neurophysiol 33:172–187.

Aizenberg M, Geffen MN (2013) Bidirectional effects of aversive learning on perceptual acuity are mediated by the sensory cortex. Nat Neurosci 16:994–996.

Aizenberg M, Mwilambwe-Tshilobo L, Briguglio JJ, Natan RG, Geffen MN (2015) Bidirectional Regulation of Innate and Learned Behaviors That Rely on Frequency Discrimination by Cortical Inhibitory Neurons. PLoS Biol 13:1–32.

Aljadeff J, Stern M, Sharpee T (2015) Transition to Chaos in Random Networks with Cell-Type-Specific Connectivity. Phys Rev Lett 114:088101.

Avermann M, Tomm C, Mateo C, Gerstner W, Petersen CCH (2012) Microcircuits of excitatory and inhibitory neurons in layer 2/3 of mouse barrel cortex. J Neurophysiol 107:3116–3134.

Bandyopadhyay S, Shamma SA, Kanold PO (2010) Dichotomy of functional organization in the mouse auditory cortex. Nat Neurosci 13:361–368.

Bassett D, Wymbs N, Porter M, Mucha P, Carlson J, Grafton S (2011) Dynamic reconfiguration of human brain networks during learning. PNAS 108:7641–7646.

Bassett DS, Bullmore E, Verchinski BA, Mattay VS, Weinberger DR, Meyer-Lindenberg A (2008) Hierarchical organization of human cortical networks in health and

schizophrenia. J Neurosci 28:9239–9248.

Bassett DS, Sporns O (2017) Network neuroscience. Nat Neurosci 20:353–364.

Bathellier B, Ushakova L, Rumpel S (2012) Discrete Neocortical Dynamics Predict Behavioral Categorization of Sounds. Neuron 76:435–449.

Bregman A (1990) Auditory scene analysis: the perceptual organization of sound. MIT Press.

Chambers B, MacLean JN (2015) Multineuronal activity patterns identify selective synaptic connections under realistic experimental constraints. J Neurophysiol 114:1837–1849.

Chen I-W, Helmchen F, Lütcke H (2015) Specific Early and Late Oddball-Evoked Responses in Excitatory and Inhibitory Neurons of Mouse Auditory Cortex. J Neurosci 35:12560–12573.

Chen QC, Jen PH-S (2000) Bicuculline application affects discharge patterns, rate–intensity functions, and frequency tuning characteristics of bat auditory cortical neurons. Hear Res 150:161–174.

DeFelipe J et al. (2013) New insights into the classification and nomenclature of cortical GABAergic interneurons. Nat Rev Neurosci 14:202–216.

Deneux T, Kempf A, Daret A, Ponsot E, Bathellier B (2016) Temporal asymmetries in auditory coding and perception reflect multi-layered nonlinearities. Nat Commun 7:12682.

Denève S, Machens CK (2016) Efficient codes and balanced networks. Nat Neurosci 19:375–382.

Dykstra AR, Koh CK, Braida LD, Tramo MJ (2012) Dissociation of Detection and Discrimination of Pure Tones following Bilateral Lesions of Auditory Cortex Yan J, ed. PLoS One 7:e44602.

Feng AS, Ratnam R (2000) Neural Basis of Hearing in Real-World Situations. Annu Rev Psychol 51:699–725.

Fino E, Packer AM, Yuste R (2013) The Logic of Inhibitory Connectivity in the Neocortex. Neurosci 19:228–237.

Fu Y, Tucciarone JM, Espinosa JS, Sheng N, Darcy DP, Nicoll RA, Huang ZJ, Stryker MP (2014) A cortical circuit for gain control by behavioral state. Cell 156:1139–1152.

Geffen MN, Gervain J, Werker JF, Magnasco MO (2011) Auditory Perception of Self-Similarity in Water Sounds. Front Integr Neurosci 5:15.

Gervain J, Werker JF, Geffen MN (2014) Category-Specific Processing of Scale-Invariant Sounds in Infancy Malmierca MS, ed. PLoS One 9:e96278.

Gimenez TL, Lorenc M, Jaramillo S (2015) Adaptive categorization of sound frequency does not require the auditory cortex in rats. J Neurophysiol 114:1137–1145.

Guo W, Hight AE, Chen JX, Klapoetke NC, Hancock KE, Shinn-Cunningham BG, Boyden ES, Lee DJ, Polley DB (2015) Hearing the light: neural and perceptual encoding of optogenetic stimulation in the central auditory pathway. Sci Rep 5:10319.

Gururangan SS, Sadovsky AJ, MacLean JN (2014) Analysis of Graph Invariants in Functional Neocortical Circuitry Reveals Generalized Features Common to Three Areas of Sensory Cortex Sporns O, ed. PLoS Comput Biol 10:e1003710.

Hamilton LS, Sohl-Dickstein J, Huth AG, Carels VM, Deisseroth K, Bao S (2013) Optogenetic activation of an inhibitory network enhances feedforward functional connectivity in auditory cortex. Neuron 80:1066–1076.

Harris KD, Bartho P, Chadderton P, Curto C, de la Rocha J, Hollender L, Itskov V, Luczak A, Marguet SL, Renart A, Sakata S (2011) How do neurons work together? Lessons from auditory cortex. Hear Res 271:37–53.

Hopfield JJ (1982) Neural networks and physical systems with emergent collective computational abilities. Proc Natl Acad Sci U S A 79:2554–2558.

Ibrahim LA, Mesik L, Ji X, Fang Q, Li H, Li Y, Zingg B, Zhang LI, Tao HW (2016) Cross-Modality Sharpening of Visual Cortical Processing through Layer-1-Mediated Inhibition and Disinhibition. Neuron 89:1031–1045.

Kato HK, Gillet SN, Isaacson JS, Kato HK, Gillet SN, Isaacson JS (2015) Flexible Sensory Representations in Auditory Cortex Driven by Behavioral Relevance Article Flexible Sensory Representations in Auditory Cortex Driven by Behavioral Relevance. Neuron 88:1027–1039.

Kepecs A, Fishell G (2014) Interneuron cell types are fit to function. Nature 505:318–326.

Ko H, Cossell L, Baragli C, Antolik J, Clopath C, Hofer SB, Mrsic-Flogel TD (2013) The emergence of functional microcircuits in visual cortex. Nature 496:96–100.

Koukouli F, Rooy M, Changeux J-P, Maskos U (2016) Nicotinic receptors in mouse prefrontal cortex modulate ultraslow fluctuations related to conscious processing. Proc Natl Acad Sci U S A 113:14823–14828.

Kuchibhotla K V, Gill J V, Lindsay GW, Papadoyannis ES, Field RE, Sten TAH, Miller KD, Froemke RC (2017) Parallel processing by cortical inhibition enables context-dependent behavior. Nat Neurosci 20:62–71.

Kuczala A, Sharpee TO (2016) Eigenvalue spectra of large correlated random matrices. Phys Rev E 94:050101.

Landau ID, Egger R, Dercksen VJ, Oberlaender M, Sompolinsky H (2016) The Impact of Structural Heterogeneity on Excitation-Inhibition Balance in Cortical Networks. Neuron 92:1106–1121.

Latham PE, Nirenberg S (2004) Computing and Stability in Cortical Networks. Neural Comput 16:1385–1412.

Lee S-H, Kwan AC, Zhang S, Phoumthipphavong V, Flannery JG, Masmanidis SC, Taniguchi H, Huang ZJ, Zhang F, Boyden ES, Deisseroth K, Dan Y (2012) Activation of specific interneurons improves V1 feature selectivity and visual perception. Nature 488:379–383.

Lee S, Kruglikov I, Huang J, Fishell G, Rudy B (2013) A disinhibitory circuit mediates motor integration in the somatosensory cortex. Nat Neurosci 16:1662–1670.

Letzkus JJ, Wolff SBE, Meyer EMM, Tovote P, Courtin J, Herry C, Lu A (2011) A disinhibitory microcircuit for associative fear learning in the auditory cortex. :0–6.

Li L -y., Xiong XR, Ibrahim LA, Yuan W, Tao HW, Zhang LI (2015) Differential Receptive Field Properties of Parvalbumin and Somatostatin Inhibitory Neurons in Mouse Auditory Cortex. Cereb Cortex 25:1782–1791.

Lin I-C, Okun M, Carandini M, Harris KD (2015) The Nature of Shared Cortical Variability. Neuron 87:644–656.

Litwin-Kumar A, Rosenbaum R, Doiron B (2016) Inhibitory stabilization and visual coding in cortical circuits with multiple interneuron subtypes. J Neurophysiol 115:1399–1409.

Liu B, Wu GK, Arbuckle R, Tao HW, Zhang LI (2007) Defining cortical frequency tuning with recurrent excitatory circuitry. Nat Neurosci 10:1594–1600.

Loewenstein Y, Yanover U, Rumpel S (2015) Predicting the Dynamics of Network Connectivity in the Neocortex. J Neurosci 35:12535–12544.

Luczak A, Barthó P, Harris KD (2009) Spontaneous Events Outline the Realm of Possible Sensory Responses in Neocortical Populations. Neuron 62:413–425.

Markram H et al. (2015) Reconstruction and Simulation of Neocortical Microcircuitry. Cell 163:456–492.

Markram H, Toledo-Rodriguez M, Wang Y, Gupta A, Silberberg G, Wu C (2004) Interneurons of the neocortical inhibitory system. Nat Rev Neurosci 5:793–807.

Marlin BJ, Mitre M, D'amour JA, Chao M V., Froemke RC (2015) Oxytocin enables maternal behaviour by balancing cortical inhibition. Nature 520:499–504.

McDermott JH, Simoncelli EP (2011) Sound Texture Perception via Statistics of the Auditory Periphery: Evidence from Sound Synthesis. Neuron 71:926–940.

McGarry LM, Packer AM, Fino E, Nikolenko V, Sippy T, Yuste R (2010) Quantitative classification of somatostatin-positive neocortical interneurons identifies three interneuron subtypes. Front Neural Circuits 4:12.

Merolla P et al. (2014) A million spiking-neuron integrated circuit with a scalable communication network and interface. Science (80-) 345:665–668.

Mesik L, Ma W, Li L, Ibrahim LA, Huang ZJ, Zhang LI, Tao HW (2015) Functional response properties of VIP-expressing inhibitory neurons in mouse visual and auditory cortex. Front Neural Circuits 09:22.

Moore AK, Wehr M (2013) Parvalbumin-Expressing Inhibitory Interneurons in Auditory Cortex Are Well-Tuned for Frequency. J Neurosci 33:13713–13723.

Naka A, Adesnik H (2016) Inhibitory Circuits in Cortical Layer 5. Front Neural Circuits 10:35.

Natan RG, Briguglio JJ, Mwilambwe-Tshilobo L, Jones SI, Aizenberg M, Goldberg EM, Geffen MN (2015) Complementary control of sensory adaptation by two types of cortical interneurons. Elife 4:1–27.

Nelken I (2014) Stimulus-specific adaptation and deviance detection in the auditory system: experiments and models. Biol Cybern 108:655–663.

Nelson A, Schneider DM, Takatoh J, Sakurai K, Wang F, Mooney R (2013) A Circuit for

Motor Cortical Modulation of Auditory Cortical Activity. J Neurosci 33:14342–14353.

Ocker GK, Litwin-Kumar A, Doiron B (2015) Self-Organization of Microcircuits in Networks of Spiking Neurons with Plastic Synapses Latham PE, ed. PLOS Comput Biol 11:e1004458.

Ohl FW, Wetzel W, Wagner T, Rech A, Scheich H (1999) Bilateral ablation of auditory cortex in Mongolian gerbil affects discrimination of frequency modulated tones but not of pure tones. Learn Mem 6:347–362.

Okun M, Steinmetz NA, Cossell L, Iacaruso MF, Ko H, Barthó P, Moore T, Hofer SB, Mrsic-Flogel TD, Carandini M, Harris KD (2015) Diverse coupling of neurons to populations in sensory cortex. Nature 521:511–515.

Oswald A-MM, Schiff ML, Reyes AD (2006) Synaptic mechanisms underlying auditory processing. Curr Opin Neurobiol 16:371–376.

Ozeki H, Finn IM, Schaffer ES, Miller KD, Ferster D (2009) Inhibitory Stabilization of the Cortical Network Underlies Visual Surround Suppression. Neuron 62:578–592.

Pachitariu M, Lyamzin DR, Sahani M, Lesica NA (2015) State-dependent population coding in primary auditory cortex. J Neurosci 35:2058–2073.

Phillips EA, Hasenstaub AR (2016) Asymmetric effects of activating and inactivating cortical interneurons. Elife 5:1–22.

Pi H-J, Hangya B, Kvitsiani D, Sanders JI, Huang ZJ, Kepecs A (2013) Cortical

interneurons that specialize in disinhibitory control. Nature 503:521–524.

Poorthuis RB, Enke L, Letzkus JJ (2014) Cholinergic circuit modulation through differential recruitment of neocortical interneuron types during behaviour. J Physiol 592:4155–4164.

Rajan K, Harvey CD, Tank DW (2016) Recurrent Network Models of Sequence Generation and Memory. Neuron 90:128–142.

Rock C, Apicella A junior (2015) Callosal Projections Drive Neuronal-Specific Responses in the Mouse Auditory Cortex. J Neurosci 35:6703–6713.

Rothschild G, Nelken I, Mizrahi A (2010) Functional organization and population dynamics in the mouse primary auditory cortex. Nat Neurosci 13:353–360.

Roux L, Stark E, Sjulson L, Buzsáki G (2014) In vivo optogenetic identification and manipulation of GABAergic interneuron subtypes. Curr Opin Neurobiol 26:88–95.

Rubin DB, Van Hooser SD, Miller KD (2015) The Stabilized Supralinear Network: A Unifying Circuit Motif Underlying Multi-Input Integration in Sensory Cortex. Neuron 85:402–417.

Rudy B, Fishell G, Lee S, Hjerling-Leffler J (2011) Three groups of interneurons account for nearly 100% of neocortical GABAergic neurons. Dev Neurobiol 71:45–61.

Sadovsky AJ, MacLean JN (2013) Scaling of topologically similar functional modules defines mouse primary auditory and somatosensory microcircuitry. J Neurosci 33:14048–14060.

Schinkel-Bielefeld N, David S V., Shamma SA, Butts DA (2012) Inferring the role of inhibition in auditory processing of complex natural stimuli. J Neurophysiol 107:3296–3307.

Schneider DM, Nelson A, Mooney R (2014) A synaptic and circuit basis for corollary discharge in the auditory cortex. Nature 513:189–194.

Seybold BA, Elizabeth AK, Schreiner CE, Hasenstaub AR, Seybold BA, Phillips EAK, Schreiner CE, Hasenstaub AR (2015) Inhibitory Actions Unified by Network Integration Viewpoint Inhibitory Actions Unified by Network Integration. Neuron 87:1181–1192.

Shamma SA, Fleshman JW, Wiser PR, Versnel H (1993) Organization of response areas in ferret primary auditory cortex. J Neurophysiol 69:367–383.

Song S, Sjöström PJ, Reigl M, Nelson S, Chklovskii DB (2005) Highly Nonrandom Features of Synaptic Connectivity in Local Cortical Circuits Friston KJ, ed. PLoS Biol 3:e68.

Spitzer NC (2017) Neurotransmitter Switching in the Developing and Adult Brain. Annu Rev Neurosci 40:1–19.

Sussillo D (2014) Neural circuits as computational dynamical systems. Curr Opin Neurobiol 25:156–163.

Talwar SK, Gerstein GL (2001) Reorganization in Awake Rat Auditory Cortex by Local Microstimulation and Its Effect on Frequency-Discrimination Behavior. J Neurophysiol 86:1555–1572.

Tan AYY, Wehr M (2009) Balanced tone-evoked synaptic excitation and inhibition in mouse auditory cortex. Neuroscience 163:1302–1315.

Timme NM, Ito S, Myroshnychenko M, Nigam S, Shimono M, Yeh F-C, Hottowy P, Litke AM, Beggs JM (2016) High-Degree Neurons Feed Cortical Computations Pillow JW, ed. PLOS Comput Biol 12:e1004858.

Tomm C, Avermann M, Petersen C, Gerstner W, Vogels TP (2014) Connection-type-specific biases make uniform random network models consistent with cortical recordings. J Neurophysiol 112:1801–1814.

Tramo MJ, Shah GD, Braida LD (2002) Functional Role of Auditory Cortex in Frequency Processing and Pitch Perception. J Neurophysiol 87:122–139.

Tsodyks M V., Skaggs WE, Sejnowski TJ, McNaughton BL (1997) Paradoxical Effects of External Modulation of Inhibitory Interneurons. J Neurosci 17:4382–4388.

Ulanovsky N, Las L, Nelken I (2003) Processing of low-probability sounds by cortical neurons. Nat Neurosci 6:391–398.

Vierling-Claassen D, Cardin JA, Moore CI, Jones SR (2010) Computational Modeling of Distinct Neocortical Oscillations Driven by Cell-Type Selective Optogenetic Drive: Separable Resonant Circuits Controlled by Low-Threshold Spiking and Fast-Spiking Interneurons. Front Hum Neurosci 4:198.

Wang J, Caspary D, Salvi RJ (2000) GABA-A antagonist causes dramatic expansion of tuning in primary auditory cortex. Neuroreport 11:1137–1140.

Wang Y, Toledo-Rodriguez M, Gupta A, Wu C, Silberberg G, Luo J, Markram H (2004) Anatomical, physiological and molecular properties of Martinotti cells in the somatosensory cortex of the juvenile rat. J Physiol 561:65–90.

Wehr M, Zador AM (2003) Balanced inhibition underlies tuning and sharpens spike timing in auditory cortex. Nature 426:442–446.

Williamson RS, Ahrens MB, Linden JF, Sahani M (2016) Input-Specific Gain Modulation by Local Sensory Context Shapes Cortical and Thalamic Responses to Complex Sounds. Neuron 91:467–481.

Wu GK, Arbuckle R, Liu B, Tao HW, Zhang LI (2008) Lateral Sharpening of Cortical Frequency Tuning by Approximately Balanced Inhibition. Neuron 58:132–143.

Yatsenko D, Josić K, Ecker AS, Froudarakis E, Cotton RJ, Tolias AS (2015) Improved Estimation and Interpretation of Correlations in Neural Circuits Pillow JW, ed. PLOS Comput Biol 11:e1004083.

Yavorska I, Wehr M (2016) Somatostatin-Expressing Inhibitory Interneurons in Cortical Circuits. Front Neural Circuits 10:76.

Zhang S, Xu M, Kamigaki T, Do J, Chang W-C, Jenvay S, Miyamichi K, Luo L, Dan Y (2014) Long-range and loca circuits for top-down modulation of visual cortex processing. Science (80-) 345:660–664.

CHAPTER 4: THE ROLE OF FEEDBACK FROM THE AUDITORY CORTEX IN SHAPING RESPONSES TO SOUNDS IN THE INFERIOR COLLICULUS

Adapted from: Blackwell JM, Rao W, De Biasi M, Geffen MN (2019) The role of feedback from the auditory cortex in shaping responses to sounds in the inferior colliculus *bioRxiv* doi: 10.1 101/584334

ABSTRACT

The extensive feedback from the auditory cortex (AC) to the inferior colliculus (IC) supports critical aspects of auditory learning, but has not been extensively characterized. Furthermore, it remains unknown whether and how intra-cortical processing of auditory information propagates to earlier stages in the auditory pathway. Previous studies demonstrated that responses of neurons in IC are altered by focal electrical stimulation and pharmacological inactivation of auditory cortex, but these methods lack the ability to selectively manipulate the activity of projection neurons. Combining viral technology with electrophysiological recordings, we measured the effects of selective optogenetic activation or suppression of cortico-collicular feedback projections on IC responses to sounds. Activation of cortico-collicular feedback generally increased spontaneous activity and decreased stimulus selectivity in IC, whereas suppression of the feedback did not affect

collicular activity. To further understand how microcircuits in the auditory cortex may control collicular activity, we tested the effects of optogenetically modulating different cortical neuronal subtypes, specifically parvalbumin-positive (PV) and somatostatin-positive (SOM) inhibitory interneurons. We found that, despite strong effects on sound-evoked responses across the layers of AC, activating either type of interneuron did not affect IC sound-evoked activity. However, suppression of SOMs, but not PVs, weakly increased spontaneous activity in IC. These findings suggest that shaping of sound responses mediated by cortical inhibition does not affect sound processing in the IC of passive awake mice. Combined, our results identify that activation of excitatory projections, but not inhibitory-driven increases in cortical activity, affects collicular sound responses.

4.1 INTRODUCTION

A common view of information processing within a sensory pathway is that the information about the stimulus ascends along the hierarchy of sensory areas, with each area performing a computation increasing in complexity. In this framework, the role of descending feedback between these nuclei is often overlooked. In the auditory system, the auditory cortex (AC) sends extensive feedback to nuclei earlier in the auditory pathway, including the auditory thalamus (Winer et al., 2001; Alitto and Usrey, 2003; Rouiller and Durif, 2004) and the auditory midbrain (Saldaña et al., 1996; Winer et al., 1998; Doucet et al., 2003; Bajo and Moore, 2005; Coomes et al., 2005; Bajo et al., 2007). Whereas the way the information is processed and integrated between brain areas along the *ascending*

pathway has been extensively studied, the mechanisms by which information processing is shaped via the *descending feedback* pathway remains poorly characterized. In this study, we examined how modulation of activity in the auditory cortex, selectively targeting excitatory projections or inhibitory interneurons, shapes spontaneous activity and sound-evoked responses in the auditory midbrain nucleus, the inferior colliculus (IC).

Previous studies demonstrated that neuronal responses to sounds in IC are altered by focal electrical stimulation and inactivation of AC. Cortical stimulation shifted tuning properties of IC neurons toward those of the stimulated neurons in frequency (Jen et al., 1998; Yan and Suga, 1998; Ma and Suga, 2001a; Jen and Zhou, 2003; Yan et al., 2005; Zhou and Jen, 2007), amplitude (Jen and Zhou, 2003; Yan et al., 2005; Zhou and Jen, 2007), azimuth (Zhou and Jen, 2005, 2007), and duration (Ma and Suga, 2001b). Stimulation of AC had mixed effects on sound-evoked responses in IC, increasing and decreasing responses in different subpopulations of neurons (Jen et al., 1998; Zhou and Jen, 2005). Consistent with this effect, different patterns of direct cortico-collicular activation enhanced or suppressed white noise-induced responses in IC (Vila et al., 2019). AC inactivation studies, on the other hand, found less consistent effects on IC responses. Whereas pharmacological inactivation of AC caused a shift in best frequency in IC neurons (Zhang et al., 1997), several studies show inactivation of AC had no effect on frequency selectivity in IC (Jen et al., 1998), but rather modulated sound-evoked and spontaneous activity (Gao and Suga, 1998; Popelář et al., 2003, 2016). Cortico-collicular feedback is critical to auditory learning, specifically learning to adapt to a unilateral earplug during sound localization (Bajo et al., 2010). Pairing electrical leg stimulation with a tone induced a shift in best frequency of IC neurons, while presentation of a tone alone was insufficient

(Gao and Suga, 1998, 2000). Furthermore, cortico-collicular feedback was necessary to induce running in response to a loud noise (Xiong et al., 2015).

In AC, interactions between excitation and inhibition shape sound responses in excitatory cell populations. Modulating activity of different inhibitory interneuron subtypes in AC narrowed frequency tuning and attenuated tone-evoked responses of excitatory neurons, while suppression had the opposite effect (Hamilton et al., 2013; Aizenberg et al., 2015; Seybold et al., 2015; Phillips and Hasenstaub, 2016). Electrical stimulation of AC, cooling or pharmacological inactivation affected the amplitude of sound-evoked responses and shifted the best frequency of neurons in IC, but it remains unknown how specific these effects are to direct feedback and whether the effects of intra-cortical inhibition propagate to the IC.

The goal of the present study is to examine the role of cortico-collicular projections in shaping sound responses in IC. We used viral transfection methods to selectively drive excitatory or inhibitory opsin expression in IC-projecting neurons in AC. We then recorded neuronal activity in IC and tested how activation or suppression of cortico-collicular projections affected spontaneous activity and sound-evoked responses in IC neurons. IC receives glutamatergic (Feliciano and Potashner, 1995) inputs from neurons originating predominantly in layer 5 of AC (Saldaña et al., 1996; Winer et al., 1998; Doucet et al., 2003; Bajo and Moore, 2005; Coomes et al., 2005; Bajo et al., 2007). As previously mentioned, inhibitory interneurons shape sound response of excitatory neurons in AC. To better understand whether and how intra-cortical network interactions propagated to IC, we manipulated the activity of the two most common inhibitory neuronal subtypes in AC, Parvalbumin-(PV) and Somatostatin-(SOM) positive interneurons (Rudy et al., 2011). We

then recorded neuronal activity in AC and IC and tested how activation or suppression of AC inhibitory interneurons affected spontaneous activity and sound-evoked responses in IC neurons and compared this to how these manipulations affected activity in AC. This study elucidates how descending auditory feedback shapes downstream auditory processing.

4.2 RESULTS

Activating direct cortico-collicular feedback modulates activity in the inferior colliculus

Our first goal was to characterize the effects of activating the direct cortico-collicular projections on tone-evoked responses in IC. We used a viral transfection strategy to deliver either an excitatory opsin, ChannelRhodopsin2 (ChR2) or an inhibitory opsin, ArchaerhodopsinT (ArchT), bilaterally, specifically to the neurons in the auditory cortex which project to the inferior colliculus. To achieve such specificity, we injected a retrograde virus that encoded Cre recombinase (Retro2 AAV.Cre) in IC. This retrograde viral construct ensured that neurons projecting to IC expressed Cre recombinase a few weeks later. At the same time, we injected a virus that encoded ChR2 or ArchT in reversed fashion under the FLEX cassette in AC (AAV.Flex.ChR2, AAV.Flex.ArchT). This strategy ensured that only neurons expressing Cre recombinase in the auditory cortex would express ChR2 or ArchT in AC. Therefore, opsin was expressed exclusively in AC-IC projecting neurons (**Figure 4.1 A,B**). Shining light over AC of these mice would therefore directly activate or suppress only these cortico-collicular feedback projections.

First, we measured and quantified neuronal spiking in IC in response to stimulation or suppression of cortico-collicular projections. To activate these neurons, we shone blue laser over AC, recorded neuronal activity in IC, and quantified the effects of manipulating feedback in the absence of sound (**Figure 4.1 E,F**). We measured the spiking activity as we varied the duration of laser manipulation (1 ms, 5 ms, 25 ms, 250 ms). As expected, activation of cortico-collicular neurons resulted, on average, in an increase in firing rate of IC neurons. This effect persisted at all laser durations we used. Specifically, for all durations the distribution of the change in activity with activation was significantly different from normally distributed around zero (**Figure 4.1E**; 1 ms: p = 3.07e-15, mean = 1.1 stdevs, median = 0.21 stdevs; 5 ms: p = 4.4e-20, mean = 1.7 stdevs, median = 0.19 stdevs; 25 ms: p = 5.5e-17, mean = 1.6 stdevs, median = -0.021 stdevs; 250 ms: p = 3.4e-12, mean = 0.58 stdevs, median = 0.101 stdevs, Kolmogorov-Smirnov test). Whereas the direction of the effect was consistent with our prior expectations, the magnitude of the effect was unexpectedly small. This suggests that AC targets a small subpopulation of IC neurons and that the effect of activation does not spread too far within IC.

We tested the effect of suppressing AC-IC neurons on firing responses in IC and, surprisingly, we detected no difference in firing in IC neurons. For all laser durations the population of responses were normally distributed around zero change in activity (**Figure 4.1F**). This result suggests that AC-IC inputs at rest do not contribute to IC responses, but rather modulate collicular activity only when activated.

Next, our goal was to characterize modulation of sound-evoked responses in IC by cortical feedback. We first tested the effects of feedback modulation on acoustic click responses. We chose clicks as the initial stimulus because they drive fast responses in both

AC and IC. Laser stimulation began 250 ms prior to click train onset to allow for the response to the laser to come to a steady state, and continued activation throughout the clicks. Activating the feedback had a weak suppressive effect on the firing rate of IC neurons in response to clicks. Consistent with previous experiments, we observed an overall increase in spontaneous activity (**Figure 4.1G**, bottom; $p = 0.0031$, spont ON = 5 ± 0.87 Hz, spont OFF = 4.3 ± 0.92 Hz). Activating feedback caused a small decrease in click-evoked response (**Figure 4.1G**, left; $p = 0.001$, click ON = 10.4 ± 1.2 Hz, click OFF = 10.7 ± 1.1 Hz).

By contrast, suppressing cortico-collicular feedback using ArchT had no effect on IC click responses (**Figure 4.1H**). Because attenuating the input does not affect the activity in IC during clicks this result further suggests that the strength of the baseline signal from AC to IC, even in the presence of cortical activity, is not sufficient to modulate IC responses.

We also tested whether the effects of cortico-collicular modulation differed across the receptive field of collicular neurons. We presented a stimulus that consisted of tones of 50 frequencies ranging from 3 to 70 kHz. To modulate the feedback from AC, we tested three different laser onsets (-100 ms, -20 ms, +8 ms) relative to tone onset to isolate the effect of timing on affecting IC responses. These delays were chosen for the following reasons: -100ms delay would allow for the laser effect on cortical activity to come to a steady state, making it easier to quantify the effect throughout the tone pip; +8 ms is set up to mimic the time scale of cortical response to a tone, effectively amplifying the onset of the cortical response; -20 ms delay is an intermediate value.

Figure 4.1

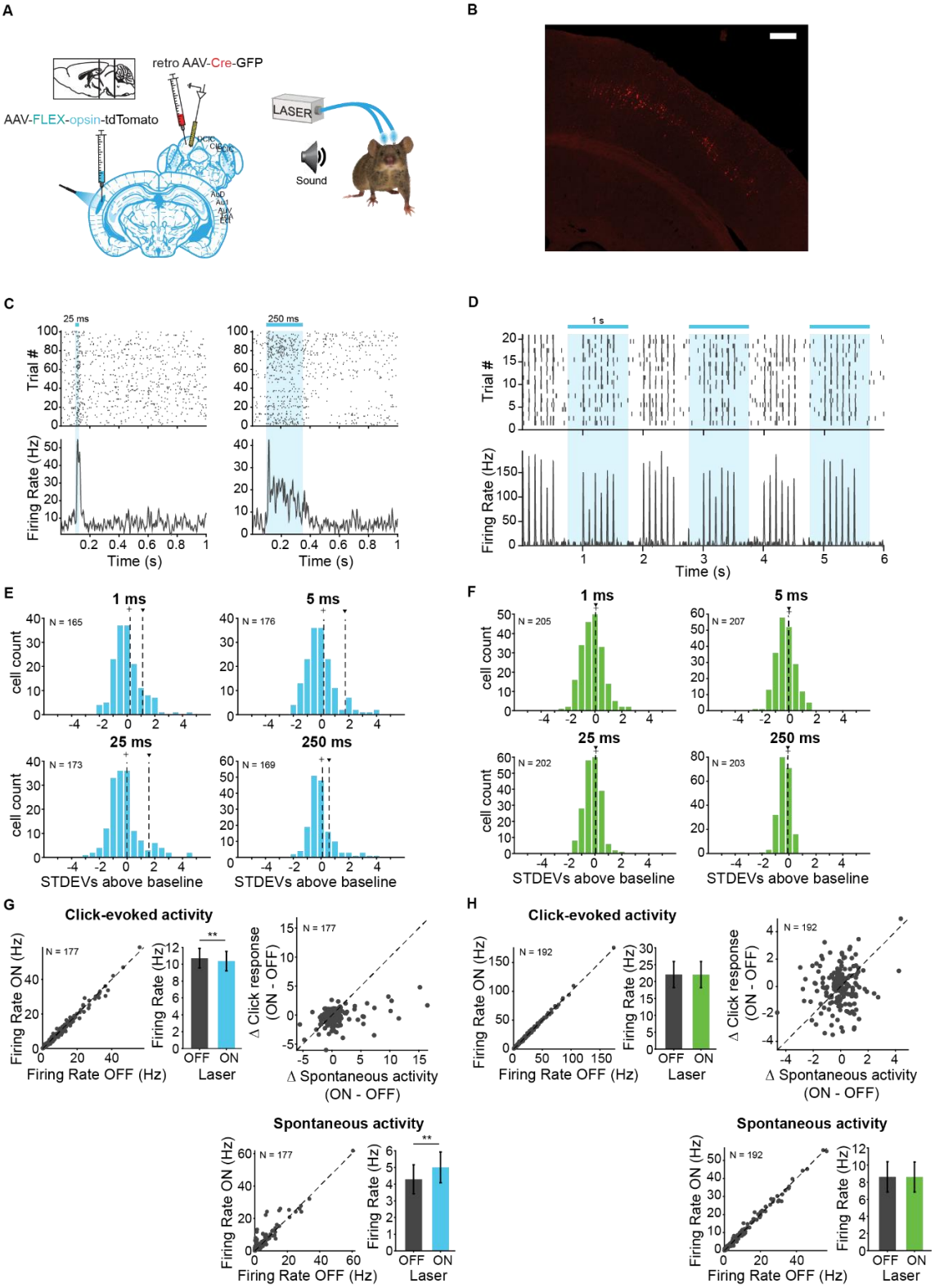
A
retro AAV-Cre-GFP
AAV-FLEX-opsin-tdTomato
LASER
Sound
B
C
25 ms
250 ms
Trial #
Firing Rate (Hz)
Time (s)
D
1 s
Trial #
Firing Rate (Hz)
Time (s)
E
1 ms
5 ms
25 ms
250 ms
N = 165
N = 176
N = 173
N = 169
cell count
STDEVs above baseline
F
1 ms
5 ms
25 ms
250 ms
N = 205
N = 207
N = 202
N = 203
cell count
STDEVs above baseline
G
Click-evoked activity
N = 177
Firing Rate ON (Hz)
Firing Rate OFF (Hz)
Firing Rate (Hz)
OFF ON
Laser
Δ Click response (ON - OFF)
Δ Spontaneous activity (ON - OFF)
Spontaneous activity
N = 177
Firing Rate ON (Hz)
Firing Rate OFF (Hz)
Firing Rate (Hz)
OFF ON
Laser
H
Click-evoked activity
N = 192
Firing Rate ON (Hz)
Firing Rate OFF (Hz)
Firing Rate (Hz)
OFF ON
Laser
Δ Click response (ON - OFF)
Δ Spontaneous activity (ON - OFF)
Spontaneous activity
N = 192
Firing Rate ON (Hz)
Firing Rate OFF (Hz)
Firing Rate (Hz)
OFF ON
Laser

Figure 4.1 Effects of modulating feedback activity on responses in IC in the absence of sounds and to clicks. **A** Experimental design: Injection of retro AAV.Cre into IC and anterograde AAV.Flex.opsin into AC and record from IC (left) in awake mice while shining laser into AC, all performed bilaterally (right). **B** Image of opsin-tdTomato expression in cortico-collicular feedback projections in AC. Scale bar: 200um. **C** Example unit response to two laser pulse durations (blue), 25 ms (left) and 250 ms (right). **D** Example unit response to clicks with (blue) and without laser. **E** Distributions of change in unit activity in response to different laser durations in ChR2 cohort (1 ms, 5 ms, 25 ms, 250 ms), + indicates median, ▼ indicates mean. These distributions are not normally distributed (Kolmogorov-Smirnov test; *1 ms*: p = 3.07e-15, mean = 1.1 stdevs, median = 0.21 stdevs; *5 ms*: p = 4.4e-20, mean = 1.7 stdevs, median = 0.19 stdevs; *25 ms*: p = 5.5e-17, mean = 1.6 stdevs, median = -0.021 stdevs; *250 ms*: p = 3.4e-12, mean = 0.58 stdevs, median = 0.101 stdevs). **F** Distributions of change in unit activity in response to different laser durations in ArchT cohort (1 ms, 5 ms, 25 ms, 250 ms), + indicates median, ▼ indicates mean. These distributions are normally distributed (Kolmogorov-Smirnov test). **G** Population response to clicks with activation shows a decrease in click response (left; p = 0.001, click ON = 10.4 ± 1.2 Hz, click OFF = 10.7 ± 1.1 Hz) and an increase in spontaneous activity (bottom; p = 0.0031, spont ON = 5 ± 0.87 Hz, spont OFF = 4.3 ± 0.92 Hz). **H** Population response to clicks with suppression shows no change in activity.

We found that whereas activating feedback increased spontaneous activity of IC neurons (**Figure 4.2A**, left; -100 ms: p = 0.022, ON = 4.3 ± 0.47 Hz; OFF = 3.6 ± 0.38; -20 ms: p = 8.6e-6, ON = 5.6 ± 0.63, OFF = 3.7 ± 0.47), overall the feedback decreased tone-evoked response magnitude in IC, which we defined as the difference between spontaneous and tone-evoked response, at all laser onsets (**Figure 4.2A**, right; *-100 ms*: p = 3.2e-5, ON = 14.2 ± 0.98 Hz; OFF = 15.5 ± 1.04 Hz; *-20 ms*: p = 1.4e-6, ON = 11.8 ± 1.08 Hz, OFF = 13.9 ± 1 Hz; *+8 ms*: p = 0.0034, ON = 13.03 ± 1.03, OFF = 13.7 ± 1.03). This suggests that the broad activation of feedback upregulates the baseline activity of IC neurons, but decreases tone-evoked response (**Figure 4.3E**). By contrast, suppressing the feedback had no effect on either spontaneous activity or tone-evoked response magnitude (**Figure 4.2B**), suggesting that at baseline, AC does not provide strong modulation of IC activity, as removing it does not affect sound-evoked effects in IC.

Figure 4.2

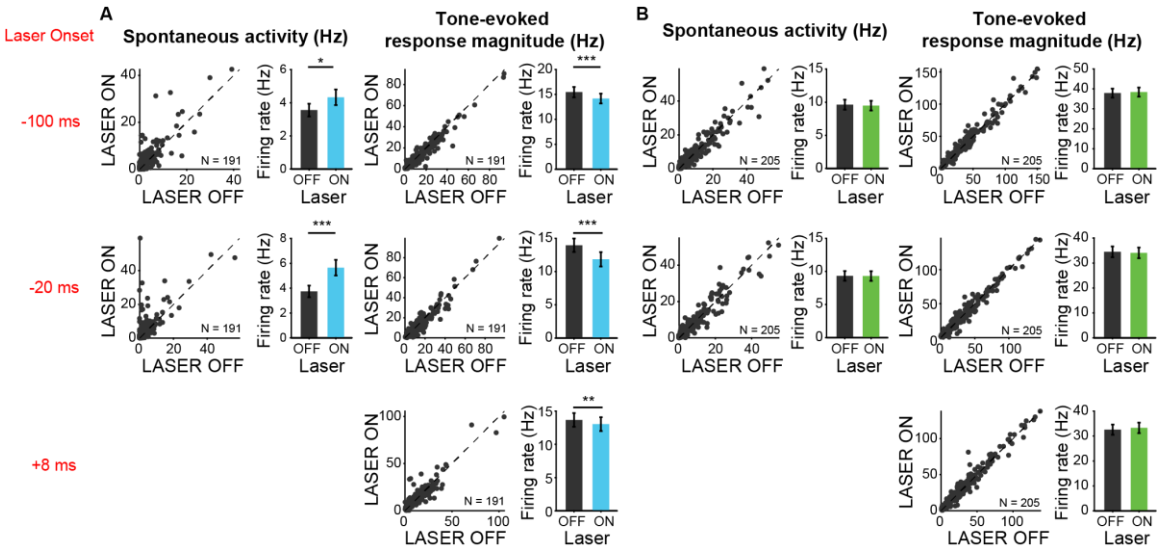
A
B
Laser Onset
Spontaneous activity (Hz)
Tone-evoked response magnitude (Hz)
-100 ms
-20 ms
+8 ms
LASER ON
LASER OFF
Firing rate (Hz)
OFF ON
Laser
N = 191
N = 205
*
**
***

Figure 4.2 Effects of modulating feedback activity on spontaneous and tone-evoked response magnitude in IC. Left panels: neuronal activity (spontaneous, left or tone-evoked, right) on laser on versus laser off trials. Right panels: Average neuronal activity (spontaneous, left or tone-evoked, right) for laser on and laser off trials. **A** Activating feedback increased spontaneous activity (left; -*100 ms*: p = 0.022, ON = 4.3 ± 0.47 Hz; OFF = 3.6 ± 0.38; -*20 ms*: p = 8.6e-6, ON = 5.6 ± 0.63, OFF = 3.7 ± 0.47) and decreased tone-evoked response magnitude (right; -*100 ms*: p = 3.2e-5, ON = 14.2 ± 0.98 Hz; OFF = 15.5 ± 1.04 Hz; -*20 ms*: p = 1.4e-6, ON = 11.8 ± 1.08 Hz, OFF = 13.9 ± 1 Hz; +*8 ms*: p = 0.0034, ON = 13.03 ± 1.03, OFF = 13.7 ± 1.03). **B** Suppressing feedback had no effect on spontaneous activity or tone-evoked response magnitude.

We then examined the effect of feedback on frequency tuning of IC units. Activation of feedback decreased frequency selectivity in the subsets of units that also showed a decrease in tone-evoked response magnitude or increase in spontaneous activity, but not in units that showed an increase in tone-evoked response magnitude or decrease in spontaneous activity (**Figure 4.3A**, mag decrease: *-20 ms*, p = 0.00031, sparse ON = 0.49 ± 0.027, sparse OFF = 0.55 ± 0.025; *+8 ms*, p = 0.00029, sparse ON = 0.46 ± 0.027, sparse OFF = 0.55 ± 0.024; spont increase: *-100 ms*, p = 0.011, sparse ON = 0.49 ± 0.032, sparse OFF = 0.56 ± 0.031; *-20 ms*, p = 0.00018, sparse ON = 0.46 ± 0.034, sparse OFF = 0.56 ± 0.029; *+8 ms*, p = 2.2e-6, sparse ON = 0.41 ± 0.032, sparse OFF = 0.55 ± 0.029**)**. Over the population of neurons with decreased tone-evoked response magnitude and/or increased spontaneous activity, the median slopes and y-intercepts of ranked linear fits to frequency responses are less than 1 and above zero, respectively (**Figure 4.3D**). These results, in combination with the decreased tone-evoked activity observed (**Figure 4.3E**, *-100 ms*: p = 0.018, ON = 19.01 ± 1.2 Hz, OFF = 18.5 ± 1.2 Hz; *+8 ms*: p = 0.007, ON = 17.3 ± 1.2 Hz; OFF = 16.9 ± 1.2 Hz), indicate the decrease in frequency selectivity was due to a decrease in response to tones at preferred frequencies, not non-preferred frequencies. This result suggests that the suppressive effect of the feedback is preferential for higher firing responses. Suppressing feedback resulted in very small (< 0.04 %) change in sparseness, therefore it did not affect frequency selectivity (**Figure 4.3B**).

Figure 4.3

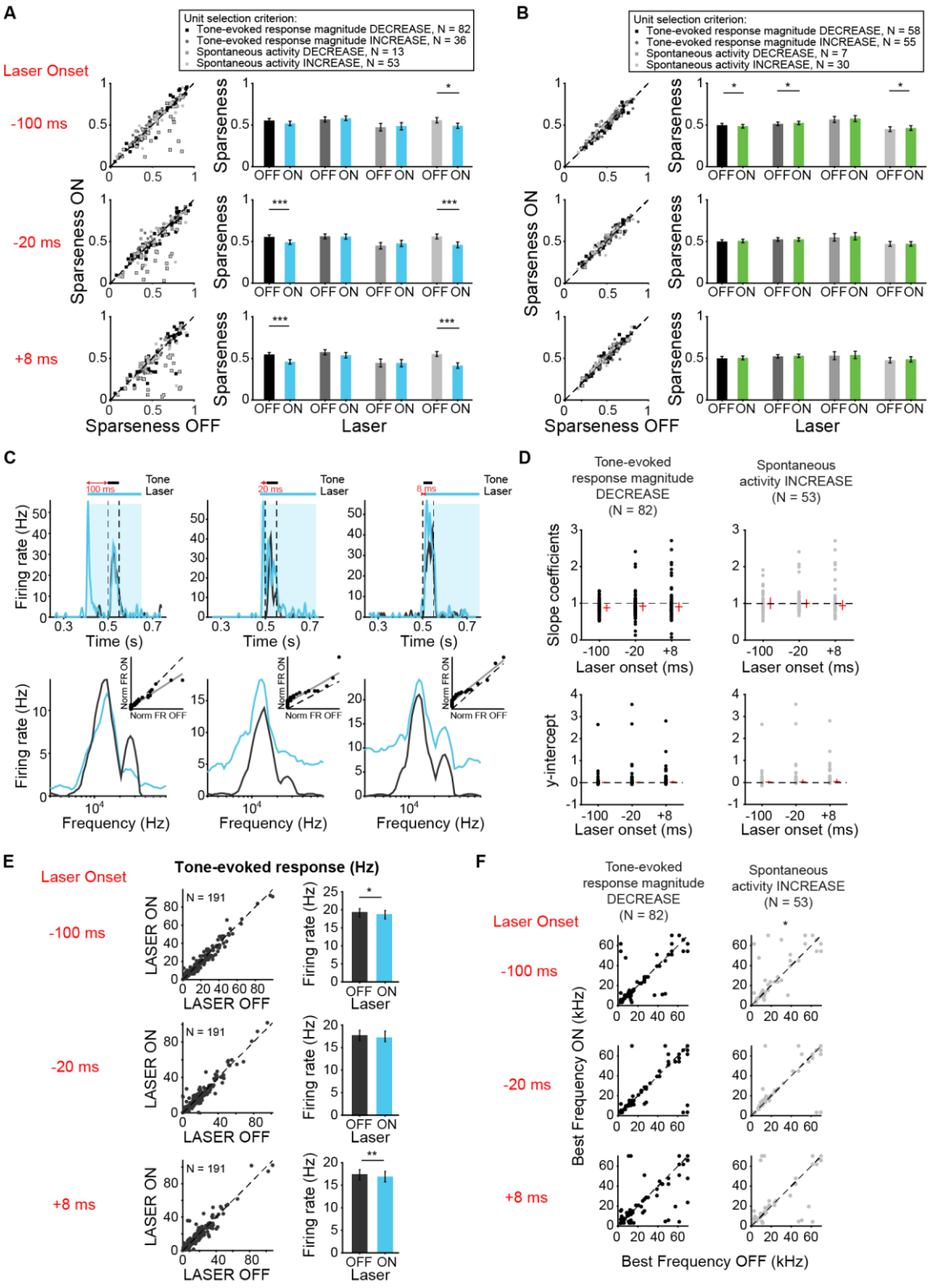
A
Unit selection criterion:
Tone-evoked response magnitude DECREASE, N = 82
Tone-evoked response magnitude INCREASE, N = 36
Spontaneous activity DECREASE, N = 13
Spontaneous activity INCREASE, N = 53
Laser Onset
-100 ms
-20 ms
+8 ms
Sparseness ON
Sparseness OFF
Sparseness
Laser
OFF ON
B
Unit selection criterion:
Tone-evoked response magnitude DECREASE, N = 58
Tone-evoked response magnitude INCREASE, N = 55
Spontaneous activity DECREASE, N = 7
Spontaneous activity INCREASE, N = 30
C
Tone
Laser
100 ms
20 ms
8 ms
Firing rate (Hz)
Time (s)
Norm FR ON
Norm FR OFF
Frequency (Hz)
D
Tone-evoked response magnitude DECREASE (N = 82)
Spontaneous activity INCREASE (N = 53)
Slope coefficients
y-intercept
Laser onset (ms)
E
Tone-evoked response (Hz)
Laser Onset
-100 ms
-20 ms
+8 ms
N = 191
LASER ON
LASER OFF
Firing rate (Hz)
OFF ON
Laser
F
Tone-evoked response magnitude DECREASE (N = 82)
Spontaneous activity INCREASE (N = 53)
Laser Onset
-100 ms
-20 ms
+8 ms
Best Frequency ON (kHz)
Best Frequency OFF (kHz)

Figure 4.3 Effect of modulating direct cortico-collicular feedback at different latencies relative to tone onset on frequency selectivity in IC. **A** Left panels: Sparseness for laser on versus laser off trials. Right panels: Average sparseness for laser on and laser off trials. Activating feedback decreased frequency selectivity in a subset of units (mag decrease: *-20 ms*, p = 0.00031, sparse ON = 0.49 ± 0.027, sparse OFF = 0.55 ± 0.025; *+8 ms*, p = 0.00029, sparse ON = 0.46 ± 0.027, sparse OFF = 0.55 ± 0.024; spont increase: *-100 ms*, p = 0.011, sparse ON = 0.49 ± 0.032, sparse OFF = 0.56 ± 0.031; *-20 ms*, p = 0.00018, sparse ON = 0.46 ± 0.034, sparse OFF = 0.56 ± 0.029; *+8 ms*, p = 2.2e-6, sparse ON = 0.41 ± 0.032, sparse OFF = 0.55 ± 0.029). **B** Left panels: Sparseness for laser on versus laser off trials. Right panels: Average sparseness for laser on and laser off trials. Suppressing feedback has little effect on frequency selectivity (mag decrease: -100 ms, p = 0.011, sparse ON = 0.53 ± 0.021, sparse OFF = 0.51 ± 0.021; mag increase: -100 ms, p = 0.019, sparse ON = 0.48 ± 0.021, sparse OFF = 0.49 ± 0.021; spont increase: -100 ms, p = 0.043, sparse ON = 0.46 ± 0.029, sparse OFF = 0.45 ± 0.029). **C** Example unit response timecourse (top) and tuning curves (bottom) for laser on (blue) and laser off (grey) conditions. Bottom insets represent ranked linear fits for example unit. **D** Slope coefficients (top, mag decrease: *-100 ms*, median = 0.88; *-20 ms*, median = 0.92; *+8 ms*, median = 0.903; spont increase: *-100 ms*, median = 0.99; *-20 ms*, median = 1; *+8 ms*, median = 0.94) and y-intercepts (bottom, mag decrease: *-100 ms*, median = 0.0086; *-20 ms*, median = 0.014; *+8 ms*, median = 0.022; spont increase: *-100 ms*, median = 0.014; *-20 ms*, median = 0.025; *+8 ms*, median = 0.037) of ranked linear fits, red horizontal lines indicate median, red vertical lines indicate interquartile range. **E** Left panels: Tone-evoked response for laser on versus laser off trials. Right panels: Average tone-evoked response for laser on and laser off trials. Activating

feedback slightly decreased tone-evoked response, averaged across 7 most preferred frequencies (*-100ms*: p = 0.018, ON = 19.01 ± 1.2 Hz, OFF = 18.5 ± 1.2 Hz; *+8ms*: p = 0.007, ON = 17.3 ± 1.2 Hz; OFF = 16.9 ± 1.2 Hz) **F** Best frequencies for laser off versus laser on trials. Activating feedback had little effect on best frequency (spont increase: *-100 ms*, p = 0.022).

To better understand the effect of modulation of cortical activity on spectro-temporal receptive field properties of IC neurons, we presented a continuous signal comprised of dynamic random chords (DRCs) sampled from a uniform distribution of loudness values per frequency bin. The unbiased nature of this stimulus allowed us to estimate the spectro-temporal receptive field of neurons (STRF), which quantifies the dynamics of sound waveform in time and frequency that lead to a neuronal response. During the DRC stimulus, we turned on the laser every other second for 250 ms to either activate or suppress cortico-collicular projections. We found that a subset of cells reduced their mean DRC-evoked firing rates (N = 56), whereas another subset of cells increased their mean DRC-evoked firing rate when we activated cortico-collicular feedback (N = 47). We next separately computed the receptive fields for each neuron when laser was off and when laser was on and compared the STRFs. To quantify those changes, we identified the positive (activation) and negative (suppressive) regions in the STRFs and compared them for laser ON and laser OFF conditions. In the subset of neurons whose firing rate increased with laser STRFs changed: only 42% of positive lobes, and 63% of negative lobes persisted with the laser (**Figure 4.4B**, left). Of those lobes that persisted, for positive lobes, there was on average a decrease in temporal width ($p = 0.00098$, ON = 0.0303 ± 0.0018 s, OFF = 0.037 ± 0.0023 s), frequency selectivity ($p = 0.00042$, ON = 6.7 ± 1.1 Hz, OFF = 9.6 ± 1.8 Hz) and STRF size ($p = 0.00036$, ON = 46.05 ± 6.9 pixels, OFF = 77.5 ± 12.04 pixels), whereas for negative lobes, we did not detect any changes (**Figure 4.4C**, left). In neurons whose firing rate was decreased, there was a much smaller change in the lobes, with 78% and 79% of positive and negative lobes persisting, respectively (**Figure 4.4B**, right). For both positive lobes and negative lobes, the only difference was an increase in the temporal

width when laser was activated (**Figure 4.4C**, right; Positive lobes: p = 0.026, ON = 0.034 ±0.0025 s, OFF = 0.032 ± 0.0025 s; Negative lobes: p = 0.02, ON = 0.037 ± 0.0028 s, OFF = 0.032 ± 0.0024 s). The decrease in STRF size in units with increased DRC-evoked response and decrease in sparseness across the population is consistent with the interpretation that the effect of the feedback leads to a decrease in responsiveness to tones that evoke the greatest responses (in the center of the receptive field) and an increase to stimuli that evoke weaker activity. In other words, neuronal firing increases overall, but selective responses to specific frequency bands decrease.

Figure 4.4

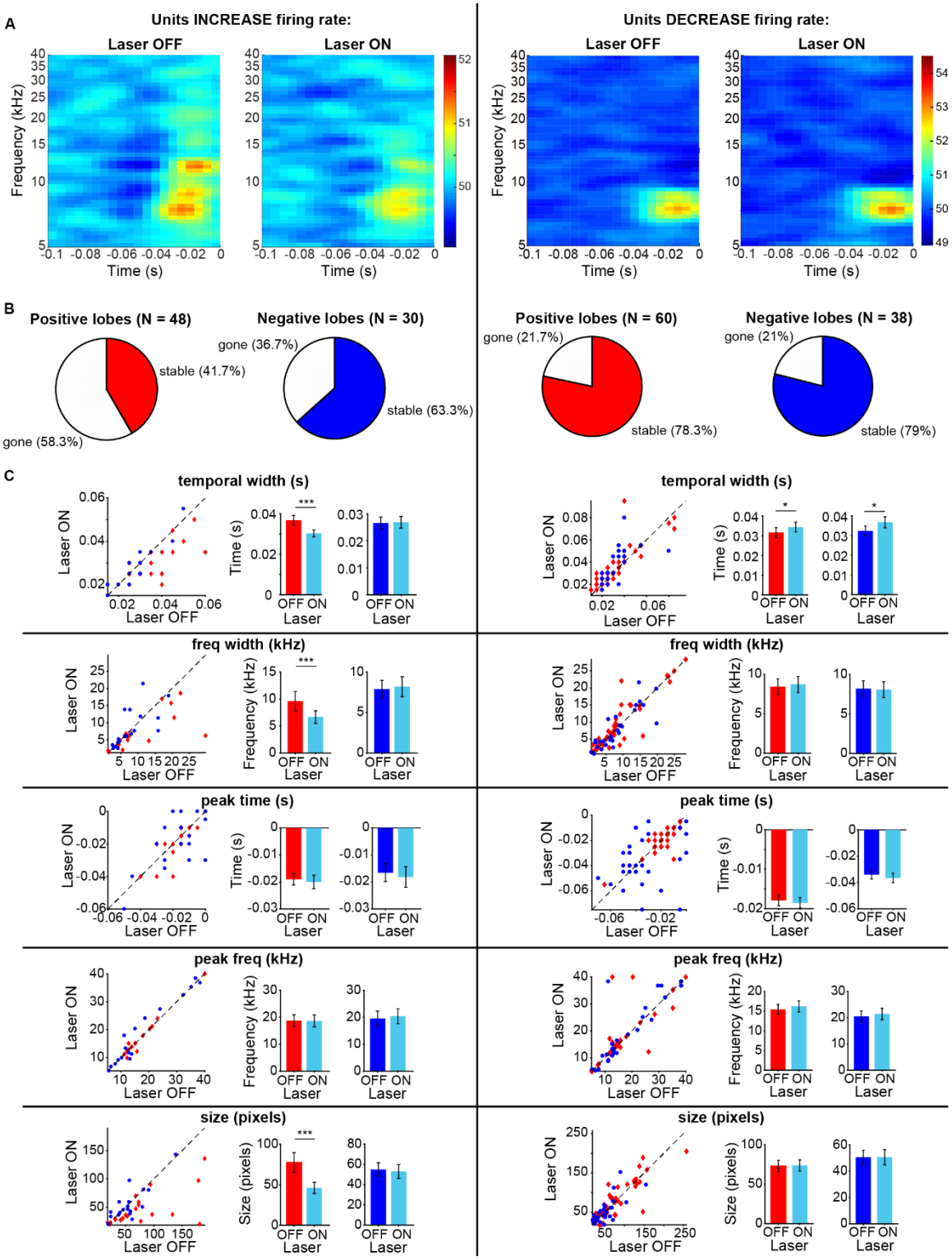
A
Units INCREASE firing rate:
Laser OFF
Laser ON
Frequency (kHz)
Time (s)
Units DECREASE firing rate:
B
Positive lobes (N = 48)
Negative lobes (N = 30)
gone (58.3%)
stable (41.7%)
gone (36.7%)
stable (63.3%)
Positive lobes (N = 60)
Negative lobes (N = 38)
gone (21.7%)
stable (78.3%)
gone (21%)
stable (79%)
C
temporal width (s)
freq width (kHz)
peak time (s)
peak freq (kHz)
size (pixels)
Laser ON
Laser OFF
Time (s)
Frequency (kHz)
Size (pixels)
OFF ON
Laser

Figure 4.4 Effects of activating direct cortico-collicular feedback on STRF properties. **A** Example STRF with and without activation of feedback for units that increase firing rate (left) and decrease firing rate (right) in response to feedback activation. **B** Number of positive and negative lobes that persisted with laser (stable). **C** Changes in STRF parameters of stable positive and negative lobes. Left panels: STRF parameter for laser off versus laser on trials. Center panels: Average positive lobe STRF parameter for laser on and laser off trials. Right panels: Average negative lobe STRF parameter for laser on and laser off trials. For units with an increase in firing rate we observed a decrease in temporal width ($p = 0.00098$, ON = 0.0303 ± 0.0018 s, OFF = 0.037 ± 0.0023 s), frequency width ($p = 0.00042$, ON = 6.7 ± 1.1 Hz, OFF = 9.6 ± 1.8 Hz), and overall size ($p = 0.00036$, ON = 46.05 ± 6.9 pixels, OFF = 77.5 ± 12.04 pixels) of positive lobes. For units with a decrease in firing rate we observed only a small increase in temporal width for both positive ($p = 0.026$, ON = 0.034 ±0.0025 s, OFF = 0.032 ± 0.0025 s) and negative ($p = 0.02$, ON = 0.037 ± 0.0028 s, OFF = 0.032 ± 0.0024 s) lobes.

Modulating inhibitory neuronal activity in AC does not affect collicular sound responses

Auditory responses in AC are shaped by interactions between excitatory and inhibitory neurons (Blackwell and Geffen, 2017; Wood et al., 2017). To determine how modulating frequency selectivity in AC might affect tone-evoked responses in IC in a frequency-selective fashion, we perturbed the excitatory-inhibitory interactions by modulating two different classes of inhibitory interneuron known to contribute to sound responses in AC: PV and SOM inhibitory interneurons. We found that modulating PV interneuron activity in AC had little effect on spontaneous and tone-evoked activity or frequency selectivity in IC (**Figure 4.5 B-E**) despite modulating frequency selectivity, spontaneous activity, and tone-evoked response magnitude in AC. Specifically, in AC, activating PVs decreased spontaneous activity and tone-evoked response magnitude (**Figure 4.5F**; spontaneous activity: p = 2.2e-9, ON = 0.88 ± 0.16 Hz, OFF = 2.7 ± 0.34 Hz; tone-evoked response magnitude: p = 8.02e-7, ON = 6.9 ± 1.06 Hz, OFF = 11.5 ± 1.3 Hz**)** and increased frequency selectivity (**Figure 4.5G**; p = 3.3e-12, ON = 0.59 ± 0.022, OFF = 0.42 ± 0.02), while suppressing PVs increased spontaneous activity (**Figure 4.5I**; p = 5.2e-5, ON = 4.08 ± 0.54 Hz, OFF = 3.06 ± 0.55 Hz) and decreased frequency selectivity (**Figure 4.5J**; p = 3.8e-5, ON = 0.34 ± 0.027, OFF = 0.41 ± 0.031). This suggests that the increase in cortical activity driven by broad PV activation does not propagate to the inferior colliculus.

Figure 4.5

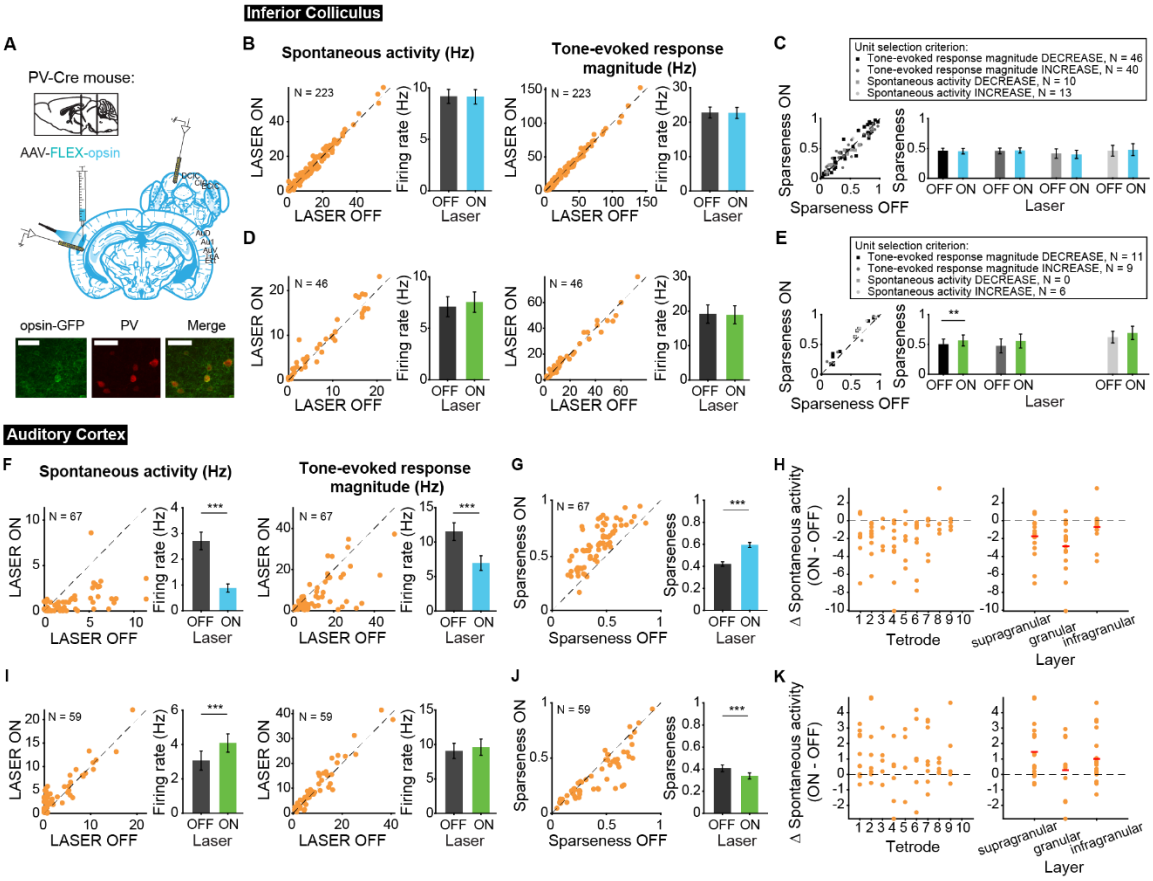
Inferior Colliculus
A
PV-Cre mouse:
AAV-FLEX-opsin
opsin-GFP
PV
Merge
B
Spontaneous activity (Hz)
Tone-evoked response magnitude (Hz)
N = 223
LASER ON
LASER OFF
Firing rate (Hz)
OFF ON
Laser
C
Unit selection criterion:
Tone-evoked response magnitude DECREASE, N = 46
Tone-evoked response magnitude INCREASE, N = 40
Spontaneous activity DECREASE, N = 10
Spontaneous activity INCREASE, N = 13
Sparseness ON
Sparseness OFF
Sparseness
D
N = 46
E
Unit selection criterion:
Tone-evoked response magnitude DECREASE, N = 11
Tone-evoked response magnitude INCREASE, N = 9
Spontaneous activity DECREASE, N = 0
Spontaneous activity INCREASE, N = 6
Auditory Cortex
F
N = 67
***
G
H
Δ Spontaneous activity (ON - OFF)
Tetrode
supragranular
granular
infragranular
Layer
I
N = 59
J
K

Figure 4.5 Effects of modulating PV interneurons in AC on tone-evoked responses in IC. **A** Stain for PV (center) and opsin-GFP (left). Scale bar: 50um. **B** Activating PVs had no effect on spontaneous activity or tone-evoked response magnitude in IC. **C** Activating PVs had no effect on frequency selectivity in IC. **D** Suppressing PVs had no effect on spontaneous activity or tone-evoked response magnitude in IC. **E** Suppressing PVs had weak effects on frequency selectivity in IC (mag decrease: $p = 0.0068$, ON = 0.57 ± 0.092, OFF = 0.5 ± 0.087). **F** Activating PVs decreased spontaneous activity ($p = 2.2e-9$, ON = 0.88 ± 0.16 Hz, OFF = 2.7 ± 0.34 Hz) and tone-evoked response magnitude ($p = 8.02e-7$, ON = 6.9 ± 1.06 Hz, OFF = 11.5 ± 1.3 Hz) in AC. **G** Activating PVs increased frequency selectivity in putative excitatory units in AC ($p = 3.3e-12$, ON = 0.59 ± 0.022, OFF = 0.42 ± 0.02). **H** Activating PVs affected putative excitatory units across all layers of AC. **I** Suppressing PVs increased spontaneous activity ($p = 5.2e-5$, ON = 4.08 ± 0.54 Hz, OFF = 3.06 ± 0.55 Hz) but does not affect tone-evoked response magnitude in AC. **J** Suppressing PVs decreased frequency selectivity in AC ($p = 3.8e-5$, ON = 0.34 ± 0.027, OFF = 0.41 ± 0.031). **K** Suppressing PVs affected putative excitatory units across all layers of AC. **B,D,F,I** Left panels: neuronal activity (spontaneous, left or tone-evoked, right) on laser on versus laser off trials. Right panels: Average neuronal activity (spontaneous, left or tone-evoked, right) for laser on and laser off trials. **C,E,G,J** Left panels: Sparseness for laser on versus laser off trials. Right panels: Average sparseness for laser on and laser off trials. **H,K** Change in spontaneous activity (laser on trials – laser off trials), left panels: for units at each tetrode; right panels: separated into supragranular: tetrodes 1-3; granular: tetrodes 5,6; infragranular: tetrodes 7-10.

Different interneuron classes may function in distinct networks, so we also tested the effects of modulating SOM interneurons. Modulating SOM interneurons had no effect on tone-evoked activity (**Figure 4.6 B,D**, right) or frequency selectivity (**Figure 4.6 C,E**), but suppressing SOM interneurons increased spontaneous activity in IC (**Figure 4.6D**, left; $p = 0.029$, ON = 6.9 ± 0.66 Hz, OFF = 6.7 ± 0.63 Hz), a change that we also observed with activation of the direct feedback projections (**Figure 4.2A**, left). Similar to PV interneurons, activating SOM interneurons decreased spontaneous activity and tone-evoked response magnitude in AC (**Figure 4.6F**; spontaneous activity: $p = 1.4e-12$, ON = 0.97 ± 0.25 Hz, OFF = 2.9 ± 0.37 Hz; tone-evoked response magnitude: $p = 1.3e-15$, ON = 3.3 ± 0.59 Hz, OFF = 11.4 ± 1.2 Hz) and increased frequency selectivity (**Figure 4.6G**; $p = 1.6e-13$, ON = 0.69 ± 0.024, OFF = 0.47 ± 0.019). In AC, suppressing SOMs reduced spontaneous activity, but had no significant effect on tone-evoked response magnitude or frequency selectivity (**Figure 4.6 I,J**; $p = 8.1e-4$, ON = 3.6 ± 0.41 Hz, OFF = 2.2 ± 0.38 Hz). This lack of effect was not due to the relatively small effect of light penetrating to the deep layers. In fact, to confirm that modulating PV and SOM activity in AC affected activity of units in L5/6 where the feedback projections we looked at changes in spontaneous activity at each tetrode which spanned the entire auditory cortex. We found that activity was modulated across the layers (**Figure 4.5-4.6 H,K**). Whereas modulating PVs did not have an effect on IC activity, SOM suppression resulted in an increase in spontaneous, but not tone-evoked activity in IC, which suggests that inhibitory modulation of sound responses in AC does not propagate to IC.

Figure 4.6

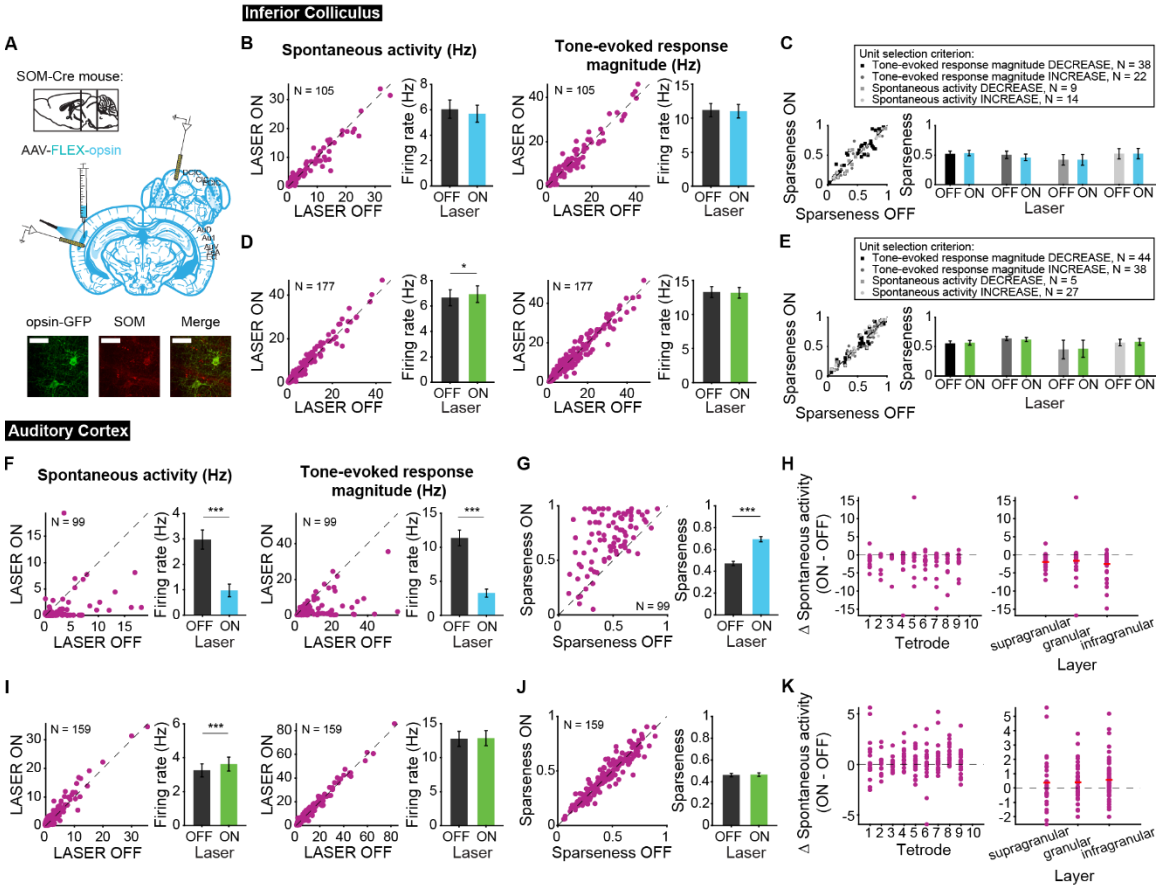
Inferior Colliculus
A
SOM-Cre mouse:
AAV-FLEX-opsin
opsin-GFP
SOM
Merge
B
Spontaneous activity (Hz)
Tone-evoked response magnitude (Hz)
N = 105
LASER ON
LASER OFF
Firing rate (Hz)
OFF ON
Laser
C
Unit selection criterion:
Tone-evoked response magnitude DECREASE, N = 38
Tone-evoked response magnitude INCREASE, N = 22
Spontaneous activity DECREASE, N = 9
Spontaneous activity INCREASE, N = 14
Sparseness ON
Sparseness OFF
Sparseness
D
N = 177
*
E
Unit selection criterion:
Tone-evoked response magnitude DECREASE, N = 44
Tone-evoked response magnitude INCREASE, N = 38
Spontaneous activity DECREASE, N = 5
Spontaneous activity INCREASE, N = 27
Auditory Cortex
F
N = 99
***
G
H
Δ Spontaneous activity (ON - OFF)
Tetrode
supragranular
granular
infragranular
Layer
I
N = 159
J
K

Figure 4.6 Effects of modulating SOM interneurons in AC on tone-evoked responses in IC. **A** Stain for SOM (center) and opsin-GFP (left). Scale bar: 50um. **B** Activating SOMs had no effect on spontaneous activity or tone-evoked response magnitude in IC. **C** Activating SOMs had no effect on frequency selectivity in IC. **D** Suppressing SOMs increased spontaneous activity ($p = 0.029$, ON = 6.9 ± 0.66 Hz, OFF = 6.7 ± 0.63 Hz) but did not affect tone-evoked response magnitude in IC. **E** Suppressing SOMs had no effect on frequency selectivity in IC. **F** Activating SOMs decreased spontaneous activity ($p = 1.4e-12$, ON = 0.97 ± 0.25 Hz, OFF = 2.9 ± 0.37 Hz) and tone-evoked response magnitude ($p = 1.3e-15$, ON = 3.3 ± 0.59 Hz, OFF = 11.4 ± 1.2 Hz) in AC. **G** Activating SOMs increased frequency selectivity in putative excitatory units in AC ($p = 1.6e-13$, ON = 0.69 ± 0.024, OFF = 0.47 ± 0.019). **H** Activating SOMs affected putative excitatory units across all layers of AC. **I** Suppressing SOMs increased spontaneous activity ($p = 8.1e-4$, ON = 3.6 ± 0.41 Hz, OFF = 2.2 ± 0.38 Hz) but did not affect tone-evoked response magnitude in AC. **J** Suppressing SOMs had no effect on frequency selectivity in AC. **K** Suppressing SOMs affected putative excitatory units across all layers of AC. **B,D,F,I** Left panels: neuronal activity (spontaneous, left or tone-evoked, right) on laser on versus laser off trials. Right panels: Average neuronal activity (spontaneous, left or tone-evoked, right) for laser on and laser off trials. **C,E,G,J** Left panels: Sparseness for laser on versus laser off trials. Right panels: Average sparseness for laser on and laser off trials. **H,K** Change in spontaneous activity (laser on trials – laser off trials), left panels: for units at each tetrode; right panels: separated into supragranular: tetrodes 1-3; granular: tetrodes 5,6; infragranular: tetrodes 7-10.

4.3 DISCUSSION

Auditory cortex sends extensive projections to IC (Saldaña et al., 1996; Winer et al., 1998; Doucet et al., 2003; Bajo and Moore, 2005; Coomes et al., 2005; Bajo et al., 2007). Our results demonstrate that activation of this cortico-collicular feedback modulates sound responses in IC by upregulating spontaneous IC activity, but decreasing frequency selectivity and reducing spectro-temporal receptive field size in IC. Interestingly, suppressing cortico-collicular feedback had little effect on IC activity, which suggests that at baseline and during passive tone presentation the feedback does not affect activity of IC neurons. We also found that SOM, but not PV inhibitory interneurons modulated IC activity, suggesting that the effects of modulation of cortical activity by PVs does not back-propagate to IC, whereas SOM-driven modulation affects spontaneous activity, but not tone-evoked responses. Overall our findings imply that direct cortico-collicular feedback can modulate responses to simple (pure tones) and more complex (DRCs) auditory stimuli by reducing, rather than increasing, sound selectivity. This modulation occurs independently of the activity of cortical inhibitory interneurons.

Effects of modulating direct cortico-collicular feedback

Whereas optogenetic manipulation allows for temporally precise control and cell-type specificity, the technique lacks the spatial specificity of electrical stimulation. Since both AC and cortico-collicular projections are tonotopically organized (Lim and Anderson, 2007; Markovitz et al., 2013; Barnstedt et al., 2015; Straka et al., 2015), spatially specific stimulation can more accurately mimic frequency-specific responses by activating specific

regions in the tonotopic map. Previous studies found that electrical stimulation of AC caused best frequencies in IC to shift towards the best frequencies of the stimulated site in AC (Gao and Suga, 1998; Yan and Suga, 1998; Gao and Suga, 2000; Ma and Suga, 2001a; Yan et al., 2005; Zhou and Jen, 2007). These results suggest that cortico-collicular feedback may be important for increasing the representation of behaviorally relevant stimuli in IC. However, when activating direct feedback, we did not observe consistent changes in IC best frequencies (**Figure 4.3F**). In this activation paradigm, we activated feedback projections across cortex, and therefore across the tonotopic map, so it is unsurprising that we did not find shifts in the best frequencies of neurons.

Previous studies found no effect of activating projection terminals on responses in the central nucleus of IC, only shell regions of IC (Xiong et al., 2015), which are the predominant targets of cortico-collicular feedback. In our study we were able to record from a larger neuronal population, revealing a subset of neurons in central IC that were modulated by feedback. The effects in central IC may be due to direct cortico-collicular feedback, intra-collicular circuits (Saldaña and Merchań, 1992; Malmierca et al., 1995; Miller et al., 2005; Sturm et al., 2014) , or a combination of these mechanisms.

Inactivation studies have shown mixed effects on sound-evoked responses in IC, but consistently demonstrated no effect on frequency selectivity. Specifically, suppression of AC increased or decreased IC sound responses in distinct subsets of cells (Popelář et al., 2003, 2016) while suppression of direct cortico-collicular feedback terminals in IC decreased sound-evoked responses (Xiong et al., 2015). However, our results show that suppression of direct cortico-collicular feedback has inconsistent effects on frequency selectivity and no effect on any other sound response properties in IC. Xiong et al. found

changes in IC responses specifically in the shell regions of IC, while our study targeted the central nucleus of IC, thus it is plausible that the difference in the recording locations might explain this discrepancy.

Our interest in central IC is due to its frequency tuning properties and that it is part of the behavioral output pathway leading to the pedunculopontine tegmental nucleus, which controls pre-pulse inhibition (PPI) of the acoustic startle reflex. Understanding how AC modulates sound responses in central IC may provide insight into how AC drives changes in auditory behaviors. Previously, we found that behavioral frequency discrimination acuity changed after differential auditory fear conditioning and these changes were driven by the auditory cortex (Aizenberg and Geffen, 2013; Aizenberg et al., 2015). The behavioral task used to test frequency discrimination acuity was a modified PPI task. Although AC can modulate this behavior, PPI is still observed after decerebration (Li and Frost, 2000) and the underlying circuit is believed to be subcortical (Fendt et al., 2001). The IC is a critical structure in the PPI circuit (Leitner and Cohen, 1985; Li et al., 1998; Fendt et al., 2001), with the central nucleus of IC receiving ascending auditory projections and the external nucleus of IC acting as the output station (Fendt et al., 2001; Li and Yue, 2002). In fact, stimulation of the central nucleus of IC also induces a running response in mice, but not if AC is silenced (Xiong et al., 2015). The broad frequency tuning in the shell regions of the IC (Syka et al., 2000; Barnstedt et al., 2015) made the central nucleus of IC, which has sharper tuning and a tonotopic organization (Syka et al., 2000; Ehret et al., 2003; Malmierca et al., 2008; Barnstedt et al., 2015), a good candidate for how AC may drive changes in frequency discrimination acuity. Limited evidence for a descending pathway

from AC to the pedunculopontine tegmental nucleus (Schofield and Motts, 2009) suggests another alternative pathway by which AC modulates frequency discrimination.

Future studies

One caveat of our study is that our experiments were performed in passively listening mice. It is possible that the lack of effect we observe with suppression of cortico-collicular feedback is due to the lack of task engagement. Previous studies have found that inactivation of this pathway affects innate responses to sound (Xiong et al., 2015) and auditory learning (Bajo et al., 2010), suggesting that activity of this pathway is critical for auditory behaviors. Studies have found that task engagement modulates neuronal responses to sounds (Fritz et al., 2003; Lakatos et al., 2013; McGinley et al., 2015; Downer et al., 2017; Kuchibhotla et al., 2017). Thus, we would expect suppression of this pathway to affect sound processing in IC during a behavioral task. Future studies should explore how activity changes with an animal actively engaged in a behavioral task.

4.4 METHODS

Animals.

All experiments were performed in adult male and female mice (supplier: Jackson Laboratories; age, 12–15 wk; weight, 22–32 g; PV-Cre mice, strain: B6; 129P2-Pvalbtm1(cre)Arbr/J; SOM-Cre mice, strain: Ssttm2.1(cre)Zjh/J; Cdh23 mice, strain: Cdh23tm2.1Kjn/J, or PV-Cre x Cdh23 or SOM-Cre x Cdh23 crosses). Mice were housed at 28°C on a 12 h light–dark cycle with water and food provided ad libitum, less than five animals per cage. In PV-Cre mice Cre recombinase (Cre) was expressed in parvalbumin-

positive interneurons, and in SOM-Cre, Cre was expressed in somatostatin-positive interneurons. All animal work was conducted according to the guidelines of University of Pennsylvanian IACUC and the AALAC Guide on Animal Research. Anesthesia by isofluorane and euthanasia by ketamine were used. All means were taken to minimize the pain or discomfort of the animals during and following the experiments. All experiments were performed during the animals' dark cycle.

Viral Vectors.

Modified AAVs encoding ArchT (AAV9-CAG-FLEX-ArchT-GFP or AAV9-CAG-FLEX-ArchT-tdTomato; UNC Vector Core) or ChR2 (AAV9-CAG-FLEX-ChR2-tdTomato; Penn Vector Core) were used for selective suppression or excitation, respectively. Retrograde AAV virus encoding Cre (retro AAV-hSyn-Cre-GFP) was custom made in our laboratory. Briefly, RetroAAV2 hSyn Cre-GFP was packaged using the Helper-Free system (Agilent) and the retrograde trafficking plasmid, Retro2, which bears capsid mutations in serotype 2.

Surgery and Virus Injection.

At least 21 days prior to electrophysiological recordings, mice were anesthetized with isoflurane to a surgical plane. The head was secured in a stereotactic holder. The mouse was subjected to a small craniotomy (2 x 2 mm) over AC under aseptic conditions. Viral particles were injected (750 nl) bilaterally using a syringe pump (Pump 11 Elite, Harvard Apparatus) targeted to AC (coordinates relative to bregma: −2.6 mm anterior, ±4.3 mm

lateral, +1 mm ventral). Fiber-optic cannulas (Thorlabs, Ø200 μm Core, 0.22 NA) were implanted bilaterally over the injection site at depth of 0.5 mm from the skull surface. For a subset of mice, to target direct feedback, the mouse was also subjected to a craniotomy over IC (1 x 4 mm). Retro AAV viral construct was injected (3 x 200 nl) via glass syringe (30-50 um diameter) using a syringe pump (Pump 11 Elite, Harvard Apparatus) bilaterally in IC. Craniotomies were covered with a removable silicon plug. A small headpost was secured to the skull with dental cement (C&B Metabond) and acrylic (Lang Dental). For postoperative analgesia, slow release Buprenex (0.1 mg/kg) and Bupivicane (2 mg/kg) were injected subcutaneously. An antibiotic (5 mg/kg Baytril) was injected subcutaneously daily (for 4 days) at the surgical site during recovery. Virus spread was confirmed postmortem by visualization of the fluorescent protein expression in fixed brain tissue, and its colocalization with PV or SOM, following immuno-histochemical processing with the appropriate antibody.

Acoustic Stimuli.

Stimuli were delivered via a magnetic speaker (Tucker-Davis Technologies) directed toward the mouse's head. Speakers were calibrated prior to the experiments to ±3 dB over frequencies between 3 and 70 kHz by placing a microphone (Brüel and Kjaer) in the location of the ear contralateral to the recorded AC hemisphere, recording speaker output and filtering stimuli to compensate for acoustic aberrations (Carruthers et al., 2013).

Clicks.

Click trains were composed of six 50 ms clicks with a 50 ms ISI. Click trains were repeated 120 times with a 450 ms ISI between trains. Alternating click trains were also paired with 1 s laser stimulation beginning 250 ms prior to click train onset.

Tuning Stimuli.

(1) To measure tuning for direct feedback cohorts, a train of 50 pure tones of frequencies spaced logarithmically between 3 and 70 kHz, at 70 dB sound pressure level relative to 20 microPascals (SPL), in pseudo-random order was presented 20 times. Each tone was 50 ms duration (5-ms cosine squared ramp up and down) with an inter-stimulus interval (ISI) of 450 ms. Alternating tones were paired with continuous 250 ms laser pulse at either -100 ms, -20 ms, or +8 ms onset relative to tone onset.

(2) For SOM-Cre and PV-Cre cohorts, a train of pure tones of 35 frequencies spaced logarithmically between 3 and 70 kHz and 8 uniformly spaced intensities from 0 to 70 dB SPL were presented 10 times in a pseudo-random order. Alternating tones were paired with continuous 250 ms laser pulse at -100 ms relative to tone onset.

Dynamic Random Chords (DRCs).

To measure spectro-temporal receptive fields (STRFs) we constructed DRCs from 20 ms chords (with 1 ms ramp) of 50 frequencies spaced logarithmically between 5 and 40 kHz with average intensity of 50 dB SPL and 20 dB SPL standard deviation. Total duration was 40 minutes with a 250 ms continuous laser pulse presented every 1 s.

Electrophysiological Recordings.

All recordings were carried out inside a double-walled acoustic isolation booth (Industrial Acoustics). Mice were placed in the recording chamber, and a headpost was secured to a custom base, immobilizing the head. Activity of neurons in AC were recorded via a custom silicon multi-channel probe (Neuronexus), lowered in the area targeting AC via a stereotactic instrument following a craniotomy at a 35-degree angle. The electrode tips were arranged in a vertical fashion that permits recording the activity of neurons across the depth of the auditory cortex and the inferior colliculus. Activity of neurons in IC were recorded via the same custom probes, lowered in the area targeting IC via a stereotactic instrument following either a craniotomy (SOM-Cre and PV-Cre cohorts) or removal of the silicon plug, vertically. Electro-physiological data from 32 channels were filtered between 600 and 6000 Hz (spike responses), digitized at 32kHz and stored for offline analysis (Neuralynx). Spikes belonging to single neurons and multi-units were detected using commercial software (Plexon). We examined the following experimental conditions (note: we do not distinguish here between PV-Cre/SOM-Cre and PV-Cre x Cdh23/SOM-Cre x Cdh23): Cdh23 + ArchT (N = 4 male mice, awake) Cdh23 + ChR2 (N = 5 male mice, awake) SOM-Cre + ChR2 (N = 15 male mice; 8 anesthetized, 7 awake) SOM-Cre + ArchT (N = 7 mice; 4 female, 3 male, 4 anesthetized, 3 awake) PV-Cre + ChR2 (N = 16 male mice; 12 anesthetized, 4 awake) PV-Cre + ArchT (N = 4 male mice, awake). For cohorts with awake and anesthetized recordings data were analyzed separately, but we observed no difference in our results so data were combined. Mice that did not show effect of laser activation or suppression in auditory cortex were excluded. The proportions of units from each of the cohorts for tone-evoked/spontaneous responses are as follows:

Cdh23 + ChR2: N = 4 single units; N = 187 multi-units

Cdh23 + ArchT: N = 22 single units; N = 181 multi-units

PV-Cre + ChR2: N = 25 single units in IC; N = 3 single units in AC; N = 198 multi-units in IC; N = 64 multi-units in AC; N = 57 units from awake animals in IC; N = 138 units from anesthetized animals in IC; N = 14 units from awake animals in AC; N = 53 units from anesthetized animals in AC.

PV-Cre + ArchT: N = 2 single units in IC; N = 3 single units in AC; N = 44 multi-units in IC; N = 56 multi-units in AC

SOM-Cre + ChR2: N = 15 single units in IC; N = 9 single units in AC; N = 90 multi-units in IC; N = 90 multi-units in AC; N = 76 units from awake animals in IC; N = 29 units from anesthetized animals in IC; N = 49 units from awake animals in AC; N = 50 units from anesthetized animals in AC.

SOM-Cre + ArchT: N = 16 single units in IC; N = 4 single units in AC; N = 161 multi-units in IC; N = 155 multi-units in AC; N = 75 units from awake animals in IC; N = 37 units from anesthetized animals in IC; N = 67 units from awake animals in AC; N = 36 units from anesthetized animals in AC.

Photostimulation of Neuronal Activity.

Neurons were stimulated by application of continuous light pulse delivered from either blue (473 nm, BL473T3-150, used for ChR2 stimulation) or green DPSS laser (532 nm, GL532T3-300, Slocs lasers, used for ArchT stimulation) through implanted cannulas. Laser power measured through cannulas was 3 mW. Timing of the light pulse was controlled with microsecond precision via a custom control shutter system, synchronized to the acoustic stimulus delivery.

Neural Response Analysis.

Unit selection. Units were selected based on pure-tone responsiveness. For each unit we identified the 7 frequencies that elicited the highest response and averaged activity across these trials (and the highest 3 amplitudes for stimulus with multiple amplitudes). Units with tone-evoked activity (75 ms window after tone onset) less than two standard deviations above the spontaneous activity (50 ms window prior to tone onset) in no laser condition were excluded from the analysis. Both single units and high quality multi-units (multi-units with <1% of spikes with <1ms inter-spike-interval) were used.

Spontaneous activity and tone-evoked response magnitude

Feedback cohort: Spontaneous activity was the average firing rate in a 20 ms window (to allow for equivalent comparison between -100 ms and -20 ms tone onset conditions) prior to tone onset of top 7 preferred frequencies.

SOM-Cre/PV-Cre cohorts: Spontaneous activity was the average firing rate in a 50 ms window prior to tone onset of top 7 preferred frequencies and 3 highest amplitudes.

All mice: Tone-evoked response magnitude was calculated as the difference between the average tone-evoked response in a 75 ms window after tone onset and the spontaneous activity.

Sparseness. To examine frequency selectivity of neurons, sparseness of frequency tuning was computed as:

$$Sparseness = 1 - \frac{\left(\sum_{i=1}^{i=n} \frac{FR_i}{n}\right)^2}{\sum_{i=1}^{i=n} \frac{FR_i^2}{n}}$$

where FR_i is tone-evoked response to tone at frequency *i*, and *n* is number of frequencies used (Weliky et al., 2003). Subgroups of neurons used in sparseness analyses were separated based on > 1 standard deviation change based on the -100 ms laser onset trials.

Linear fits across frequencies. Linear fits were calculated using linear regression (fitlm.m; MATLAB) over 50 data points, one for each of the 50 frequencies tested (Natan et al., 2017b). The 50 data points were separately calculated as the mean FR over all repeats of each frequency.

Best Frequency. Best frequency was defined as the frequency that elicited the maximum response.

STRF Analysis. To calculate the STRF we separated the stimulus into 1-second chunks, concatenating the 250 ms laser ON chunks and the 250 ms laser OFF chunks immediately preceding laser onset. These data were then used to calculate the average spectrogram preceding a spike. To allow for finer temporal resolution of the STRFs we upsampled the DRCs using nearest neighbor interpolation. Subsequently we averaged the STRF across the eight stimulus files. To determine the significance of the cluster, the *z*-score of pixels was computed relative to the baseline values from an STRF generated with scrambled spike trains, using Stat4ci toolbox (Chauvin et al., 2005; Natan et al., 2017a). We ran this significance test 100 times and any pixel identified as significant more than 90 times was considered significant. Clusters were matched between laser ON and laser OFF trials by comparing the overlap of the clusters, requiring a 50% overlap of the smallest cluster size to be a match. From STRF, the peak time, temporal width, peak frequency, and frequency

width of the positive and negative clusters were measured (Woolley et al., 2006; Shechter and Depireux, 2007; Schneider and Woolley, 2010).

Statistical Analyses.

Significant differences and *P* values were calculated using paired Wilcoxon sign-rank test (unless noted otherwise) with standard MATLAB routine. For the laser alone data, to compare distributions to standard normal distribution data were normalized by mean and standard deviation and then significant differences and *P* values were calculated by Kolmogorov-Smirnoff test with standard MATLAB routine. Mean ± standard error of the mean was reported unless stated otherwise. * indicates $p < 0.05$, ** indicates $p < 0.01$, *** indicates $p < 0.001$.

4.4 REFERENCES

Aizenberg M, Geffen MN (2013) Bidirectional effects of aversive learning on perceptual acuity are mediated by the sensory cortex. Nat Neurosci 16:994–996.

Aizenberg M, Mwilambwe-Tshilobo L, Briguglio JJ, Natan RG, Geffen MN (2015) Bidirectional Regulation of Innate and Learned Behaviors That Rely on Frequency Discrimination by Cortical Inhibitory Neurons. PLoS Biol 13:1–32.

Alitto HJ, Usrey WM (2003) Corticothalamic feedback and sensory processing. Curr Opin Neurobiol 13:440–445.

Bajo VM, Moore DR (2005) Descending projections from the auditory cortex to the

inferior colliculus in the gerbil, Meriones unguiculatus. J Comp Neurol 486:101–116.

Bajo VM, Nodal FR, Bizley JK, Moore DR, King a. J (2007) The Ferret Auditory Cortex: Descending Projections to the Inferior Colliculus. Cereb Cortex 17:475–491.

Bajo VM, Nodal FR, Moore DR, King AJ (2010) The descending corticocollicular pathway mediates learning-induced auditory plasticity. Nat Neurosci 13:253–260.

Barnstedt O, Keating P, Weissenberger Y, King AJ, Dahmen JC (2015) Functional Microarchitecture of the Mouse Dorsal Inferior Colliculus Revealed through In Vivo Two-Photon Calcium Imaging. J Neurosci 35:10927–10939.

Blackwell JM, Geffen MN (2017) Progress and challenges for understanding the function of cortical microcircuits in auditory processing. Nat Commun 8:2165.

Carruthers IM, Natan RG, Geffen MN (2013) Encoding of ultrasonic vocalizations in the auditory cortex. J Neurophysiol 109:1912–1927.

Chauvin A, Worsley KJ, Schyns PG, Arguin M, Gosselin F (2005) Accurate statistical tests for smooth classification images. J Vis 5:659–667.

Coomes DL, Schofield RM, Schofield BR (2005) Unilateral and bilateral projections from cortical cells to the inferior colliculus in guinea pigs. Brain Res 1042:62–72.

Doucet JR, Molavi DL, Ryugo DK (2003) The source of corticocollicular and corticobulbar projections in area Te1 of the rat. Exp Brain Res 153:461–466.

Downer JD, Rapone B, Verhein J, O'Connor KN, Sutter ML (2017) Feature-Selective Attention Adaptively Shifts Noise Correlations in Primary Auditory Cortex. J

Neurosci 37:5378–5392.

Ehret G, Egorova M, Hage SR, Müller BA (2003) Spatial map of frequency tuning-curve shapes in the mouse inferior colliculus. Neuroreport 14:1365–1369.

Feliciano M, Potashner SJ (1995) Evidence for a Glutamatergic Pathway from the Guinea Pig Auditory Cortex to the Inferior Colliculus. J Neurochem 65:1348–1357.

Fendt M, Li L, Yeomans JS (2001) Brain stem circuits mediating prepusle inhibition of the startle reflex. Psychopharmacology (Berl) 156:216–224.

Fritz J, Shamma S, Elhilali M, Klein D (2003) Rapid task-related plasticity of spectrotemporal receptive fields in primary auditory cortex. Nat Neurosci 6:1216–1223.

Gao E, Suga N (1998) Experience-dependent corticofugal adjustment of midbrain frequency map in bat auditory system. PNAS 95:12663–12670.

Gao E, Suga N (2000) Experience-dependent plasticity in the auditory cortex and the inferior colliculus of bats : Role of the corticofugal system. PNAS 97:8081–8086.

Hamilton LS, Sohl-Dickstein J, Huth AG, Carels VM, Deisseroth K, Bao S (2013) Optogenetic activation of an inhibitory network enhances feedforward functional connectivity in auditory cortex. Neuron 80:1066–1076.

Jen PH-S, Chen QC, Sun XD (1998) Corticofugal regulation of auditory sensitivity in the bat inferior colliculus. J Comp Physiol A 183:683–697.

Jen PH-S, Zhou X (2003) Corticofugal modulation of amplitude domain processing in the

midbrain of the big brown bat, Eptesicus fuscus. Hear Res 184:91–106.

Kuchibhotla K V, Gill J V, Lindsay GW, Papadoyannis ES, Field RE, Sten TAH, Miller KD, Froemke RC (2017) Parallel processing by cortical inhibition enables context-dependent behavior. Nat Neurosci 20:62–71.

Lakatos P, Musacchia G, O'Connel MN, Falchier AY, Javitt DC, Schroeder CE (2013) The spectrotemporal filter mechanism of auditory selective attention. Neuron 77:750–761.

Leitner DS, Cohen ME (1985) Role of the inferior colliculus in the inhibition of acoustic startle in the rat. Physiol Behav 34:65–70.

Li L, Frost BJ (2000) Azimuthal directional sensitivity of prepulse inhibition of the pinna startle reflex in decerebrate rats. Brain Res Bull 51:95–100.

Li L, Korngut LM, Frost BJ, Beninger RJ (1998) Prepulse inhibition following lesions of the inferior colliculus: prepulse intensity functions. Physiol Behav 65:133–139.

Li L, Yue Q (2002) Auditory gating processes and binaural inhibition in the inferior colliculus. Hear Res 168:98–109.

Lim HH, Anderson DJ (2007) Antidromic Activation Reveals Tonotopically Organized Projections From Primary Auditory Cortex to the Central Nucleus of the Inferior Colliculus in Guinea Pig. J Neurophysiol 97:1413–1427.

Ma X, Suga N (2001a) Plasticity of Bat's Central Auditory System Evoked by Focal Electric Stimulation of Auditory and/or Somatosensory Cortices. J Neurophysiol

85:1078–1087.

Ma X, Suga N (2001b) Corticofugal modulation of duration-tuned neurons in the midbrain auditory nucleus in bats. PNAS 98:14060–14065.

Malmierca MS, Izquierdo MA, Cristaudo S, Hernandez O, Perez-Gonzalez D, Covey E, Oliver DL (2008) A Discontinuous Tonotopic Organization in the Inferior Colliculus of the Rat. J Neurosci 28:4767–4776.

Malmierca MS, Rees A, Le Beau FEN, Bjaalie JG (1995) Laminar organization of frequency-defined local axons within and between the inferior colliculi of the guinea pig. J Comp Neurol 357:124–144.

Markovitz CD, Tang TT, Lim HH (2013) Tonotopic and localized pathways from primary auditory cortex to the central nucleus of the inferior colliculus. Front Neural Circuits 7:1–11.

McGinley MJ, David S V, McCormick DA (2015) Cortical Membrane Potential Signature of Optimal States for Sensory Signal Detection. Neuron 87:179–192.

Miller KE, Casseday JH, Covey E (2005) Relation between intrinsic connections and isofrequency contours in the inferior colliculus of the big brown bat, Eptesicus fuscus. Neuroscience 136:895–905.

Natan RG, Carruthers IM, Mwilambwe-Tshilobo L, Geffen MN (2017a) Gain Control in the Auditory Cortex Evoked by Changing Temporal Correlation of Sounds. Cereb cortex 27:2385–2402.

Natan RG, Rao W, Geffen MN (2017b) Cortical Interneurons Differentially Shape Frequency Tuning following Adaptation. Cell Rep 21:878–890.

Phillips EA, Hasenstaub AR (2016) Asymmetric effects of activating and inactivating cortical interneurons. Elife 5:1–22.

Popelář J, Nwabueze-Ogbo FC, Syka J (2003) Changes in Neuronal Activity of the Inferior Colliculus in Rat after Temporal Inactivation of the Auditory Cortex. Physiol Res 52:615–628.

Popelář J, Šuta D, Lindovský J, Bureš Z, Pysanenko K, Chumak T, Syka J (2016) Cooling of the auditory cortex modifies neuronal activity in the inferior colliculus in rats. Hear Res 332:7–16.

Rouiller EM, Durif C (2004) The dual pattern of corticothalamic projection of the primary auditory cortex in macaque monkey. Neurosci Lett 358:49–52.

Rudy B, Fishell G, Lee S, Hjerling-Leffler J (2011) Three groups of interneurons account for nearly 100% of neocortical GABAergic neurons. Dev Neurobiol 71:45–61.

Saldaña E, Feliciano M, Mugnaini E (1996) Distribution of descending projections from primary auditory neocortex to inferior colliculus mimics the topography of intracollicular projections. J Comp Neurol 371:15–40.

Saldaña E, Merchań MA (1992) Intrinsic and commissural connections of the rat inferior colliculus. J Comp Neurol 319:417–437.

Schneider DM, Woolley SMN (2010) Discrimination of Communication Vocalizations by

Single Neurons and Groups of Neurons in the Auditory Midbrain. J Neurophysiol 103:3248–3265.

Schofield BR, Motts SD (2009) Projections from auditory cortex to cholinergic cells in the midbrain tegmentum of guinea pigs. Brain Res Bull 80:163–170.

Seybold BA, Elizabeth AK, Schreiner CE, Hasenstaub AR, Seybold BA, Phillips EAK, Schreiner CE, Hasenstaub AR (2015) Inhibitory Actions Unified by Network Integration Viewpoint Inhibitory Actions Unified by Network Integration. Neuron 87:1181–1192.

Shechter B, Depireux DA (2007) Stability of spectro-temporal tuning over several seconds in primary auditory cortex of the awake ferret. Neuroscience 148:806–814.

Straka MM, Hughes R, Lee P, Lim HH (2015) Descending and tonotopic projection patterns from the auditory cortex to the inferior colliculus. Neuroscience 300:325–337.

Sturm J, Nguyen T, Kandler K (2014) Development of intrinsic connectivity in the central nucleus of the mouse inferior colliculus. J Neurosci 34:15032–15046.

Syka J, Popelář J, Kvašňák E, Astl J (2000) Response properties of neurons in the central nucleus and external and dorsal cortices of the inferior colliculus in guinea pig. Exp Brain Res 133:254–266.

Vila C-H, Williamson RS, Hancock KE, Polley DB (2019) Optimizing optogenetic stimulation protocols in auditory corticofugal neurons based on closed-loop spike feedback. bioRxiv.

Weliky M, Fiser J, Hunt RH, Wagner DN (2003) Coding of Natural Scenes in Primary Visual Cortex. Neuron 37:703–718.

Winer JA, Diehl JJ, Larue DT (2001) Projections of auditory cortex to the medial geniculate body of the cat. J Comp Neurol 430:27–55.

Winer JA, Larue DT, Diehl JJ, Hefti BJ (1998) Auditory cortical projections to the cat inferior colliculus. J Comp Neurol 400:147–174.

Wood KC, Blackwell JM, Geffen MN (2017) Cortical inhibitory interneurons control sensory processing. Curr Opin Neurobiol 46:200–207.

Woolley SMN, Gill PR, Theunissen FE (2006) Stimulus-Dependent Auditory Tuning Results in Synchronous Population Coding of Vocalizations in the Songbird Midbrain. J Neurosci 26:2499–2512.

Xiong XR, Liang F, Zingg B, Ji X, Ibrahim LA, Tao HW, Zhang LI (2015) Auditory cortex controls sound-driven innate defense behaviour through corticofugal projections to inferior colliculus. Nat Commun 6:7224.

Yan J, Zhang Y, Ehret G, Yan J (2005) Corticofugal shaping of frequency tuning curves in the central nucleus of the inferior colliculus of mice. J Neurophysiol 93:71–83.

Yan W, Suga N (1998) Corticofugal modulation of the midbrain frequency map in the bat. Nat Neurosci 1:54–58.

Zhang Y, Suga N, Yan J (1997) Corticofugal modulation of frequency processing in bat auditory system. Nature 387:900–903.

Zhou X, Jen PH-S (2005) Corticofugal modulation of directional sensitivity in the midbrain of the big brown bat, Eptesicus fuscus. Hear Res 203:201–215.

Zhou X, Jen PH-S (2007) Corticofugal Modulation of Multi-Parametric Auditory Selectivity in the Midbrain of the Big Brown Bat. J Neurophysiol 98:2509–2516.

CHAPTER 5: CONCLUSIONS

In this dissertation we described experiments that explore whether and how distinct neuronal subtypes in auditory cortex shape and encode both simple and complex sound properties. In chapter 2, we tested how neurons in the auditory cortex encode sounds that exhibit scale-invariant statistics, but vary across multiple scale magnitudes. Scale invariance is a property of sounds whose temporal modulation within spectral bands scale with the center frequency of the band. We found that for these naturalistic sounds, although neurons exhibited selectivity for subsets of stimuli with specific statistics, over the population responses were stable over large changes in stimulus statistics. In chapter 4, we tested how direct feedback from the auditory cortex to the inferior colliculus modulated sound responses in the inferior colliculus. We found that this feedback modulated responses to simple and complex auditory stimuli by reducing sound selectivity, specifically by decreasing responsiveness to tones that evoke the greatest responses and an increasing response to stimuli that evoke weaker activity. Furthermore, we tested the effects of perturbing intra-cortical inhibitory-excitatory networks on sound responses in the inferior colliculus by modulating the activity of distinct inhibitory subtypes in auditory cortex. We found that modulation of neither PV- nor SOM-interneurons affected sound-evoked responses in the inferior colliculus, despite significant modulation of cortical responses (also described in chapter 3). Overall our findings imply that direct cortico-collicular feedback can modulate responses to simple and more complex auditory stimuli independently of the activity of cortical inhibitory interneurons. Together these results

provide evidence supporting the importance of the auditory cortex in sound processing. Here we discuss the implications of our results and suggest future questions we would like to address.

Role of attention in modulating cortico-collicular feedback

Previous studies have demonstrated the behavioral consequences of inactivating this pathway, causing impairments in auditory learning (Bajo et al., 2010) and innate noise-evoked running response (Xiong et al., 2015). These results suggest that cortico-collicular feedback can modulate auditory processing. In chapter 4, however, we found that suppression of cortico-collicular feedback had no effect on spontaneous activity or sound-evoked responses in the inferior colliculus. Cortico-collicular feedback may not be active in the absence of behavioral task engagement. In our experiments, mice were awake and passively listening to sounds, which may explain the lack of effect we observed with suppression of cortico-collicular feedback.

Previous studies have found that task engagement modulates neuronal responses to sounds (Fritz et al., 2003; Lakatos et al., 2013; McGinley et al., 2015; Downer et al., 2017; Kuchibhotla et al., 2017). Engagement in a tone detection task enhanced STRF representation of the behaviorally relevant frequency and changes in STRF parameters are correlated with behavioral performance (Fritz et al., 2003). Given the evidence suggesting the importance of this pathway in auditory behaviors and the effects of attention on receptive field plasticity, we would expect suppression of this pathway to affect sound processing in IC during a behavioral task. Future studies should explore how activity changes with an animal actively engaged in a behavioral task.

Of particular interest would be testing the effects of modulating cortico-collicular feedback in frequency discrimination. Based on effects we observed with activation we would expect broad activation of feedback across auditory cortex would impair behavioral performance due to the decrease in selectivity. Stimulation of neurons in auditory cortex with specific preferred frequencies increased and enhanced representation of those frequencies in the inferior colliculus (Jen et al., 1998; Yan and Suga, 1998; Ma and Suga, 2001; Jen and Zhou, 2003; Yan et al., 2005; Zhou and Jen, 2007). These results suggest that specific activation of cortico-collicular projection neurons tuned to behaviorally relevant frequency would enhance discrimination and suppression of cortico-collicular feedback might impair discrimination. Cortico-collicular feedback is necessary for sound-localization adaptation after a unilateral earplug (Bajo et al., 2010). Our lab has demonstrated that auditory cortex drives changes in frequency discrimination acuity after differential auditory fear conditioning (Aizenberg and Geffen, 2013). The role of cortico-collicular feedback in auditory learning suggests that cortico-collicular feedback is a candidate pathway by which auditory cortex modulates this behavior. We therefore expect that inactivation of cortico-collicular feedback following differential auditory fear conditioning would attenuate changes in frequency discrimination acuity observed after learning.

Local cortical circuits modulating cortico-collicular feedback

We observed little effect of modulating AC inhibitory interneurons on activity in IC despite the changes observed in AC (**Figures 4.5, 4.6**), which suggests there may be another neuron subtype that plays a modulatory role during cortico-collicular plasticity in

driving feedback modulation. One possibility that was not explored here are cholinergic inputs from the nucleus basalis. The nucleus basalis (NB), a cholinergic nucleus in the basal forebrain, has been implicated as a key structure in learning-induced auditory plasticity. Studies have found that pairing NB stimulation with presentation of a tone has been sufficient to induce receptive field plasticity in AC (Kilgard and Merzenich, 1998; Kilgard et al., 2001; Weinberger, 2003) and that blocking muscarinic receptors in AC impairs this plasticity (Miasnikov et al., 2008). Of greater interest is the receptive field plasticity also observed in IC. Acetylcholine applied to AC increased spontaneous and tone-evoked activity in both AC and IC (Ji et al., 2001). Furthermore, pairing AC stimulation with nucleus basalis stimulation (Ma and Suga, 2003) or pairing tone presentation with nucleus basalis stimulation (Zhang et al., 2005) shifted best frequencies in both AC and IC and application of atropine in AC inhibited this IC plasticity (Zhang et al., 2005). It is plausible that NB cholinergic inputs may be responsible for driving responses of IC neurons rather than PV or SOM inhibitory interneurons. However, SOMs in AC are depolarized by application of cholinergic agonist (Kuchibhotla et al., 2017). Furthermore, the lack of effect we observe with inhibitory interneuron activation is consistent with our results from suppressing cortico-collicular feedback. Thus, while another neuronal subtype may be responsible for driving feedback activity in a behavioral context, inhibitory interneurons may still play a role in shaping responses of feedback once active

Combined, our studies reveal two novel aspects of computation in the cortical and sub-cortical areas of the central auditory pathway. These studies open new avenues for

probing how the auditory cortex functions in everyday acoustic environments and elucidate the function of cortical and sub-cortical microcircuits in learning.

Technical limitations of optogenetic activation of cortico-collicular feedback

In chapter 4 we found that only optogenetic activation of cortico-collicular feedback had any measurable effect on activity in IC. There are several technical limitations to the design of our experiments that are important to consider when interpreting these results.

First, whereas optogenetic manipulation allows for temporal precision and cell-type specificity, the technique lacks the spatial specificity of electrical stimulation. Both AC and cortico-collicular projections are tonotopically organized (Lim and Anderson, 2007; Markovitz et al., 2013; Barnstedt et al., 2015; Straka et al., 2015). In our experiments we activated feedback projections across cortex and, therefore, across the tonotopic map. For any given stimulus, only a subset of neurons tuned to those stimulus properties will be active. Previous studies found that electrical stimulation of AC caused best frequencies in IC to shift towards the best frequencies of the stimulated site in AC (Gao and Suga, 1998, 2000; Yan and Suga, 1998; Ma and Suga, 2001; Yan et al., 2005; Zhou and Jen, 2007). These results suggest that cortico-collicular feedback may be important for increasing the representation of behaviorally relevant stimuli in IC. Stimulating frequency region-specific subsets of feedback projections would more accurately mimic natural neuronal activation patterns and provide better insight as to how cortico-collicular feedback stimulus-specific responses.

Second, we chose to activate cortico-collicular neurons by shining light in the cortex, thus initiating spikes at the level of the cell body as would occur in response to a sound. An important consideration with this method, however, is that these neurons do not only send collaterals to IC, but also to the auditory thalamus (Asokan et al., 2018; Williamson and Polley, 2019), amygdala (Asokan et al., 2018), and striatum (Asokan et al., 2018). There is also evidence of descending projections to IC from thalamus (Winer et al., 2002) and amygdala (Marsh et al., 2002). When interpreting our results it is important to consider that the effects we observe from activating cortico-collicular feedback may also be due, at least in part, to these secondary pathways.

Future experiments should take into account the technical limitations of our current study. To explore the role of cortico-collicular projections in shaping sound responses in IC we propose taking advantage of two-photon imaging in IC. This technique would allow for identification of direct targets of cortico-collicular feedback using fluorescent tagging to visualize cortico-collicular axon terminals. We could then differentiate activity of direct and indirect targets of cortico-collicular feedback. We then propose identifying subsets of of cortico-collicular axons in IC active in response to particular tones and then using holographic optogenetics (Pégard et al., 2017) in order to activate a similar pattern of neurons as we observe in response to sounds while silencing AC to prevent antidromic spikes. These experiments would (1) further our understanding of how cortico-collicular feedback shapes sound responses in IC both directly (measuring activity of direct synaptic targets) and indirectly (measure activity of non-synaptic targets) and (2) measure more precisely the contribution of direct projections from AC to IC in shaping sound responses by using more natural patterns of activation.

5.1 References

Aizenberg M, Geffen MN (2013) Bidirectional effects of aversive learning on perceptual acuity are mediated by the sensory cortex. Nat Neurosci 16:994–996.

Asokan MM, Williamson RS, Hancock KE, Polley DB (2018) Sensory overamplification in layer 5 auditory corticofugal projection neurons following cochlear nerve synaptic damage. Nat Commun 9:2468.

Bajo VM, Nodal FR, Moore DR, King AJ (2010) The descending corticocollicular pathway mediates learning-induced auditory plasticity. Nat Neurosci 13:253–260.

Barnstedt O, Keating P, Weissenberger Y, King AJ, Dahmen JC (2015) Functional Microarchitecture of the Mouse Dorsal Inferior Colliculus Revealed through In Vivo Two-Photon Calcium Imaging. J Neurosci 35:10927–10939.

Downer JD, Rapone B, Verhein J, O'Connor KN, Sutter ML (2017) Feature-Selective Attention Adaptively Shifts Noise Correlations in Primary Auditory Cortex. J Neurosci 37:5378–5392.

Fritz J, Shamma S, Elhilali M, Klein D (2003) Rapid task-related plasticity of spectrotemporal receptive fields in primary auditory cortex. Nat Neurosci 6:1216–1223.

Gao E, Suga N (1998) Experience-dependent corticofugal adjustment of midbrain frequency map in bat auditory system. PNAS 95:12663–12670.

Gao E, Suga N (2000) Experience-dependent plasticity in the auditory cortex and the

inferior colliculus of bats : Role of the corticofugal system. PNAS 97:8081–8086.

Jen PH-S, Chen QC, Sun XD (1998) Corticofugal regulation of auditory sensitivity in the bat inferior colliculus. J Comp Physiol A 183:683–697.

Jen PH-S, Zhou X (2003) Corticofugal modulation of amplitude domain processing in the midbrain of the big brown bat, Eptesicus fuscus. Hear Res 184:91–106.

Ji W, Gao E, Suga N (2001) Effects of Acetylcholine and Atropine on Plasticity of Central Auditory Neurons Caused by Conditioning in Bats. J Neurophysiol 86:211–225.

Kilgard MP, Merzenich MM (1998) Cortical Map Reorganization Enabled by Nucleus Basalis Activity. Science (80-) 279:1714–1718.

Kilgard MP, Pandya PK, Vazquez J, Gehi A, Schreiner CE, Merzenich MM (2001) Sensory Input Directs Spatial and Temporal Plasticity in Primary Auditory Cortex. J Neurophysiol 86:326–338.

Kuchibhotla K V, Gill J V, Lindsay GW, Papadoyannis ES, Field RE, Sten TAH, Miller KD, Froemke RC (2017) Parallel processing by cortical inhibition enables context-dependent behavior. Nat Neurosci 20:62–71.

Lakatos P, Musacchia G, O'Connel MN, Falchier AY, Javitt DC, Schroeder CE (2013) The spectrotemporal filter mechanism of auditory selective attention. Neuron 77:750–761.

Lim HH, Anderson DJ (2007) Antidromic Activation Reveals Tonotopically Organized Projections From Primary Auditory Cortex to the Central Nucleus of the Inferior Colliculus in Guinea Pig. J Neurophysiol 97:1413–1427.

Ma X, Suga N (2001) Plasticity of Bat's Central Auditory System Evoked by Focal Electric Stimulation of Auditory and/or Somatosensory Cortices. J Neurophysiol 85:1078–1087.

Ma X, Suga N (2003) Augmentation of Plasticity of the Central Auditory System by the Basal Forebrain and/or Somatosensory Cortex. J Neurophysiol 89:90–103.

Markovitz CD, Tang TT, Lim HH (2013) Tonotopic and localized pathways from primary auditory cortex to the central nucleus of the inferior colliculus. Front Neural Circuits 7:1–11.

Marsh RA, Fuzessery ZM, Grose CD, Wenstrup JJ (2002) Projection to the Inferior Colliculus from the Basal Nucleus of the Amygdala. J Neurosci 22:10449–10460.

McGinley MJ, David S V, McCormick DA (2015) Cortical Membrane Potential Signature of Optimal States for Sensory Signal Detection. Neuron 87:179–192.

Miasnikov AA, Chen JC, Weinberger NM (2008) Specific auditory memory induced by nucleus basalis stimulation depends on intrinsic acetylcholine. Neurobiol Learn Mem 90:443–454.

Pégard NC, Mardinly AR, Oldenburg IA, Sridharan S, Waller L, Adesnik H (2017) Three-dimensional scanless holographic optogenetics with temporal focusing (3D-SHOT). Nat Commun 8:1228.

Straka MM, Hughes R, Lee P, Lim HH (2015) Descending and tonotopic projection patterns from the auditory cortex to the inferior colliculus. Neuroscience 300:325–337.

Weinberger NM (2003) The nucleus basalis and memory codes: Auditory cortical plasticity and the induction of specific, associative behavioral memory. Neurobiol Learn Mem 80:268–284.

Williamson RS, Polley DB (2019) Parallel systems for sound processing and functional connectivity among layer 5 and 6 auditory corticothalamic neurons. bioRxiv doi:10.1101/447276.

Winer JA, Chernock ML, Larue DT, Cheung SW (2002) Descending projections to the inferior colliculus from the posterior thalamus and the auditory cortex in rat, cat, and monkey. Hear Res 168:181–195.

Xiong XR, Liang F, Zingg B, Ji X, Ibrahim LA, Tao HW, Zhang LI (2015) Auditory cortex controls sound-driven innate defense behaviour through corticofugal projections to inferior colliculus. Nat Commun 6:7224.

Yan J, Zhang Y, Ehret G, Yan J (2005) Corticofugal shaping of frequency tuning curves in the central nucleus of the inferior colliculus of mice. J Neurophysiol 93:71–83.

Yan W, Suga N (1998) Corticofugal modulation of the midbrain frequency map in the bat. Nat Neurosci 1:54–58.

Zhang Y, Hakes JJ, Bonfield SP, Yan J (2005) Corticofugal feedback for auditory midbrain plasticity elicited by tones and electrical stimulation of basal forebrain in mice. Eur J Neurosci 22:871–879.

Zhou X, Jen PH-S (2007) Corticofugal Modulation of Multi-Parametric Auditory Selectivity in the Midbrain of the Big Brown Bat. J Neurophysiol 98:2509–2516.